Quantum Corrections to the Kink-Antikink Potential

by

Zander Lee

Thesis presented in partial fulfilment of the requirements for the degree of Master of Science in Physics in the Faculty of Science at Stellenbosch University

Supervisor: Prof. Herbert Weigel

March 2017

Declaration

By submitting this thesis electronically, I declare that the entirety of the work contained therein is my own, original work, that I am the sole author thereof (save to the extent explicitly otherwise stated), that reproduction and publication thereof by Stellenbosch University will not infringe any third party rights and that I have not previously in its entirety or in part submitted it for obtaining any qualification.

Date: March 2017 .....

Abstract

Quantum Corrections to the Kink-Antikink Potential

Z. Lee

Department of Physics,
Stellenbosch University,
Private Bag X1, Matieland 7602, South Africa.

Thesis: MSc (Physics)

March 2017

In quantum field theory vacuum polarization effects may drastically alter the classical properties of non-perturbative field configurations. This is especially the case when comparing the vacuum polarization energy (VPE) of configurations with different topological sectors which correspond to different particle numbers. For this reason we calculate the one-loop quantum correction to the kink-antikink potential by computing the VPE as a function of the kink-antikink separation. Being a quantum field theory calculation a proper renormalization must be applied. We compute the VPE by utilizing the spectral method which makes use of scattering data for fluctuations around the static kink-antikink configuration. In a first step we compare our numerical results for the kink background in the ϕ^4 and sine-Gordon models to analytical results from literature. In the next step the VPE is computed for backgrounds that have a kink and an antikink at a certain separation. Above a certain separation an unstable mode appears in the bound state spectrum of the symmetric channel. This unstable mode arises due to fluctuations which correspond to the variation of the separation distance. We exclude these fluctuations, because each calculation must be performed at a fixed separation. This enforces an orthogonality constraint in the symmetric channel. Ultimately, the $\mathcal{O}(\hbar)$ quantum correction to the kink-antikink potential is extracted from the calculation of the VPE.

Uittreksel

Kwantumkorreksies aan die Kink-Antikink Potensiaal

("Quantum Corrections to the Kink-Antikink Potential")

Z. Lee

Fisika Departement,
Stellenbosch Universiteit,
Privaatsak X1, Matieland 7602, Suid-Afrika.

Tesis: MSc (Fisika)

Maart 2017

In kwantumveldteorie kan die klassieke eienskappe van nie-perturbatiewe konfigurasies drasties verander word deur vakuum-polarisasie effekte. Hierdie is veral die geval wanneer die vakuum-polarisasie energie (VPE) van konfigurasies met verskillende topologiese sektore, wat ooreenstem met verskillende deeltjie nommers, vergelyk word. Vir hierdie rede bereken ons die een-lus kwantumkorreksie aan die kink-antikink potensiaal deur die VPE te bereken as 'n funksie van die kink-antikink skeiding. 'n Behoorlike hernormaliseering moet toegepas word omdat die 'n veldteorie berekening is. Ons bereken die VPE deur gebruik te maak van die spektrale metode, wat gebruik maak van spreidingsdata vir fluktuasies rondom die statiese kink-antikink konfigurasie. In 'n eerste stap vergelyk ons ons numeriese resultate vir die kink agtergrond in die ϕ^4 en sine-Gordon modelle met analitiese resultate van literatuur. In die volgende stap word die VPE bereken vir agtergronde wat 'n kink en 'n antikink het op 'n sekere skeiding. Bo 'n sekere skeiding verskyn 'n onstabiele modus in die gebondetoestand spektrum van die simmetriese kanaal. Die onstabiele modus ontstaan as gevolg van fluktuasies wat ooreenstem met die variasie van die skeidingsafstand. Hierdie fluktuasies word uitgesluit omdat elke berekening gedoen moet word teen 'n vaste skeiding. Hierdie dwing 'n ortogonaliteit beperking in die simmetriese kanaal. Uiteindelik word die $\mathcal{O}(\hbar)$ kwantumkorreksie aan die kink-antikink potensiaal uit die berekening van die VPE gehaal.

Acknowledgements

I would like to express my sincere gratitude to my supervisor, Professor Herbert Weigel, for his guidance, patience and encouragement over the course of this thesis. I am thankful for the support of my wife, Nadine Lee, and my family. Finally I would like to thank the National Institute for Theoretical Physics (NITheP) for funding my degree in the form of a bursary.

Contents

List of Figures

List of Tables

Chapter 1

Introduction

In this thesis we calculate the one-loop quantum corrections to the classical energy of soliton-antisoliton pairs in the ϕ^4 and sine-Gordon models in one space and time dimensions. In this introduction we will motivate this calculation. It is also necessary to discuss the properties of solitons and provide examples of their applications, which appear in many fields of physics.

1.1 Solitons in Field Theory

Quantum field theory (QFT) is the theoretical framework which reconciles quantum mechanics and Einstein's theory of special relativity. It also provides a full explanation of particle-wave dualism. Historically, the first achievement of QFT was the development of quantum electrodynamics (QED), which describes the interaction of matter and light. It is the most accurately tested physical theory currently known, with QED predicting the anomalous magnetic moment of the electron up to 10 significant digits [1]. At the time of writing, QFT describes three of the four known fundamental forces of Nature in the framework of the Standard Model of particle physics.

When a field theory is elevated to a quantum theory, the classical wave solutions lead to elementary quanta that can naturally be interpreted as particles. However, many non-linear field theories produce classical solutions which already have particle properties. These solutions possess a localized energy density which moves undistorted with constant velocity, and are called solitary waves or solitons [2]. They are non-perturbative solutions, i.e. they cannot be obtained by considering a linearized version of the field equations and treating the non-linear terms by perturbation theory.

These solitary waves were first discovered by John S. Russell in 1834 [3]. In 1895, Korteweg and De Vries (KdV) expanded upon Russell's experimental work by deriving the non-linear wave equation which bears their name [4]. They found that the solutions to the KdV equation have a permanent form and move undistorted. The first evidence for a special class of solitary wave solutions which maintain their shape after interaction was given by Perring and Skyrme in 1962 during their numerical investigation of the sine-Gordon model [5]. These solutions were called "solitons" by

Zabusky and Kruskal who found that the solutions to the KdV equation also have this property [6].

Solitary waves and solitons are distinguished according to Ref. [2] as follows: A solitary wave is a localized, non-singular solution to a non-linear field equation whose energy density is localized and moves undistorted with constant velocity. A soliton is a particular solitary wave whose energy density profile is asymptotically ($t \to \infty$) restored to its original shape and velocity after interaction. Throughout this thesis, however, we will use the term soliton to refer to both solitary waves and solitons.

Since the discovery of solitons they have been used in various branches of physics to study a wide variety of physical phenomena. They are ubiquitous in non-linear optics[7–9] and have been used to study Bose-Einstein condensates [10; 11], ferromagnets [12] and other topics in condensed matter physics [13; 14], as well as biophysics [15–17]. The use of solitons in particle physics originated with the Skyrme model [18], whose soliton solutions (skyrmions) can be interpreted as baryons[1] [20; 21]. These skyrmions and other solitons found in particle physics are called topological solitons, since they are characterized by a topological index which is related to their behavior at spatial infinity. This index becomes a conserved quantum number in the quantized theory. As an example, the topological charge of the skyrmion is the baryon number. Topological quantum numbers do not originate from continuous symmetries of the Lagrangian, but from boundary conditions.

The properties of solitons allow them to be interpreted as extended particles in classical field theory. The mass of the particle is given by the integrated energy density, which typically overestimates the actual mass since quantum corrections are omitted. This is not problematic when investigating the properties of a single particle. However, the quantum corrections may become important when comparing configurations with different particle numbers as it occurs, for example, when computing the binding energies of compound objects. In these cases the quantum corrections could drastically alter the properties of the configuration, such as possibly stabilizing a classically unstable configuration. The leading quantum correction to the soliton energy is the vacuum polarization energy (VPE). The VPE has already been investigated for various soliton configurations, such as the kinks of the ϕ^4 [22] and sine-Gordon models [23; 24], the skyrmion as a model for baryons [25–27] and cosmic strings in the standard model [28; 29]. The VPE has also been studied for configurations with different particle numbers, such as the H-dibaryon ($B = 2$) in the Skyrme model which is strongly bound classically [30]. It is very interesting to see that the estimated[2] VPE reduces this binding considerably [31].

In this thesis we consider a soliton and an antisoliton separated by a distance $2R$. These types of configurations mimic particle-antiparticle interactions. We calculate the VPE of the soliton-antisoliton potential in one time and one space dimensions for two models, the ϕ^4 model, which has a quartic self-interaction, and the sine-Gordon model.

[1] For a recent review on soliton models for baryons see Ref. [19].

[2] The VPE contribution calculated by Ref. [31] is only an estimate since the Skyrme model is not renormalizable.

1.2 Notation and Conventions

Throughout this thesis we will be working in natural units $\hbar = c = 1$, unless otherwise stated. The standard covariant tensor notation is used, with space-time coordinates being represented by the contravariant four-vector

$$x^\mu = \left(x^0, \boldsymbol{x}\right)^\mu, \tag{1.2.1}$$

where x^0 is the time component and $\boldsymbol{x} = (x^1, x^2, x^3)$ are the three spatial components. A four-vector is defined as any four-component set that transforms according to

$$x'^\mu = \Lambda^\mu{}_\nu x^\nu = \sum_{\nu=0}^{3} \Lambda^\mu{}_\nu x^\nu \tag{1.2.2}$$

where $\Lambda^\mu{}_\nu$ is the Lorentz transformation. The Minkowski metric tensor,

$$g_{\mu\nu} = g^{\mu\nu} = \begin{pmatrix} 1 & 0 & 0 & 0 \\ 0 & -1 & 0 & 0 \\ 0 & 0 & -1 & 0 \\ 0 & 0 & 0 & -1 \end{pmatrix}_{\mu\nu}, \tag{1.2.3}$$

is used to transform a contravariant four-vector into a covariant one:

$$x_\nu = g_{\mu\nu} x^\mu = \left(x^0, -\boldsymbol{x}\right)_\nu. \tag{1.2.4}$$

The covariant and contravariant derivatives are given by

$$\frac{\partial}{\partial x^\mu} = \partial_\mu = (\partial_t, \boldsymbol{\partial})_\mu \quad \text{and} \quad \frac{\partial}{\partial x_\mu} = \partial^\mu = (\partial_t, -\boldsymbol{\partial})^\mu, \tag{1.2.5}$$

respectively, where ∂_t refers to differentiation with respect to time and $\boldsymbol{\partial}$ is the nabla operator, $\boldsymbol{\partial} = \nabla$. Another operator of importance is the d'Alembert operator

$$\partial_\mu \partial^\mu = \partial^2 = \partial_t^2 - \boldsymbol{\partial}^2 = \partial_t^2 - \nabla^2. \tag{1.2.6}$$

In this thesis we will mostly work in $(1+1)$ dimensions, so $\mu = 0, 1$. We also use $\dot{\phi}$ and ϕ' to refer to differentiation with respect to time ($x^0 = t$) and space ($x^1 = x$) variables, respectively. Finally, operators are indicated by hats, $\hat{A}$, and the Einstein summation convention for doubled indexes is assumed (already indicated in Eq. (1.2.2)).

1.3 Lagrangian Formalism

Consider a dynamical system with its configuration space given by the manifold $\Omega \subseteq \mathbb{R}^d$, where d is the number of space-time degrees of freedom. As an example consider $d = 1$, which describes a single point particle moving along an infinitely long, straight line. The possible configurations of this particle are the positions along the line. For sufficiently large d, the system describes the continuous displacement of a field $\phi(\boldsymbol{x}, t)$ in space-time. The Lagrange function of the system is given as the spatial integral of the system's Lagrangian density, $\mathcal{L}(\phi, \partial_t\phi, \boldsymbol{\partial}\phi)$, which is a function

of the field $\phi(\boldsymbol{x},t)$ and its first temporal and spatial derivatives. The action of the system is given by

$$S[\phi] = \int_{t_1}^{t_2} \mathrm{d}t\, L(t) = \int_{\Omega} \mathrm{d}^4x\ \mathcal{L}(\phi(x), \partial_\mu\phi(x)), \tag{1.3.1}$$

where $\phi(x) = \phi(\boldsymbol{x},t)$ and the integration is over the space-time manifold Ω with the boundary $\partial\Omega$. If we solve the variational problem $\delta S = 0$ for a variation of this field, $\phi \to \phi + \delta\phi$, subject to the boundary condition $\delta\phi = 0$ on $\partial\Omega$, then we obtain the Euler-Lagrange equation

$$\frac{\partial\mathcal{L}(\phi,\partial_\mu\phi)}{\partial\phi} - \partial_\nu \frac{\partial\mathcal{L}(\phi,\partial_\mu\phi)}{\partial(\partial_\nu\phi)} = 0. \tag{1.3.2}$$

This equation is the field equation of motion for this system. Other quantities of interest are the canonical conjugate field momentum, given by

$$\pi(\boldsymbol{x},t) = \frac{\partial\mathcal{L}}{\partial(\partial_t\phi)} = \frac{\partial\mathcal{L}}{\partial\dot{\phi}}, \tag{1.3.3}$$

and the energy-momentum tensor

$$T^{\mu\nu} = \frac{\partial\mathcal{L}}{\partial(\partial_\mu\phi)}\partial^\nu\phi - g^{\mu\nu}\mathcal{L}, \tag{1.3.4}$$

which is obtained from the application of Noether's theorem for translation invariance [32]. The energy-momentum tensor obeys the continuity equation $\partial_\mu T^{\mu\nu} = 0$ and produces the conserved charge

$$P^\nu = \int \mathrm{d}^3x\, T^{0\nu} \quad \text{with} \quad \partial_t P^\nu = 0. \tag{1.3.5}$$

From the time component of the above conserved charge we obtain the total energy P^0 with energy density T^{00}, and from the spatial components we obtain the field momentum P^i with momentum density T^{0i}, where $i = 1,2,3$.

1.4 Thesis Organization

This thesis is organized as follows: In Chapter 2 we provide an introduction to the spectral method and define the VPE. We briefly review one-dimensional potential scattering theory as it is necessary to understand the spectral method. We also outline the quantization of the small-amplitude fluctuations and illustrate the implementation of the calculation of the VPE using the variable phase approach, both with and without a constraint applied to the fluctuations.

In Chapter 3 we introduce the ϕ^4 model and calculate the VPE of the single kink background, while in Chapter 4 we do the same for the sine-Gordon model. In Chapter 5 we construct the kink-antikink configurations for both models, and calculate the VPE for these configurations as a function of the half-separation distance.

Finally, we summarize our results and conclude in Chapter 6. The appendices contain a review of three-dimensional scattering theory, a proof of Levinson's theorem in (1+1) dimensions in the antisymmetric channel, details on calculations too long for the main text and an overview of the numerical methods used.

Chapter 2

The Spectral Method

The spectral method is an accurate, reliable and efficient procedure for performing calculations in renormalizable quantum field theories in the presence of time-independent background field configurations. The spectral method uses various tools from scattering theory to compute the spectra of quantum fluctuations, as well as to handle the necessary regularization and renormalization. These calculations are exact to one-loop, which includes all quantum effects up to $\mathcal{O}(\hbar)$. The method can be straightforwardly applied to configurations that allow for a partial wave decomposition.

In this chapter we discuss the spectral method and how it is used to calculate quantities of interest for our current problem. The chapter is laid out as follows: Section 2.1 discusses the vacuum polarization energy (VPE) while Section 2.2 provides a review of scattering theory to the extent necessary to understand the spectral method and its application to the current problem. In Section 2.3 we derive the equations necessary to perform the calculation of the VPE. Finally, Sections 2.4 and 2.5 illustrate numerical implementations of the calculation of VPE using the Variable Phase Approach (VPA) without and with a constraint, respectively.

2.1 Vacuum Polarization Energy

The leading quantum correction to the classical energy of a system is called the vacuum polarization energy (VPE). The VPE measures the change in energy caused by the polarization of the single particle modes, which occurs due to the interaction of a quantum field with a background configuration [33, pg. 4–5]. It is obtained from the sum of all one-loop diagrams with any number of insertions of the background field configuration [34]

$E_{\text{vac}} =$ 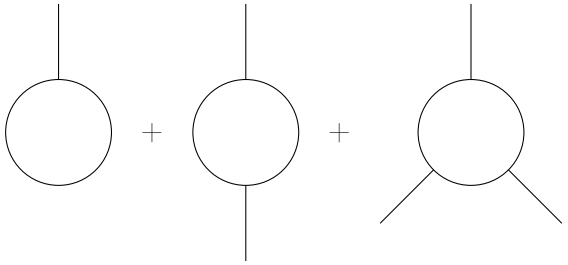 $+ \ \ldots \ ,$ (2.1.1)

where each external line corresponds to one insertion of the background field configuration. This expression is divergent and must be renormalized.

The VPE can also be obtained by recalling that each mode of a quantum field is associated with a quantum harmonic oscillator when adopting the small-amplitude approximation for each mode. Since the ground state, or zero-point, energy of a quantum harmonic oscillator is nonzero, the system will have nonzero energy in its vacuum state corresponding to the sum of the vacuum energy of these field modes. The VPE is then calculated as the renormalized sum of the shifts of the zero-point energies of the quantum fluctuations due to their interaction with the background configuration:

$$E_{\text{vac}} = \frac{1}{2}\sum_i \left(\omega_i - \omega_i^{(0)}\right)\Big|_{\text{ren.}}, \tag{2.1.2}$$

where ω_i and $\omega_i^{(0)}$ are the energies of the interacting and free cases, respectively, and the trailing subscript refers to the need for renormalization.

It must be stated that there are, however, two problems with Eq. (2.1.2). Firstly, we need to carefully apply regularization and renormalization techniques in order to ensure that the final result is finite and unambiguous. The final answer after renormalization can be of the same order of magnitude as the smallest energies in the sum, and so enumerating the spectrum of states correctly is of the utmost importance.

Secondly, the system could contain both discrete bound states and continuous scattering states. This means that the above sum is not only a sum and therefore we also require an integral over the continuous scattering states. Since we want to use the tools of scattering theory, our actual calculation must not discretize the system using boundary conditions. A consistent enumeration of the spectrum of small oscillation modes is necessary in order to avoid the under- or over-counting of states. As stated above, if we neglect even a single ω_i or sum a slightly different number of terms for ω_i and $\omega_i^{(0)}$, our final result would be drastically changed [33, pg. 4–5].

Using the second representation (2.1.2) and weighing both the bound states and scattering states of the system appropriately, we calculate the VPE as

$$E_{\text{vac}} = \frac{1}{2}\sum_j^{b.s.} \omega_j + \frac{1}{2}\int_0^\infty \mathrm{d}k\, \omega(k)\Big[\rho(k) - \rho^{(0)}(k)\Big]\Big|_{\text{ren.}}, \tag{2.1.3}$$

where ω_j are the bound state energies with $|\omega_j| < m$; m being the mass of the fluctuations. Furthermore, $\omega(k) = \sqrt{k^2 + m^2}$ are the scattering state energies with continuous momentum k. Finally, $\rho(k)$ and $\rho^{(0)}(k)$ are the densities of states for the interacting and free cases, respectively. In Section 2.2.1 we will relate this difference to scattering data. That relation will be at the center of the spectral method.

It is possible to formally derive Eq. (2.1.3) by calculating the integral of the vacuum energy density, $\epsilon(x)$, which is defined as the renormalized vacuum expectation value of the energy-momentum tensor (before subtracting the non-interacting part $\sim \omega^{(0)}$)

$$\epsilon(x) = \left\langle \Omega \middle| \hat{T}_{00}(x) \middle| \Omega \right\rangle \Big|_{\text{ren.}}, \tag{2.1.4}$$

where $|\Omega\rangle$ is the vacuum of the system with the background configuration. This derivation can be found in Ref. [35].

2.2 Review of Potential Scattering Theory

In order to understand the spectral method, one needs to understand potential scattering theory. For this reason, we provide a basic review of one-dimensional scattering theory in this section. A review of scattering theory in three spatial dimensions is provided in Appendix A. For a more complete discussion on this topic, see the standard texts on scattering theory, such as Ref. [36] and Ref. [37].

Suppose that we have a spinless particle in one spatial dimension, which scatters off a symmetric potential, $V(x) = V(-x)$, that is locally integrable and satisfies

$$\int_{-\infty}^{\infty} \mathrm{d}x\,(1+|x|)|V(x)| < \infty. \tag{2.2.1}$$

The wave function obeys the time-independent Schrödinger equation[1]

$$\left[-\frac{\mathrm{d}^2}{\mathrm{d}x^2} + V(x)\right]\psi(k,x) = k^2\psi(k,x). \tag{2.2.2}$$

In potential scattering theory, the standard method is to find asymptotic solutions[2] to the equation in question. In the one dimensional case we can only obtain forward-scattered and backward-scattered waves, unlike the infinite number of scattering angles in two and three spatial dimensions. The scattering wave function has the asymptotic behavior (where k is real and positive)

$$\psi_1(k,x) \sim \begin{cases} e^{ikx} + s_{12}(k)e^{-ikx} & x \to -\infty \\ s_{11}(k)e^{ikx} & x \to \infty \end{cases} \tag{2.2.3}$$

$$\psi_2(k,x) \sim \begin{cases} s_{22}(k)e^{-ikx} & x \to -\infty \\ e^{-ikx} + s_{21}(k)e^{ikx} & x \to \infty. \end{cases} \tag{2.2.4}$$

In the time-dependent scenario, ψ_1 is a component of a wave packet that for $t \to -\infty$ describes a (plane) wave e^{ikx} at negative spatial infinity. As t increases the wave packet propagates to the right. At $t = \infty$, the wave packet has been partially reflected to the left (the $s_{12}(k)e^{-ikx}$ term) and partially transmitted to the right (the $s_{11}(k)e^{ikx}$ term). The two coefficients, s_{12} and s_{11}, are the reflection (to the left) and transmission (to the right) coefficients, respectively. Similarly, the solution ψ_2 describes the situation for an incident wave from the right (i.e. $x \to -\infty$ and $x \to \infty$ are exchanged), where s_{21} and s_{22} are the right-reflection and left-transmission coefficients. The matrix of these coefficients,

$$S(k) = \begin{pmatrix} s_{11}(k) & s_{12}(k) \\ s_{21}(k) & s_{22}(k) \end{pmatrix}, \tag{2.2.5}$$

[1] The essential difference to non-relativistic scattering is the dispersion relation $\omega^2 = k^2 + m^2$; not $\omega = k^2/2m$.

[2] Solutions that are so "far away" that the potential is effectively nonexistent and its effects can thus be ignored.

is the S-matrix of Eq. (2.2.2). The S-matrix must be unitary, due to the conservation of probability; this property, along with time-reversal invariance and the symmetric nature of the potential, enforces the relations

$$s_{11}(k) = s_{22}(k) \quad \text{and} \quad s_{12}(k) = s_{21}(k). \tag{2.2.6}$$

Since $V(x)$ is symmetric, $\psi(k,-x)$ is also a solution to Eq. (2.2.2). Therefore the problem separates into wave functions of even (ψ_+) and odd (ψ_-) parity,[3] which have the asymptotic behavior at large x,

$$\lim_{x\to\infty} \psi_\pm(k,x) \simeq e^{-ikx} \pm S_\pm(k) e^{ikx}, \tag{2.2.7}$$

with

$$S(k) = \begin{pmatrix} S_+(k) & 0 \\ 0 & S_-(k) \end{pmatrix} = \begin{pmatrix} e^{2i\delta_+(k)} & 0 \\ 0 & e^{2i\delta_-(k)} \end{pmatrix}, \tag{2.2.8}$$

where $\delta_\pm(k)$ is the scattering phase shift for the even/odd wave, which is a real-valued quantity that depends on the energy (i.e. depends on k).[4]

There are two other important sets of solutions to Eq. (2.2.2): The regular solutions, $\phi_\pm(k,x)$, which satisfy the boundary conditions[5]

$$\begin{aligned} \phi_+(k,0) &= 1 \quad \text{and} \quad \phi'_+(k,0) = 0 \\ \phi_-(k,0) &= 0 \quad \text{and} \quad \phi'_-(k,0) = 1, \end{aligned} \tag{2.2.9}$$

and the Jost solutions[6], $f(\pm k,x)$, that satisfy the boundary conditions

$$\lim_{x\to\infty} \left[f(\pm k,x) - e^{\pm ikx} \right] = 0. \tag{2.2.10}$$

In the upper complex k-plane, the Volterra integral equation for $f(k,x)$ has a unique solution and $f(k,x)$ is holomorphic and continuous as $\operatorname{Im} k \to 0$. The two Jost solutions are linearly independent for $k \neq 0$, so we may write the regular solutions as their linear combination

$$\begin{aligned} \phi_+(k,x) &= \frac{1}{2}[G(k)f(-k,x) + G(-k)f(k,x)] \\ \phi_-(k,x) &= \frac{i}{2k}[F(k)f(-k,x) - F(-k)f(k,x)], \end{aligned} \tag{2.2.11}$$

where the Jost functions, $G(k)$ and $F(k)$, are constructed from the Jost solutions by

$$G(k) = \frac{f'(k,0)}{ik} \quad \text{and} \quad F(k) = f(k,0). \tag{2.2.12}$$

[3] This is analogous to the partial wave decomposition in three spatial dimensions.

[4] We may write the S-matrix elements as pure phases, because it is unitary and therefore $|S_\pm|^2 = 1$. Also, the change of basis from Eq. (2.2.5) to Eq. (2.2.8) is unitary and does not affect the phase shifts.

[5] We use the shorthand $\phi'_\pm(k,0) = \partial\phi_\pm(k,x)/\partial x \big|_{x=0}$.

[6] These are the analogue of the Jost solutions which solve the radial Schrödinger equation in three dimensions.

The boundary conditions, Eq. (2.2.9) with zero on the right-hand side trivially hold true. Using the Wronskian of the Jost solutions,

$$W[f(-k,x),f(k,x)] = f(-k,x)f'(k,x) - f(k,x)f'(-k,x) = 2ik, \tag{2.2.13}$$

we see that the nonzero boundary conditions of the regular solutions (2.2.9) also hold:

$$\phi_+(k,0) = \phi'_-(k,0) = \frac{1}{2ik}\big[f(-k,0)f'(k,0) - f(k,0)f'(-k,0)\big] = 1. \tag{2.2.14}$$

The scattering wave functions satisfy the boundary conditions at the origin

$$\psi'_+(k,0) = 0 \quad \text{and} \quad \psi_-(k,0) = 0, \tag{2.2.15}$$

which, along with their asymptotic behavior (2.2.7), leads to

$$\begin{aligned} \psi_+(k,x) &= \frac{1}{2}[f(-k,x) + S_+(k)f(k,x)] \\ \psi_-(k,x) &= \frac{i}{2}[f(-k,x) - S_-(k)f(k,x)], \end{aligned} \tag{2.2.16}$$

where

$$\begin{aligned} S_+(k) &= e^{2i\delta_+(k)} = \frac{G(-k)}{G(k)} = \frac{G(k)^*}{G(k)} \\ S_-(k) &= e^{2i\delta_-(k)} = \frac{F(-k)}{F(k)} = \frac{F(k)^*}{F(k)}. \end{aligned} \tag{2.2.17}$$

The Jost functions have the following important properties [37]:

1. The Jost functions are holomorphic in the upper complex k-plane ($\operatorname{Im} k \geq 0$), except at $k = 0$ for $G(k)$.
2. They satisfy the symmetry relations $F(-k^*) = F(k)^*$ and $G(-k^*) = G(k)^*$ (used in Eq. (2.2.17)).
3. In the upper complex k-plane ($\operatorname{Im} k \geq 0$) the limits $F(k) \to 1$ and $G(k) \to 1$ as $|k| \to \infty$ hold.
4. Every zero of the Jost functions in the upper complex k-plane ($\operatorname{Im} k \geq 0$) corresponds to a bound state and lies on the imaginary axis, $k_j = i\kappa_j$ with $\kappa_j \in \mathbb{R}$; these zeros are finite in number and simple.

The third property implies that

$$\lim_{k\to\infty} \delta_\pm(k) = 0. \tag{2.2.18}$$

The phase shifts also satisfy

$$\delta_\pm(-k) = -\delta_\pm(k) \quad \text{for} \quad k \geq 0,\ k \in \mathbb{R}, \tag{2.2.19}$$

as a combination of Eq. (2.2.17) and property 2.

2.2.1 Phase Shift and the Density of States

We are ultimately interested in calculating the VPE for a specific system. Recall that once we know the change in density of states due to the polarization of the quantum fluctuations by the background, we can calculate the VPE (2.1.3). However, obtaining the density of states for our calculation isn't very practical, so instead we seek to find a relation between the density of states and a quantity that will be more useful, such as the phase shift.

To motivate the form of this relation, consider the small oscillation wave functions $\phi_k(x)$ which obey the one-dimensional relativistic Klein-Gordon equation with a potential $V(x)$ which is symmetric under $x \to -x$:

$$\left[-\frac{\mathrm{d}^2}{\mathrm{d}x^2} + V(x)\right]\phi_k(x) = k^2\phi_k(x). \tag{2.2.20}$$

In the antisymmetric channel, the free solution to this equation is $\phi_k^{(0)}(x) = \sin kx$. We expect that the interacting case will asymptotically approach the free solution, but with a possible phase shift

$$\lim_{x\to\infty}\left[\phi_k(x) - \sin(kx + \delta_-(k))\right] = 0. \tag{2.2.21}$$

We require the phase shift to be a continuous function of k which vanishes as $k \to \infty$, since it is only defined modulo π.

We begin by placing the system inside a 'box' by enforcing the boundary condition $\phi_k(L) = 0$ for large L. We then obtain a discrete spectrum of possible values of k,

$$kL + \delta_-(k) = n\pi, \tag{2.2.22}$$

where n is the number of states with momentum less than k. The density of states is calculated as

$$\rho_-(k) = \frac{\mathrm{d}n}{\mathrm{d}k} = \frac{1}{\pi}\left(L + \frac{\mathrm{d}\delta_-(k)}{\mathrm{d}k}\right). \tag{2.2.23}$$

We wish to return to the continuum by taking the limit $L \to \infty$. In this limit the density of states diverges, so in order to obtain a finite result we consider the difference of the density of states between the interacting and free cases

$$\Delta\rho_-(k) = \rho_-(k) - \rho_-^{(0)}(k) = \frac{1}{\pi}\frac{\mathrm{d}\delta_-(k)}{\mathrm{d}k}. \tag{2.2.24}$$

Following the same procedure in the symmetric channel yields

$$\Delta\rho_+(k) = \frac{1}{\pi}\frac{\mathrm{d}\delta_+(k)}{\mathrm{d}k}, \tag{2.2.25}$$

and so we have

$$\Delta\rho(k) = \frac{1}{\pi}\sum_{p=\pm}\frac{\mathrm{d}\delta_p(k)}{\mathrm{d}k}. \tag{2.2.26}$$

This relation can also be obtained from a more rigorous derivation in three spatial dimensions that uses the Green's function, $G_\ell(r, r', k)$, to show that [35]

$$\Delta\rho_\ell(k) = \frac{2k}{\pi}\,\mathrm{Im}\int_0^\infty \mathrm{d}r\left[G_\ell(r, r, k + i\epsilon) - G_\ell^{(0)}(r, r, k + i\epsilon)\right] = \frac{1}{\pi}\frac{\mathrm{d}\delta_\ell}{\mathrm{d}k}, \tag{2.2.27}$$

where $G_\ell^{(0)}(r, r, k + i\epsilon)$ is the free Green's function of the ℓ^{th} partial wave.

Using this result (2.2.26) we can rewrite the VPE equation (2.1.3) as

$$E_{\text{vac}} = \frac{1}{2}\sum_j^{b.s.} \omega_j + \sum_{p=\pm} \int_0^\infty \frac{\mathrm{d}k}{2\pi}\omega(k)\frac{\mathrm{d}\delta_p(k)}{\mathrm{d}k}\bigg|_{\text{ren.}}. \tag{2.2.28}$$

2.2.2 Levinson's Theorem

We mentioned in Section 2.1 that maintaining a consistent counting of the modes over which we sum when calculating the VPE is of extreme importance. Specifically, we wish to sum over the same number of modes in both the free and interacting case. An important result which enforces this requirement in the continuum case is Levinson's theorem, first published in 1949 [38]. The theorem states that for regular potentials that permit n bound states we obtain [39]

$$\delta(0) - \delta(\infty) = \begin{cases} n_-\pi & \text{antisymmetric channel} \\ (n_+ - \frac{1}{2})\pi & \text{symmetric channel,} \end{cases} \tag{2.2.29}$$

where $n = n_- + n_+$. If they exist, constant threshold states ($k = 0$) only contribute $1/2$ to the number of bound states. Note that the $1/2$ which appears in the symmetric channel is related to the fact that in this channel the derivative of the wave function vanishes at $x = 0$ and not the wave function itself. The importance of the $1/2$ term in the symmetric channel can be seen from the free case where the phase shift is zero in both channels, but there exists a half-bound state ($n_+ = 1/2$) in the symmetric channel. From Eq. (2.2.18) we have $\delta(\infty) = 0$, which is sensible since we do not expect a particle with infinite energy to be perturbed by a regular potential. This result, along with the relation between the density of states and the phase shift (2.2.26), implies

$$\int_0^\infty dk\, \Delta\rho(k) + n - \frac{1}{2} = 0. \tag{2.2.30}$$

So any change in the total number of states in the continuum is balanced by the appearance of a corresponding number of bound states.

We will now prove Levinson's theorem for the symmetric channel.[7] We wish to evaluate the integral

$$I = \int_0^\infty \frac{\mathrm{d}k}{\pi}\frac{\mathrm{d}\delta_+(k)}{\mathrm{d}k} = -\frac{1}{2\pi i}\int_0^\infty \mathrm{d}k\, \frac{\mathrm{d}}{\mathrm{d}k}[\ln G(k) - \ln G(-k)], \tag{2.2.31}$$

where we used Eq. (2.2.17) to write the phase shift in terms of the Jost function $G(k)$. We may extend the integration range to $-\infty$, since the above integrand is even in k. Doing so we obtain

$$I = -\frac{1}{2\pi i}\int_{-\infty}^\infty \mathrm{d}k\, \frac{\dot{G}(k)}{G(k)} = -\frac{1}{2\pi i}\lim_{\substack{R\to\infty \\ \epsilon\to 0}} \left\{ \left[\int_{-R}^{-\epsilon} + \int_\epsilon^R\right] \mathrm{d}k\, \frac{\dot{G}(k)}{G(k)} \right\}, \tag{2.2.32}$$

[7] See Appendix B for the proof in the antisymmetric channel.

where the dot denotes differentiation with respect to k. Now consider the contour $\mathcal{C}$ which goes along the real axis from $-R$ to $-\epsilon$, avoids the origin with a small semicircle $\mathcal{C}_\epsilon$ of radius ϵ above the real axis, continues along the real axis from ϵ to R, and finally returns via a semicircle $\mathcal{C}_R$ of radius R in the upper half plane (see Fig. 2.1). So we have

$$\oint_{\mathcal{C}} \mathrm{d}k \, \frac{\dot{G}(k)}{G(k)} = \left\{ \left[\int_{-R}^{-\epsilon} + \int_{\mathcal{C}_\epsilon} + \int_{\epsilon}^{R} + \int_{\mathcal{C}_R} \right] \mathrm{d}k \, \frac{\dot{G}(k)}{G(k)} \right\}. \tag{2.2.33}$$

In the limit $R \to \infty$, the integral along the semicircle $\mathcal{C}_R$ is zero, since $G(k) \to 1$ as $|k| \to \infty$ (property 3 of the Jost function), so for large $|k|$ $\dot{G}(k)/G(k)$ goes like $|k|^{-2}$ in the upper complex k-plane. Also, recall that all of the zeros of the Jost function lie on the imaginary axis, correspond to the bound states of the system and are finite in number and simple (property 4). Integrating along the contour $\mathcal{C}$, we can use Cauchy's argument principle since we are avoiding the pole at $k = 0$ and $G(k)$ has no other poles in the upper complex plane (property 1), or any zeros on the contour. This gives

$$\oint_{\mathcal{C}} \mathrm{d}k \, \frac{\dot{G}(k)}{G(k)} = 2\pi i \sum_{j}^{b.s.} 1 = 2\pi i n_+, \tag{2.2.34}$$

where n_+ is the number of bound states in the symmetric channel. Using Eq. (2.2.12) we see that the integral along the small semicircle $\mathcal{C}_\epsilon$ is given by

$$\lim_{\epsilon \to 0} \int_{\mathcal{C}_\epsilon} \mathrm{d}k \, \frac{\dot{G}(k)}{G(k)} = -\lim_{\epsilon \to 0} \int_{\mathcal{C}_\epsilon} \mathrm{d}k \, \frac{1}{k} = -i \int_{\pi}^{0} \mathrm{d}\theta = i\pi, \tag{2.2.35}$$

since $f'(0,0) \neq 0$. Combining these results produces

$$\lim_{\substack{R \to \infty \\ \epsilon \to 0}} \left\{ \left[\int_{-R}^{-\epsilon} + \int_{\epsilon}^{R} \right] \mathrm{d}k \, \frac{\dot{G}(k)}{G(k)} \right\} = 2\pi i n_+ - i\pi, \tag{2.2.36}$$

which we substitute into Eq. (2.2.32) and thereby obtain Levinson's theorem in the symmetric channel,

$$\delta_+(0) - \delta_+(\infty) = \left(n_+ - \frac{1}{2} \right) \pi. \tag{2.2.37}$$

Using Levinson's theorem we can rewrite Eq. (2.2.28) as

$$E_{\mathrm{vac}} = \frac{1}{2} \sum_{j}^{b.s.} (\omega_j - m) + \sum_{p=\pm} \int_0^\infty \frac{\mathrm{d}k}{2\pi} (\omega - m) \frac{\mathrm{d}\delta_p(k)}{\mathrm{d}k} \bigg|_{\mathrm{ren.}}. \tag{2.2.38}$$

This formulation allows us to ignore any possible half-bound states, which would have $\omega_j = m$.

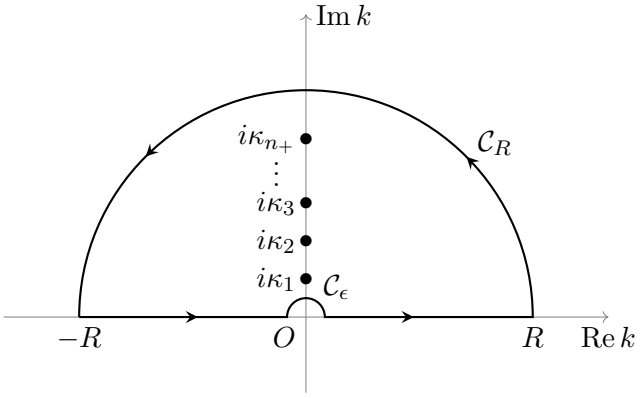

Figure 2.1: The integration contour for Levinson's theorem in the symmetric channel.

2.2.3 Born Approximation and Renormalization

We have now shown that we can write the VPE in terms of the phase shift. This is a key part of the spectral method, since we can numerically calculate the phase shift relatively easily (see Sections 2.4 and 2.5). However, in order to obtain a finite and unambiguous result for the VPE, we need to properly apply a renormalization procedure to Eq. (2.2.38).

Firstly, we note that the phase shift $\delta(k)$ typically goes like $1/k$ as $k \to \infty$, which results in a logarithmically divergent integral in Eq. (2.2.38). The divergences arise from the large k behavior and corresponds to the standard logarithmic divergences of scalar field theory in (1+1) dimensions. Recall that the Born approximation is exact at large k, so it could be a candidate for counteracting the logarithmic divergence in the integral. The Born approximation is not a good approximation for low-energy scattering data, but our calculation would not rely on its accuracy in this regime. Also, the Born approximation has no bound states, so it only affects the continuum [33]. With these properties in mind, we see that if we subtract the Born approximation from our phase shift, then the integral will converge. We can add the subtracted terms back in to the energy equation in the form of Feynman diagrams. We may do this because the terms of the Born series can be identified with Feynman diagrams: both are (formally) an expansion in the strength of the background potential. The divergences of the calculation are then fully contained within these diagrams, which are renormalized in the usual way of introducing counterterms to the Lagrangian.

To illustrate this connection, we consider a quantum field ϕ in d spacetime dimensions, which is coupled to a static background field $\sigma(\boldsymbol{x})$ with the Lagrangian density[8]

$$\begin{aligned}\mathcal{L} &= \frac{1}{2}\big[(\partial_\mu\phi)(\partial^\mu\phi) - \big(m^2 + \sigma(\boldsymbol{x}) - i\varepsilon\big)\phi^2\big] \\ &= \frac{1}{2}\phi\big[-\partial^2 - m^2 - \sigma(\boldsymbol{x}) + i\varepsilon\big]\phi,\end{aligned} \tag{2.2.39}$$

[8]The following argument is from Sections 3.3 and 3.5 of Ref. [33], which should be consulted for further details.

up to total derivative terms that do not involve the background. The energy density is obtained from the vacuum expectation value of the $\hat{T}_{00}$ component of the energy-momentum tensor. Using functional techniques this yields

$$\epsilon(x) = \frac{1}{2}\frac{\int [\mathrm{d}\phi]\phi(x)\hat{T}_x\phi(x)e^{i\int \mathrm{d}^d y \frac{1}{2}\left[(\partial_t\phi)^2-(\boldsymbol{\partial}\phi)^2-\left(m^2+\sigma-i\varepsilon\right)\phi^2\right]}}{\int [\mathrm{d}\phi]e^{i\int \mathrm{d}^d y \frac{1}{2}\left[(\partial_t\phi)^2-(\boldsymbol{\partial}\phi)^2-(m^2+\sigma-i\varepsilon)\phi^2\right]}}, \tag{2.2.40}$$

where the coordinate space operator, $\hat{T}_x$, is given by

$$\hat{T}_x = \overleftarrow{\partial}_t\overrightarrow{\partial}_t + \overleftarrow{\boldsymbol{\partial}}\cdot\overrightarrow{\boldsymbol{\partial}} + m^2 + \sigma(\boldsymbol{x}). \tag{2.2.41}$$

Arrows indicate the direction of differentiation. Since the expression for the energy density is quadratic in the field ϕ, we couple $\phi\hat{T}_x\phi$ linearly to a source, compute the logarithmic derivative with respect to this source and then set the source to zero. Doing so yields

$$\begin{aligned}\epsilon(x) &= \frac{i}{2}\,\mathrm{Tr}\left\{\left[-\partial^2-(m^2+\sigma-i\varepsilon)\right]^{-1}\delta^d(\hat{x}-x)\left[-\partial_t^2-\boldsymbol{\partial}^2+(m^2+\sigma)\right]\right\}\\ &= -i\,\mathrm{Tr}\left\{\left[-\partial^2-(m^2+\sigma-i\varepsilon)\right]^{-1}\delta^d(\hat{x}-x)\partial_t^2\right\}+\ldots,\end{aligned} \tag{2.2.42}$$

where the ellipsis in the second line refers to non-dynamical contributions that do not involve σ and the trace includes spacetime integration. We can write the above propagator as $\left[-\partial^2-(m^2+\sigma-i\varepsilon)\right]^{-1} = \left[1-S_0\sigma\right]^{-1}S_0$, where $S_0 = \left[-\partial^2-m^2+i\varepsilon\right]^{-1}$ is the free propagator. Because the background field is static, we may introduce frequency states $|\omega\rangle$ such that $\langle\omega|\sigma|\omega'\rangle = \sigma\delta(\omega-\omega')$. The ν^{th} order term in the Feynman series of the energy density is then

$$\epsilon^{(\nu)}_{\mathrm{FD}}(\boldsymbol{x}) = i\int\frac{\mathrm{d}\omega}{2\pi}\,\mathrm{Tr}'\left\{\omega^2[S_0(\omega)\sigma]^\nu S_0(\omega)\delta^{d-1}(\boldsymbol{x}-\hat{\boldsymbol{x}})\right\}, \tag{2.2.43}$$

where $S_0(\omega) = \left(\omega^2+\boldsymbol{\partial}^2-m^2+i\varepsilon\right)^{-1}$ and Tr' is the trace over all of the remaining degrees of freedom excluding integration over the time coordinate. The above expression is the $\mathcal{O}(\sigma^\nu)$ contribution to the energy density and therefore it corresponds to the Feynman diagram (with ν external legs) contribution to the energy density, up to total derivatives which do not contribute to the integrated density. We integrate the energy density to obtain

$$\begin{aligned}E^{(\nu)}_{\mathrm{FD}} = \int \mathrm{d}^{d-1}x\,\epsilon^{(\nu)}_{\mathrm{FD}}(\boldsymbol{x}) &= i\int\frac{\mathrm{d}\omega}{2\pi}\,\mathrm{Tr}'\left\{\omega^2 S_0(\omega)[S_0(\omega)\sigma]^\nu\right\}\\ &= -\frac{i}{2}\int\frac{\mathrm{d}\omega}{2\pi}\,\mathrm{Tr}'\left\{\omega\left(\frac{\partial}{\partial\omega}S_0(\omega)\right)[\sigma S_0(\omega)\sigma S_0(\omega)\sigma\ldots]\right\},\end{aligned} \tag{2.2.44}$$

with ν factors of σ but only $\nu-1$ factors of $S_0(\omega)$ in the square bracket in the second line. Integration by parts picks up derivatives from the $\nu-1$ propagators. Each of these terms gives an equal contribution due to the cyclic property of the trace, so we have

$$E^{(\nu)}_{\mathrm{FD}} = \frac{i}{2}\int\frac{\mathrm{d}\omega}{2\pi}\,\mathrm{Tr}'\left\{[S_0(\omega)\sigma]^\nu + (\nu-1)\omega\left(\frac{\partial}{\partial\omega}S_0(\omega)\right)[\sigma S_0(\omega)\sigma S_0(\omega)\sigma\ldots]\right\}. \tag{2.2.45}$$

Identifying the derivative terms in Eqs. (2.2.44) and (2.2.45) leads to

$$E_{\mathrm{FD}}^{(\nu)} = \frac{i}{2\nu}\int \frac{\mathrm{d}\omega}{2\pi}\,\mathrm{Tr}'\left[S_0(\omega)\sigma\right]^{\nu}. \tag{2.2.46}$$

In order to obtain the $\mathcal{O}(\sigma)$ diagrams, we consider the coordinate space operator $\hat{T}_x = \hat{T}_x^{(0)} + \hat{T}_x^{(1)}$, where the superscripts indicates that it contains pieces to zeroth- and first-order in the background $\sigma(\boldsymbol{x})$. Augmenting these operators with δ-functions, as in Eq. (2.2.42), and computing them in momentum space yields

$$\begin{aligned}\left\langle k'\middle|\hat{T}_x^{(0)}\delta^d(x-\hat{x})\middle|k\right\rangle &= e^{i(k'-k)x}\left[k'^0k^0 + \boldsymbol{k}'\cdot\boldsymbol{k} + m^2\right]\\ \left\langle k'\middle|\hat{T}_x^{(1)}\delta^d(x-\hat{x})\middle|k\right\rangle &= \sigma(\boldsymbol{x})e^{i(k'-k)x}.\end{aligned} \tag{2.2.47}$$

We define the tadpole graph, which is divergent in two or more spacetime dimensions, by employing dimension regularization to $d = (s+1)$ spacetime dimensions,

$$\frac{1}{2i}\,\mathrm{Tr}'\left[\hat{T}_x^{(1)}\delta^{d-1}(\boldsymbol{x}-\hat{\boldsymbol{x}})\left(-\partial^2 - m^2\right)^{-1}\right] = \frac{i}{2}\sigma(\boldsymbol{x})\int\frac{\mathrm{d}^dk}{(2\pi)^d}\frac{1}{k^2-m^2}. \tag{2.2.48}$$

This diagram is the only divergent $\mathcal{O}(\sigma)$ diagram in dimensions $d \leq 4$.[9] To obtain the total energy we integrate the above expression

$$E_{\mathrm{FD}}^{(1)} = \frac{i}{2}\int \mathrm{d}^sx\,\sigma(\boldsymbol{x})\cdot\int\frac{\mathrm{d}^dk}{(2\pi)^d}\frac{1}{k^2-m^2} = \frac{\langle\sigma\rangle}{2(4\pi)^{\frac{s+1}{2}}}\Gamma\left(\frac{1-s}{2}\right)m^{s-1}, \tag{2.2.49}$$

where

$$\langle\sigma\rangle = \int \mathrm{d}^sx\,\sigma(\boldsymbol{x}) = \frac{2\pi^{\frac{s}{2}}}{\Gamma\left(\frac{s}{2}\right)}\int_0^\infty \mathrm{d}r\,r^{s-1}\sigma(r). \tag{2.2.50}$$

It can be explicitly shown that the energy contribution from the first Born approximation to the phase shift is exactly equal to the tadpole graph (2.2.49)[33]. This diagram is renormalized by adding a counterterm $c_1\sigma(\boldsymbol{x})$ to the Lagrangian density (or equivalently, subtracting it from $\hat{T}_{00}$). The definition of the coefficient c_1 must be fixed by physical input. We employ the no-tadpole condition, such that the quantum corrections do not alter the stationary point of the Lagrangian which produces the background field σ. This means that the counterterm contribution precisely cancels Eq. (2.2.49). This ensures that the vacuum expectation value of the background field is fixed. This condition is possible since the diagram is local and proportional to $\sigma(\boldsymbol{x})$.

This procedure is the standard approach for performing renormalization in the spectral method: Subtract a sufficient number of Born approximations from the phase shifts to render the integral convergent. Add the subtracted terms back in as Feynman diagrams, which are then combined with the counterterms of the one-loop renormalized theory in order to produce a finite result. Following this approach

[9] The other $\mathcal{O}(\sigma)$ diagram has a single insertion of σ and $\hat{T}_x^{(0)}$, and can be shown to be finite in all dimensions $d \leq 4$[35]. Also, since this graph is a total derivative, it will not contribute to the vacuum energy.

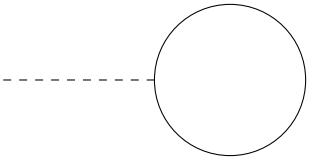

Figure 2.2: The tadpole diagram, which corresponds to one insertion of the background configuration σ, through the operator $\hat{T}_x^{(1)}$.

yields[10]

$$E_{\rm vac} = \frac{1}{2}\sum_{j}^{b.s.}(\omega_j - m) + \sum_{p=\pm}\int_0^\infty \frac{{\rm d}k}{2\pi}(\omega - m)\frac{\rm d}{{\rm d}k}[\delta_p(k)]_N + E_{\rm FD} + E_{\rm CT}, \quad (2.2.51)$$

where $E_{\rm FD}$ and $E_{\rm CT}$ are the energy contributions from the Feynman diagrams and counterterms, respectively, and

$$[\delta_p(k)]_N = \delta_p(k) - \sum_{i=1}^{N}\delta_p^{(i)}(k), \quad (2.2.52)$$

with $\delta_p^{(i)}(k)$ being the $i^{\rm th}$ Born approximation to the phase shift in the p channel.

For a scalar field theory in (1+1) dimensions, a single subtraction is all that is necessary. In this case only the local tadpole diagram occurs, as we discussed above. With the no-tadpole renormalization scheme, the energy contributions from the Feynman diagram and the counterterms cancel exactly, i.e. $E_{\rm FD} + E_{\rm CT} = 0$. Then Eq. (2.2.51) becomes

$$E_{\rm vac} = \frac{1}{2}\sum_{j}^{b.s.}(\omega_j - m) + \sum_{p=\pm}\int_0^\infty \frac{{\rm d}k}{2\pi}(\omega - m)\frac{\rm d}{{\rm d}k}\Big[\delta_p(k) - \delta_p^{(1)}(k)\Big]. \quad (2.2.53)$$

Note that the subtraction of the rest mass m avoids any possible infrared divergences from $\delta_p^{(1)}$. For an in-depth discussion of renormalization, the interested reader is directed to Ref. [40].

2.3 Small-Amplitude Quantum Corrections

Consider a scalar field $\phi(x,t)$ in (1+1) dimensions with the Lagrangian density

$$\mathcal{L}(x,t) = \frac{1}{2}\partial_\mu\phi\,\partial^\mu\phi - V(\phi), \quad (2.3.1)$$

where $V(\phi)$ is a self-interacting potential. Suppose that there exists a time-independent configuration $\phi_0(x)$, which is either a static solution to the Euler-Lagrange equation of the above Lagrangian, or it is held in place by an additional source field that couples linearly to the field variable. The configuration is then a stationary point of the classical action and has the classical energy $E_{\rm cl}$, which is

[10] In three spatial dimensions the sum over p is replaced by a sum over all partial waves ℓ.

finite. We are interested in finding the leading-order quantum corrections to this classical energy.

We begin by defining the fluctuations $\eta(x,t)$ around this background configuration as

$$\phi(x,t) = \phi_0(x) + \eta(x,t). \tag{2.3.2}$$

Applying this to the above Lagrangian (2.3.1), we find

$$\mathcal{L}(x,t) = \mathcal{L}_{\text{cl}}(x) + \mathcal{L}_{\text{cor}}(x,t) + \mathcal{O}\big(\eta^3\big), \tag{2.3.3}$$

where

$$\mathcal{L}_{\text{cl}}(x) = -\left[\frac{1}{2}\left(\frac{\partial\phi_0}{\partial x}\right)^2 + V(\phi_0)\right], \tag{2.3.4}$$

is the classical part from the background configuration and

$$\mathcal{L}_{\text{cor}}(x,t) = \frac{1}{2}\partial_\mu\eta\,\partial^\mu\eta - \frac{1}{2}U(\phi_0)\eta^2 \quad \text{with} \quad U(\phi_0) = \left.\frac{\mathrm{d}^2V(\phi)}{\mathrm{d}\phi^2}\right|_{\phi=\phi_0}, \tag{2.3.5}$$

is the Lagrangian for the fluctuations, which contains terms quadratic in η. There are no terms linear in η, due to the fact that ϕ_0 is an extremum of $V(\phi)$. As stated above, we are only interested in the leading-order quantum corrections, so we may ignore effects of $\mathcal{O}\big(\eta^3\big)$. In order for this fluctuation to be a quantum field, we must elevate it to an operator, $\hat{\eta}(x,t)$, that acts on the Hilbert space of the system described by the above Lagrangian density (2.3.5). We enforce the equal-time commutation relations

$$\big[\hat{\eta}(x,t), \hat{\pi}(x',t)\big] = i\hbar\delta(x-x') \tag{2.3.6}$$

$$\big[\hat{\eta}(x,t), \hat{\eta}(x',t)\big] = 0 \tag{2.3.7}$$

$$\big[\hat{\pi}(x,t), \hat{\pi}(x',t)\big] = 0. \tag{2.3.8}$$

where $\hat{\pi}(x,t)$ is the conjugate momentum of the field, given by Eq. (1.3.3),

$$\hat{\pi}(x,t) = \partial_t\hat{\eta}(x,t). \tag{2.3.9}$$

From Eqs. (2.3.6) and (2.3.9) we note that the fluctuations are $\mathcal{O}\big(\hbar^{1/2}\big)$. Using the Euler-Lagrange equations we find the equation of motion for the field operator,

$$\partial^2\hat{\eta}(x,t) + U(\phi_0)\hat{\eta}(x,t) = 0. \tag{2.3.10}$$

We make the stationary ansatz, such that

$$\hat{\eta}(x,t) = e^{-i\omega t}\hat{\eta}_\omega(x). \tag{2.3.11}$$

and so the particles associated with these fluctuations obey the stationary wave equation

$$\left[-\frac{\mathrm{d}^2}{\mathrm{d}x^2} + U(\phi_0)\right]\eta_\omega(x) = \omega^2\eta_\omega(x), \tag{2.3.12}$$

where $\omega = \sqrt{k^2+m^2}$ with $k > 0$ for the scattering states and $k_j = i\kappa_j$ for the bound states.

We are interested in calculating the quantum contribution to the energy. The total energy to $\mathcal{O}(\hbar)$ is given by

$$E = E_{\text{cl}} + E_{\text{vac}}, \tag{2.3.13}$$

where, using Eqs. (1.3.4) and (1.3.5),

$$E_{\text{cl}} = \int \mathrm{d}^3x \left[\frac{1}{2}\left(\frac{\partial\phi_0}{\partial x}\right)^2 + V(\phi_0)\right], \tag{2.3.14}$$

is the classical energy and

$$\int \mathrm{d}x\, \epsilon(x) = \int \mathrm{d}x \left\langle \Omega \middle| \hat{T}_{00}(x) \middle| \Omega \right\rangle \Big|_{\text{ren.}}, \tag{2.3.15}$$

is the energy contribution from the quantum fluctuations, $\hat{\eta}$, with $|\Omega\rangle$ being the vacuum of the system. If we now perform a Fock decomposition of $\hat{\eta}$, apply this to the above equation and subtract the analogue quantity for $U(\phi_0) = m^2$, we arrive at Eq. (2.1.2). Its properly renormalized extension is the master formula, Eq. (2.2.53).

2.4 Variable Phase Approach in One Space Dimension

The goal of this project is to numerically compute the VPE in an efficient and accurate manner. In order to do this, we require an expression for the VPE which is numerically tractable. In a previous section we obtained Eq. (2.2.53), which contains the derivative of the phase shift in the integral term. However, we do not wish to calculate numerical derivatives and thereby introduce an additional layer of numerical error. Instead, we utilize integration by parts to write

$$\int_0^\infty \mathrm{d}k\,(\omega - m)\frac{\mathrm{d}}{\mathrm{d}k}\Big[\delta_p(k) - \delta_p^{(1)}(k)\Big] = (\omega - m)\Big[\delta_p(k) - \delta_p^{(1)}(k)\Big]\Big|_0^\infty - \int_0^\infty \mathrm{d}k\,\frac{k}{\omega}\Big[\delta_p(k) - \delta_p^{(1)}(k)\Big]. \tag{2.4.1}$$

Recall that the Born approximation is exact for large k, and thus

$$\lim_{k\to\infty} k^2\Big[\delta_p(k) - \delta_p^{(1)}(k)\Big] = 0.$$

For $k = 0$ we have $\omega = m$, and so since $\delta(0)$ is finite (Levinson's theorem) we have $(\omega - m)\delta_p(0) = 0$. Also, $\delta^{(1)}(0)$ is $\mathcal{O}(1/k)$ while ω approaches m at $\mathcal{O}\big(k^2\big)$, therefore the first term on the right-hand side of Eq. (2.4.1) is indeed zero. The equation for the VPE then becomes

$$E_{\text{vac}} = \frac{1}{2}\sum_j^{b.s.}(\omega_j - m) - \sum_{p=\pm}\int_0^\infty \frac{\mathrm{d}k}{2\pi}\frac{k}{\sqrt{k^2+m^2}}\Big[\delta_p(k) - \delta_p^{(1)}(k)\Big]. \tag{2.4.2}$$

This expression is amenable to numerical computation, as long as we can calculate the phase shift and its Born approximation efficiently. To achieve this, we will utilize the generalizations of the variable phase approach [41].

We begin by rewriting the stationary wave equation (2.3.12) in the form

$$\left[-\frac{\mathrm{d}^2}{\mathrm{d}x^2}+\sigma(x)\right]\eta_k = k^2\eta_k \quad \text{where} \quad \sigma(x) = U(\phi_0(x)) - m^2. \tag{2.4.3}$$

This is exactly Eq. (2.2.2), so we can use the results from Section 2.2. Recall from Section 2.2 that the Jost solution, which is just a plane wave in the free case, solves Eq. (2.4.3). We parameterize it as

$$f(k,x) = e^{ikx+i\beta(k,x)}, \tag{2.4.4}$$

where $\beta(k,x)$ satisfies the differential equation

$$-i\beta''(k,x) + 2k\beta'(k,x) + \left[\beta'(k,x)\right]^2 + \sigma(x) = 0. \tag{2.4.5}$$

The boundary conditions for this differential equation are obtained by recalling the asymptotic behavior of the Jost solution (2.2.10), which implies that

$$\lim_{x\to\infty}\beta(k,x) = 0 \quad \text{and} \quad \lim_{x\to\infty}\beta'(k,x) = 0. \tag{2.4.6}$$

To proceed further we need to consider each channel individually.

2.4.1 Antisymmetric Channel

In the antisymmetric channel the Jost function is related to the Jost solution by Eq. (2.2.12),

$$F(k) = f(k,0) = e^{i\beta(k,0)}. \tag{2.4.7}$$

The phase shift is obtained from the Jost function by Eq. (2.2.17), therefore

$$\delta_-(k) = \frac{1}{2i}[\ln F(-k) - \ln F(k)] = \frac{1}{2i}[\ln F^*(k) - \ln F(k)]. \tag{2.4.8}$$

Using the two above equations, (2.4.7) and (2.4.8), we find

$$\delta_-(k) = -\operatorname{Re}\beta(k,0). \tag{2.4.9}$$

The Born approximation to the phase shift is extracted from the linearized version of the differential equation (2.4.5) and iterating:

$$-i\beta''^{(1)}(k,x) + 2k\beta'^{(1)}(k,x) + \sigma(x) = 0 \tag{2.4.10}$$

$$-i\beta''^{(2)}(k,x) + 2k\beta'^{(2)}(k,x) + \left[\beta'^{(1)}(k,x)\right]^2 = 0 \tag{2.4.11}$$

$$\vdots$$

with the boundary conditions

$$\lim_{x\to\infty}\beta^{(i)}(k,x) = 0 \quad \text{and} \quad \lim_{x\to\infty}\beta'^{(i)}(k,x) = 0, \quad \forall\, i, \tag{2.4.12}$$

and using

$$\delta_-^{(i)}(k) = -\operatorname{Re}\beta^{(i)}(k,0). \tag{2.4.13}$$

We have thus found an efficient method of computing the phase shift and its Born approximations in the antisymmetric channel.

2.4.2 Symmetric Channel

The relation between the Jost function and the Jost solution in the symmetric channel is given by Eq. (2.2.12), and therefore

$$G(k) = \left[1 + \frac{\beta'(k,0)}{k}\right] e^{i\beta(k,0)} = \left[1 + \frac{\beta'(k,0)}{k}\right] F(k). \tag{2.4.14}$$

Using the relation between the S-matrix and the Jost function (2.2.17), we obtain the phase shift, up to additions of $\pi/2$ necessary to turn it into a continuous function,

$$\begin{aligned}
\delta_+(k) &= \frac{1}{2i}[\ln(G(k)^*) - \ln G(k)] \\
&= \frac{1}{2i}\left[\ln F^*(k) - \ln F(k) + \ln\left(\frac{k + \beta'^*(k,0)}{k + \beta'(k,0)}\right)\right] \\
&= -\operatorname{Re}\beta(k,0) - \arctan\left[\frac{\operatorname{Im}\beta'(k,0)}{k + \operatorname{Re}\beta'(k,0)}\right].
\end{aligned} \tag{2.4.15}$$

The first Born approximation in the symmetric channel is obtained by linearizing Eq. (2.4.15) and recalling that $\beta^{(1)}$ is the leading contribution to β,

$$\delta_+^{(1)}(k) = -\operatorname{Re}\beta^{(1)}(k,0) - \frac{\operatorname{Im}\beta'^{(1)}(k,0)}{k}. \tag{2.4.16}$$

We can therefore calculate the phase shift in the antisymmetric and symmetric channel by solving the differential equations (2.4.5) and (2.4.10) to obtain $\beta(k,x)$, its derivative $\beta'(k,x)$ and its first Born approximation $\beta^{(1)}(k,x)$, with its derivative $\beta'^{(1)}(k,x)$. Using these functions we can then calculate the phase shift via the relations (2.4.9), (2.4.13), (2.4.15) and (2.4.16). Once we have obtained the phase shift and its Born approximation, we can perform the integral in Eq. (2.4.2) to calculate the VPE.[11]

2.5 Variable Phase Approach with Constraint

In Chapter 5 we shall see that it is necessary to formulate a method for calculating the phase shift for a wave function η_k subject to a constraint

$$\int_{-\infty}^{\infty} \mathrm{d}x\, z(x)\eta_k(x) = 0. \tag{2.5.1}$$

We shall only consider a symmetric constraint function, $z(-x) = z(x)$, and thus the constraint only affects the symmetric channel. Without loss of generality the constraint function can be taken to be normalized,

$$\int_{-\infty}^{\infty} \mathrm{d}x\, z(x)^2 = 1, \tag{2.5.2}$$

and to vanish at spatial infinity,

$$\lim_{x\to\pm\infty} z(x) = 0. \tag{2.5.3}$$

[11] A method for calculating the bound states numerically is discussed in Appendix D.1.

The constraint can then be included in the wave equation (2.4.3) using a Lagrange multiplier α,

$$-\eta_k''(x) + \sigma(x)\eta_k(x) + \alpha z(x) = k^2\eta_k(x). \tag{2.5.4}$$

We multiply the wave equation by $z(x)$ and integrate

$$\int_{-\infty}^{\infty} \mathrm{d}x \left[-\eta_k''(x) + \sigma(x)\eta_k(x) + \alpha z(x)\right] z(x) = k^2 \int_{-\infty}^{\infty} \mathrm{d}x\, z(x)\eta_k(x)$$
$$\int_{-\infty}^{\infty} \mathrm{d}x \left[-\eta_k''(x) + \sigma(x)\eta_k(x)\right] z(x) + \alpha = 0,$$

where we used the constraint (2.5.1) and the fact that $z(x)$ is normalized (2.5.2). Next we integrate by parts twice and use that $z(x)$ vanishes at spatial infinity (2.5.3) to identify the Lagrange multiplier as

$$\alpha = \int_{-\infty}^{\infty} \mathrm{d}x \left[z''(x) - \sigma(x)z(x)\right]\eta_k(x). \tag{2.5.5}$$

We substitute this result into the wave equation (2.5.4) to obtain the linear integro-differential equation

$$-\eta_k''(x) + \sigma(x)\eta_k(x) + z(x)\int_{-\infty}^{\infty} \mathrm{d}y \left[z''(y) - \sigma(y)z(y)\right]\eta_k(y) = k^2\eta_k(x). \tag{2.5.6}$$

By multiplying this equation with $z(x)$ on both sides and integrating, we find that the constraint (2.5.1) is imposed for $k \neq 0$.

Before we begin deriving the equations necessary to calculate the phase shift, there are two topics we want to discuss. Firstly, suppose that the constraint function was not normalized, such that

$$-\eta_k''(x) + \sigma(x)\eta_k(x) + \alpha\bar{z}(x) = k^2\eta_k(x) \quad \text{with} \quad \bar{z}(x) = Nz(x). \tag{2.5.7}$$

The constraint (2.5.1) also imposes

$$\int_{-\infty}^{\infty} \mathrm{d}x\, \bar{z}(x)\eta_k(x) = 0, \tag{2.5.8}$$

which yields the Lagrange multiplier

$$\alpha = \frac{1}{N^2}\int_{-\infty}^{\infty} \mathrm{d}x \left[\bar{z}''(x) - \sigma(x)\bar{z}(x)\right]\eta_k(x). \tag{2.5.9}$$

In this case the integro-differential equation becomes

$$-\eta_k''(x) + \sigma(x)\eta_k(x) + \frac{\bar{z}(x)}{N^2}\int_{-\infty}^{\infty} \mathrm{d}y \left[\bar{z}''(y) - \sigma(y)\bar{z}(y)\right]\eta_k(y) = k^2\eta_k(x), \tag{2.5.10}$$

which is identical to Eq. (2.5.6). As long as we impose the constraint in the form $\int \mathrm{d}x\, z(x)\eta_k(x)$, the normalization of the constraint function $z(x)$ is irrelevant.

Secondly, we need to consider the definition of a conserved current. We start with the time-dependent equations

$$\ddot{\eta}(x,t) - \eta''(x,t) + \left[\sigma(x) + m^2\right]\eta(x,t) + z(x)\int \mathrm{d}y\, g(y)\eta(y,t) = 0, \tag{2.5.11}$$

$$\ddot{\eta}^*(x,t) - \eta^{*\prime\prime}(x,t) + \left[\sigma(x) + m^2\right]\eta^*(x,t) + z(x)\int \mathrm{d}y\, g(y)\eta^*(y,t) = 0, \tag{2.5.12}$$

where

$$g(y) = z''(y) - \sigma(y)z(y). \tag{2.5.13}$$

Now we multiply the first equation by $\eta^*(x,t)$, the second one by $\eta(x,t)$ and integrate their difference over space to find

$$\int \mathrm{d}x\,[\eta^*(x,t)\ddot{\eta}(x,t) - \eta(x,t)\ddot{\eta}^*(x,t)] - \int \mathrm{d}x\,\left[\eta^*(x,t)\eta''(x,t) - \eta(x,t)\eta^{*\prime\prime}(x,t)\right]$$
$$= \int \mathrm{d}x \int \mathrm{d}y\, g(y)z(x)[\eta(x,t)\eta^*(y,t) - \eta^*(x,t)\eta(y,t)]. \tag{2.5.14}$$

The double integral vanishes due to the constraint[12], and therefore we obtain the conserved current

$$j^\mu(x,t) = \frac{i}{2}[\eta^*(x,t)\partial^\mu\eta(x,t) - \eta(x,t)\partial^\mu\eta^*(x,t)], \tag{2.5.15}$$

with $\int \mathrm{d}x\,\partial_\mu j^\mu = 0$. Current conservation implies that the reflected and transmitted fluxes sum to one. Therefore we must have a unitary scattering matrix, which implies real phase shifts in the diagonal channels.

We can now begin to rewrite the second-order integro-differential equation (2.5.6) into two coupled first-order integro-differential equations. This is necessary for the numerical implementation of the calculation of the phase shift.

2.5.1 Symmetric Channel

We begin by discussing the more complicated situation in the symmetric channel, where the constraint is imposed. We need to decompose the second-order integro-differential equation (2.5.6) into two coupled first-order integro-differential equations. Usually one would define a second function $h_k(x) = \eta_k'(x)$, but for our problem there is a more advantageous parameterization which will lead to the variable phase approach. Since we are in the symmetric channel, we can write [41]

$$\eta_k(x) = a_s(x)\cos\left[kx + \delta_s(x)\right], \tag{2.5.16}$$

where $\delta_s(x)$ is *not* the physical phase shift. Similar to defining $h_k(x) = \eta_k'(x)$, we must choose a condition which relates the derivatives $a_s'(x)$ and $\delta_s'(x)$ to the functions themselves. Using $c(x) = \cos\left[kx + \delta_s(x)\right]$ and $s(x) = \sin\left[kx + \delta_s(x)\right]$ in order to simplify our notation, we choose the condition[13]

$$a_s'(x)c(x) = a_s(x)s(x)\delta_s'(x), \tag{2.5.17}$$

[12] The constraint implies $\int \mathrm{d}x\, z(x)\eta^*(x,t) = 0$ when z real, otherwise z^* appears in Eqs. (2.5.12) and (2.5.14).

[13] This is essentially a particular form of the variation of constants method for differential equations.

with the initial conditions

$$a_s(0) = 1 \quad \text{and} \quad \delta_s(0) = 0, \tag{2.5.18}$$

which, along with the above condition (2.5.17), ensures that Eq. (2.5.16) is symmetric under spatial reflection. The physical phase shift can be found by taking the limit

$$\delta_+(k) = \lim_{x\to\infty} \delta_s(x). \tag{2.5.19}$$

We now compute the derivatives of the wave function, which are given by

$$\begin{aligned}
\eta_k'(x) &= -k a_s(x) s(x) \\
\eta_k''(x) &= -k a_s'(x) s(x) - k a_s(x) c(x) \big[k + \delta_s'(x)\big] \\
&= -k a_s(x) \frac{s(x)^2}{c(x)} \delta_s'(x) - k a_s(x) c(x) \big[k + \delta_s'(x)\big] \\
&= -k^2 a_s(x) c(x) - \frac{k a_s(x)}{c(x)} \delta_s'(x),
\end{aligned} \tag{2.5.20}$$

where we have used the condition (2.5.17). Applying this parameterization to the second-order integro-differential equation (2.5.6), we find the first-order integro-differential equation

$$\frac{\mathrm{d}\delta_s(x)}{\mathrm{d}x} = -\frac{\sigma(x)}{k} c(x)^2 + \frac{z(x)c(x)}{k a_s(x)} \int_{-\infty}^{\infty} \mathrm{d}y \, \big[\sigma(y) z(y) - z''(y)\big] a_s(y) c(y), \tag{2.5.21}$$

which must be solved along with

$$\frac{\mathrm{d}a_s(x)}{\mathrm{d}x} = a_s(x) \tan\left[kx + \delta_s(x)\right] \frac{\mathrm{d}\delta_s(x)}{\mathrm{d}x}. \tag{2.5.22}$$

It is clear that Eq. (2.5.22) does not contain a singularity in the region of $c(x) \sim 0$, since Eq. (2.5.21) must be substituted on the right-hand side.

Using the fact that the integral in Eq. (2.5.21) does not depend on x and is simply the Lagrange multiplier α, we have the coupled differential equations

$$\begin{aligned}
\frac{\mathrm{d}\delta_s(x)}{\mathrm{d}x} &= -\frac{\sigma(x)}{k} c(x)^2 + \alpha \frac{z(x)c(x)}{k a_s(x)} \\
\frac{\mathrm{d}a_s(x)}{\mathrm{d}x} &= -\frac{1}{k} s(x) [\sigma(x) a_s(x) c(x) - \alpha z(x)],
\end{aligned} \tag{2.5.23}$$

together with the constraint that defines α self-consistently. We cannot have $\eta_k(x)$ and $\eta_k'(x)$ simultaneously zero due to current conservation. For this reason

$$a_s(x)^2 = \eta_k(x)^2 + \eta_k'(x)^2/k^2 \neq 0, \tag{2.5.24}$$

which implies that $a_s(x) > 0$, since $a_s(0) = 1$. Therefore we can parameterize $a_s(x) = e^{\nu(x)}$, which allows us to rewrite the coupled differential equations (2.5.23) as

$$\begin{aligned}
\frac{\mathrm{d}\delta_s(x)}{\mathrm{d}x} &= -\frac{1}{k} c(x) \Big[\sigma(x) c(x) - \alpha z(x) e^{-\nu(x)}\Big] \\
\frac{\mathrm{d}\nu(x)}{\mathrm{d}x} &= -\frac{1}{k} s(x) \Big[\sigma(x) c(x) - \alpha z(x) e^{-\nu(x)}\Big],
\end{aligned} \tag{2.5.25}$$

with the initial conditions

$$\delta_s(0) = 0 \quad \text{and} \quad \nu(0) = 0. \tag{2.5.26}$$

These two coupled differential equations are solved by adjusting α in such a way that the constraint

$$\int_0^\infty \mathrm{d}x\, z(x)c(x)e^{\nu(x)} = 0, \tag{2.5.27}$$

holds. This will be done by implementing a root-finding algorithm. The resulting value of α can be checked using the self-consistency condition

$$\alpha = 2\int_0^\infty \mathrm{d}x \left[\sigma(x)z(x) - z''(x)\right]c(x)e^{\nu(x)}. \tag{2.5.28}$$

The physical phase shift can then be computed from the limit (2.5.19). For the unconstrained problem we have $\alpha = 0$, and thus the differential equations (2.5.25) decouple and we only need to solve the equation for $\delta_s(x)$. The first Born approximation is calculated from the unconstrained problem,[14]

$$\frac{\mathrm{d}\delta_s^{(1)}(x)}{\mathrm{d}x} = -\frac{\sigma(x)}{k}\cos^2(kx), \quad \text{with} \quad \delta_s^{(1)}(0) = 0, \tag{2.5.29}$$

and taking the limit

$$\delta_+^{(1)}(k) = \lim_{x\to\infty} \delta_s^{(1)}(x). \tag{2.5.30}$$

One may wonder whether this constraint will have an impact on the bound states of the system. This turns out to be the case, as the constraint sets a bound state to the zero mode. To illustrate this, we define the free basis states $|n\rangle$ with

$$\langle x|n\rangle \sim \cos\left[\left(n - \frac{1}{2}\right)\pi\frac{x}{L}\right] \quad \text{where} \quad n = 1, 2, \ldots. \tag{2.5.31}$$

The momentum states are discretized by the box size L. We use this basis to diagonalize the projector

$$\hat{P} = \mathbb{1} - |z\rangle\langle z|\,, \tag{2.5.32}$$

which defines the new basis states $|m\rangle' = \sum_n V_{nm}\,|n\rangle$ with real matrix elements V_{nm}. With respect to $\hat{P}$ all states have unit eigenvalues, except for the state $|m_0\rangle'$ which has an eigenvalue of zero. We then calculate the matrix elements

$$H'_{lk} = {}'\langle l|\hat{H}|k\rangle' = \sum_{n,m} V_{nl}\,\langle n|\hat{H}|m\rangle\,V_{mk}, \tag{2.5.33}$$

which is simply $H' = V^T H V$. The (infinitely dimensional) subspace whose elements satisfy the constraint is constructed by setting

$$H'_{n,m_0} = 0 \quad \text{and} \quad H'_{m_0,n} = 0, \quad \forall\, n. \tag{2.5.34}$$

[14] The reason for using the Born approximation for the unconstrained problem will be given in Chapter 5.

The bound states are then calculated by finding the eigenvalues of this reduced Hamiltonian that are below the mass m of the system. The decoupled state must be counted as a bound state, otherwise Levinson's theorem does not hold.[15] This is sensible, since we have found the spectrum of $\hat{P}H\hat{P}$ which contains a zero eigenvalue.

As a final remark, consider the wave equation for imaginary momenta ($k = it$)

$$-\eta_t''(x) + \sigma(x)\eta_t(x) + \alpha z(x) + t^2\eta_t(x) = 0. \tag{2.5.35}$$

For real momenta the Jost solution behaves like a plane wave e^{ikx} at large x, so the correct parameterization is $\eta_t(x) = a(x)e^{-tx}$, which produces

$$a''(x) - 2ta'(x) = \sigma(x)a(x) + \alpha z(x)e^{tx}. \tag{2.5.36}$$

Unless the constraint function $z(x)$ decays more rapidly than the exponential function, which is unlikely, $a(x)$ grows exponentially with x for sufficiently large t. This means that the Jost solution will not be analytic in the upper complex k-plane ($\mathrm{Im}\, k \geq 0$). However, the validity of Levinson's theorem is suggested by Ref. [42] (assuming full separability) and Ref. [43] (assuming full symmetry). We will numerically show in Chapter 5 that this is the case when counting the zero eigenvalue of the reduced Hamiltonian as a bound state.

2.5.2 Antisymmetric Channel

In the antisymmetric channel we parameterize the wave function as

$$\eta_k(x) = a_a(x)\sin\left[kx + \delta_a(x)\right]. \tag{2.5.37}$$

We again need to relate the functions to their derivatives; in this case we choose

$$a_a'(x)\sin\left[kx + \delta_a(x)\right] = -a_a(x)\cos\left[kx + \delta_a(x)\right]\delta_a'(x). \tag{2.5.38}$$

There is no constraint in the antisymmetric channel, so the differential equations decouple giving

$$\frac{\mathrm{d}\delta_a(x)}{\mathrm{d}x} = -\frac{\sigma(x)}{k}\sin^2\left[kx + \delta_a(x)\right], \tag{2.5.39}$$

which has the initial condition $\delta_a(0) = 0$. Once again we find the physical phase shift by taking the limit

$$\delta_-(k) = \lim_{x\to\infty}\delta_a(x). \tag{2.5.40}$$

The first Born approximation is calculated from

$$\frac{\mathrm{d}\delta_a^{(1)}(x)}{\mathrm{d}x} = -\frac{\sigma(x)}{k}\sin^2(kx), \quad \text{with} \quad \delta_a^{(1)}(0) = 0, \tag{2.5.41}$$

and taking the limit

$$\delta_-^{(1)}(k) = \lim_{x\to\infty}\delta_a^{(1)}(x). \tag{2.5.42}$$

[15] This will be illustrated with the numerical results in Chapter 5.

Chapter 3

The ϕ^4 Model

In this chapter we will introduce the ϕ^4 model, which corresponds to the Klein-Gordon model with a quartic interaction term. The field equation of this model has two static solutions of interest, called the kink and antikink, which represent a dissipationless spin-0 bosonic particle and antiparticle. The kink solution is often used as a prototype configuration for other, more involved soliton systems which appear in field theory [2].

We begin this chapter by defining the Lagrangian and basic properties of the ϕ^4 model in Section 3.1. In Section 3.2 we derive the static solutions of the field equation for the model. Finally, in Section 3.3, the calculation of the quantum correction to the kink solution is performed using the methods of Chapter 2, specifically Sections 2.4 and 2.5. This has already been done analytically [22], and we will illustrate that our numerical method can accurately reproduce the results from literature.

3.1 The Model

Consider a scalar field $\phi(x,t)$ in (1+1) dimensions with its dynamics being governed by the Lagrangian density

$$\mathcal{L}(x,t) = \frac{1}{2}\partial_\mu\phi\,\partial^\mu\phi - V(\phi), \tag{3.1.1}$$

with the potential

$$V(\phi) = \frac{\lambda}{4}\left(\phi^2 - \frac{m^2}{2\lambda}\right)^2. \tag{3.1.2}$$

The parameters λ and m are positive, where λ is a coupling constant and m will turn out to be the mass of the quantum fluctuations. The reason for the negative sign in front of the $m^2/2\lambda$ term is to ensure that the potential does not have a unique minimum and thus allows the existence of static solutions [2, Chapter 2]. The potential has two degenerate minima at $\phi = \pm m/\sqrt{2\lambda}$. The Lagrangian is invariant with respect to the transformation $\phi \to -\phi$, but this symmetry is spontaneously broken when choosing a specific vacuum configuration. Since we are working in (1+1) dimensions, the field itself must be dimensionless and we conclude that the coupling constant λ is thus not dimensionless. This implies that the actual parameter which dictates weak or strong coupling is the ratio λ/m^2 [44, pg. 7].

3.2 Static Solutions

Using the Euler-Lagrange equation, we find that the equation of motion for the ϕ^4 model is given by

$$\frac{\partial^2\phi}{\partial t^2} - \frac{\partial^2\phi}{\partial x^2} + \left(\lambda\phi^3 - \frac{m^2}{2}\phi\right) = 0. \tag{3.2.1}$$

We are interested in the static solutions to the field equation, $\phi = \phi(x)$, so therefore we must solve

$$-\frac{\mathrm{d}^2\phi}{\mathrm{d}x^2} + \left(\lambda\phi^3 - \frac{m^2}{2}\phi\right) = 0. \tag{3.2.2}$$

The static solutions are stationary points of the potential energy

$$\int \mathrm{d}x \left[\frac{1}{2}\left(\frac{\mathrm{d}\phi}{\mathrm{d}x}\right)^2 + \frac{\lambda}{4}\left(\phi^2 - \frac{m^2}{2\lambda}\right)^2\right], \tag{3.2.3}$$

The static field equation (3.2.2) is clearly solved by the constant vacuum solutions

$$\phi_{\text{vac}} = \pm\frac{m}{\sqrt{2\lambda}}. \tag{3.2.4}$$

The question we now wish to answer is whether or not there exists other configurations which are extrema of the potential energy.

3.2.1 Kink and Antikink Solutions

As in Ref. [2] we multiply the static field equation (3.2.2) by $\mathrm{d}\phi/\mathrm{d}x$ and integrate, using the boundary condition $\mathrm{d}\phi/\mathrm{d}x \to 0$ as $x \to -\infty$, to obtain

$$\frac{\mathrm{d}\phi}{\mathrm{d}x} = \pm\sqrt{\frac{\lambda}{2}}\left(\phi^2 - \frac{m^2}{2\lambda}\right). \tag{3.2.5}$$

We integrate this differential equation

$$\sqrt{\frac{\lambda}{2}}(x - x_0) = \pm\int_{\phi(x_0)}^{\phi(x)} \frac{\mathrm{d}\phi}{\phi^2 + \left(\frac{im}{\sqrt{2\lambda}}\right)^2}, \tag{3.2.6}$$

which leads to

$$\phi(x) = \pm\frac{m}{\sqrt{2\lambda}}\tanh\left[\frac{m}{2}(x - x_0)\right]. \tag{3.2.7}$$

Here the constant x_0 is the point in space where $\phi(x_0) = 0$. We have thus obtained two solutions, namely the positive kink solution

$$\phi_K(x) = \frac{m}{\sqrt{2\lambda}}\tanh\left(\frac{mx}{2}\right), \tag{3.2.8}$$

and the negative antikink solution

$$\phi_{\overline{K}}(x) = -\frac{m}{\sqrt{2\lambda}}\tanh\left(\frac{mx}{2}\right), \tag{3.2.9}$$

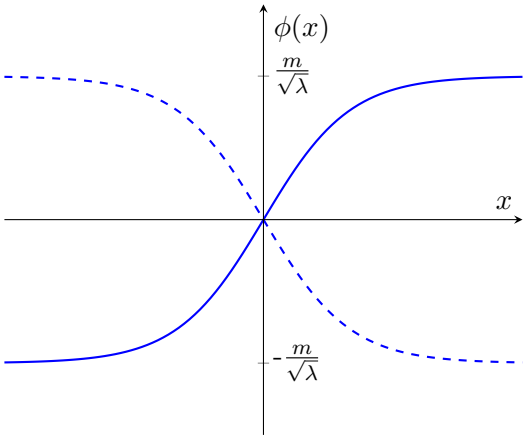

Figure 3.1: The static kink (solid line) and antikink (dashed line) solutions.

where we have chosen $x_0 = 0$. These two solutions are related by spatial reflection $x \to -x$. They also connect the two vacuum solutions ϕ_{vac}:

$$\phi_K(x) \to \pm\frac{m}{\sqrt{2\lambda}} \quad \text{and} \quad \phi_{\overline{K}}(x) \to \mp\frac{m}{\sqrt{2\lambda}} \quad \text{as} \quad x \to \pm\infty. \tag{3.2.10}$$

These solutions are plotted in Fig. 3.1.

Finally, we also construct moving kink (antikink) solutions by simply taking the Lorentz boost

$$x' = \gamma(x - vt) \quad \text{and} \quad t' = \gamma(t - vx) \quad \text{where} \quad \gamma = \frac{1}{\sqrt{1-v^2}}, \tag{3.2.11}$$

which yields

$$\phi(x,t) = \pm\frac{m}{\sqrt{2\lambda}} \tanh\left[\frac{m\gamma}{2}(x - vt)\right], \tag{3.2.12}$$

where $|v| < 1$ is the velocity of the kink (antikink). It can be straightforwardly verified that Eq. (3.2.12) is a solution to the full wave equation (3.2.1).

3.2.2 Energy Density and the Classical Kink Mass

The total energy of a field $\phi(x,t)$ is calculated using Eqs. (1.3.4) and (1.3.5)

$$E[\phi] = \int_{-\infty}^{\infty} \mathrm{d}x\, \epsilon(x,t), \tag{3.2.13}$$

where

$$\epsilon(x,t) = T^{00} = \frac{1}{2}\left(\frac{\partial\phi}{\partial t}\right)^2 + \frac{1}{2}\left(\frac{\partial\phi}{\partial x}\right)^2 + V(\phi). \tag{3.2.14}$$

So for the kink solution we have

$$\begin{aligned}\epsilon(x,t) = \epsilon(x) &= \frac{1}{2}\left(\frac{\partial\phi_K}{\partial x}\right)^2 + V(\phi_K) = 2V(\phi_K) \\ &= \frac{\lambda}{2}\left(\phi_K^2 - \frac{m^2}{2\lambda}\right)^2 = \frac{m^4}{8\lambda}\operatorname{sech}^4\left(\frac{mx}{2}\right).\end{aligned} \tag{3.2.15}$$

This classical density is illustrated in Fig. 3.2. It shows that the energy density is localized. The total energy (referred to as the classical kink mass) is given by the spatial integral

$$E[\phi_K] = \int_{-\infty}^{\infty} \mathrm{d}x \, \frac{m^4}{8\lambda} \operatorname{sech}^4\Big(\frac{mx}{2}\Big) = \frac{m^3}{3\lambda}, \tag{3.2.16}$$

which is finite. The antikink has the same energy. The total energy of the moving kink (3.2.12) is given by

$$\begin{aligned} E[\phi(x,t)] &= \int_{-\infty}^{\infty} \mathrm{d}x \left[\frac{1}{2}\Big(\frac{\partial \phi_K}{\partial t}\Big)^2 + \frac{1}{2}\Big(\frac{\partial \phi_K}{\partial x}\Big)^2 + V(\phi_K)\right] \\ &= \int_{-\infty}^{\infty} \mathrm{d}x \, \frac{m^4}{16\lambda}\left(\frac{v^2}{1-v^2} + \frac{1}{1-v^2} + 1\right) \operatorname{sech}^4\Big[\frac{m\gamma}{2}(x-vt)\Big] \\ &= \int_{-\infty}^{\infty} \mathrm{d}x \, \frac{m^4}{8\lambda(1-v^2)} \operatorname{sech}^4\Big[\frac{m\gamma}{2}(x-vt)\Big] \\ &= \gamma \frac{m^3}{3\lambda} = \gamma E[\phi_K]. \end{aligned} \tag{3.2.17}$$

This shows that the kink and antikink solutions are indeed solitons and can be interpreted as extended particles with a relativistic dispersion.

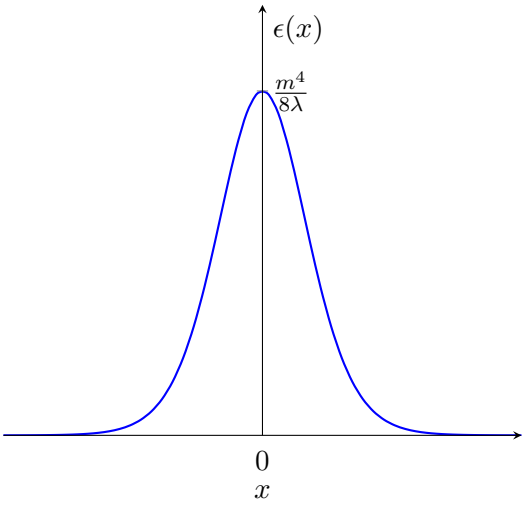

Figure 3.2: The energy density of the kink.

3.2.3 Translational Invariance

Consider the translation $x \to x + x_0$ of the kink solution. This simply gives the kink solution centered at the point $-x_0$:

$$\phi_K(x + x_0) = \frac{m}{\sqrt{2\lambda}} \tanh\Big[\frac{m}{2}(x + x_0)\Big]. \tag{3.2.18}$$

If we now calculate the total energy of this solution we find

$$E[\phi_K(x+x_0)] = \int_{-\infty}^{\infty} \mathrm{d}x\, \frac{m^4}{8\lambda} \operatorname{sech}^4\left[\frac{m}{2}(x+x_0)\right] = \frac{m^3}{3\lambda}. \tag{3.2.19}$$

Therefore we see that translating the kink solution does not change its energy. Any fluctuation that parameterizes the translation of the kink is thus a zero energy mode [2, Chapter 5]. The same holds for the antikink solution.

3.2.4 Topological Indexes

We briefly discuss the idea of topological indexes that are conserved in time and take on the role of 'quantum numbers' in the corresponding quantum field theory of the system. These indexes do not originate, like other conserved quantities, from Noether's theorem. We will first discuss the more general case of a field $\phi(x,t)$ in (1+1) dimensions, subject to a potential $V(\phi)$ which has a discrete (possibly infinite) number of degenerate absolute minima, and then see how it applies to the ϕ^4 model. The potential has the value $V(g_i) = 0$, where g_i is any one of its minima.

Consider the non-singular, finite energy solutions to the system with this potential $V(\phi)$. For the energy, given by Eqs. (3.2.13) and (3.2.14), to be finite, the field must approach one of the minima of $V(\phi)$ at every point on spatial infinity, for any instant of time t. In one spatial dimension spatial infinity is given by $x \to \pm\infty$. At some time t_0 we have

$$\lim_{x\to\infty} \phi(x,t_0) = \phi_1 \quad \text{with} \quad \phi_1 \in \{g_i\}. \tag{3.2.20}$$

The field $\phi(x,t)$ evolves continuously in time, as governed by its equation of motion. However, for the energy of the field to remain finite, it must always be located at one of the minima of $V(\phi)$ for $x \to \infty$. It cannot jump from ϕ_1 to another minimum and must thus remain stationary at ϕ_1 for all t. The same holds for $x \to -\infty$, at which point the field has the value $\phi_2 \in \{g_i\}$. Note that ϕ_1 and ϕ_2 are not necessarily the same minima. The space of all these non-singular, finite energy solutions can then be divided into sectors which are described by two indexes: the time-independent values of the field as $x \to \pm\infty$. These sectors are topologically unconnected, i.e. it is not possible to continuously distort the fields from one sector into another; doing so would violate the finite energy requirement. Therefore the solutions of one sector stays in that sector as time evolves. If $V(\phi)$ had a unique minimum, then there is only one sector of solutions, since $\phi(x,t)$ has only one allowed value for $x \to \pm\infty$.

Now we turn our attention to the ϕ^4 model. The potential in this case has two degenerate minima at $\phi = \pm m/\sqrt{2\lambda}$. The non-singular, finite energy solutions therefore fall into four topological sectors, which are described by the indexes

$(\phi(x \to -\infty), \phi(x \to \infty))$:

$$\left(\frac{m}{\sqrt{2\lambda}}, \frac{m}{\sqrt{2\lambda}}\right) \quad \text{contains} \quad \phi_{\text{vac}}(x) = \frac{m}{\sqrt{2\lambda}} \tag{3.2.21}$$

$$\left(-\frac{m}{\sqrt{2\lambda}}, \frac{m}{\sqrt{2\lambda}}\right) \quad \text{contains} \quad \phi_K(x) \tag{3.2.22}$$

$$\left(\frac{m}{\sqrt{2\lambda}}, -\frac{m}{\sqrt{2\lambda}}\right) \quad \text{contains} \quad \phi_{\overline{K}}(x) \tag{3.2.23}$$

$$\left(-\frac{m}{\sqrt{2\lambda}}, -\frac{m}{\sqrt{2\lambda}}\right) \quad \text{contains} \quad \phi_{\text{vac}}(x) = -\frac{m}{\sqrt{2\lambda}}, \tag{3.2.24}$$

where we have indicated which static solutions are elements of which sectors. If, for example, a kink (from the far left) and an antikink (from the far right) approach one another, the field configuration will belong to the sector (3.2.24). After they collide, the resulting field configuration will still belong to this sector.

We can define a topological current

$$J^\mu = \frac{\sqrt{2\lambda}}{2m}\epsilon^{\mu\nu}\partial_\nu\phi, \tag{3.2.25}$$

where $\epsilon^{\mu\nu}$ is the antisymmetric tensor with $\epsilon^{01} = 1$ and $\epsilon^{\mu\nu} = -\epsilon^{\nu\mu}$, which guarantees that the current is conserved, $\partial_\mu J^\mu = 0$. This produces the conserved topological charge

$$Q = \int_{-\infty}^{\infty} \mathrm{d}x\, J^0 = \frac{\sqrt{2\lambda}}{2m}[\phi(x \to \infty) - \phi(x \to -\infty)], \tag{3.2.26}$$

with $Q = 1$ for the kink solution and $Q = -1$ for the antikink solution. We require both $\phi(\infty)$ and $\phi(-\infty)$ in order to identify a topological sector, not just Q.[1] Solutions with $Q = 0$ are called non-topological and ones with $Q \neq 0$ are called topological. Therefore the kink and antikink are topological solutions, whereas the vacuum solutions are non-topological. Note that this charge does not arise from a continuous symmetry of the Lagrangian, but from boundary conditions. It is conserved by the finiteness of energy.

Finally, we can state that these indexes are related to symmetry breaking. If the Lagrangian is invariant under some symmetry transformation, then the complete set of minima must be mapped onto the same set by the transformation. However, each individual minimum is not required to be invariant under this transformation. In the ϕ^4 model, the Lagrangian is invariant under $\phi \to -\phi$, but the two minima are not; they are transformed into one another. There is therefore a connection between non-trivial topological sectors and the existence of degenerate minima of the potential, which is itself often related to spontaneous symmetry breaking [2].

3.3 Quantization of the Kink Solution

In order to demonstrate the effectiveness of the spectral method, we consider the first quantum correction to the kink solution, $\phi_K(x)$. Recall from Chapter 2 that

[1] As an example, both sectors (3.2.21) and (3.2.24) have $Q = 0$.

we begin by defining the fluctuations η around the kink configuration, such that $\phi(x,t) = \phi_K(x) + \eta(x,t)$. These fluctuations obey the wave equation (2.3.12), which in this case becomes

$$\left[-\frac{\mathrm{d}^2}{\mathrm{d}x^2} + m^2 - \frac{3m^2}{2}\operatorname{sech}^2\left(\frac{mx}{2}\right)\right]\eta_\omega = \omega^2\eta_\omega, \tag{3.3.1}$$

where we have factorized the time-dependence, $\eta(x,t) = e^{-i\omega t}\eta_\omega(x)$. The fluctuations are quantized as in Section 2.3, and therefore their vacuum energy contribution is the leading-order quantum correction to the classical energy. The above potential

$$\sigma(x) = -\frac{3m^2}{2}\operatorname{sech}^2\left(\frac{mx}{2}\right), \tag{3.3.2}$$

is the $n = 2$ member of the Pöschl-Teller family of exactly solvable potentials [45],

$$V_n(x) = -\left(\frac{n+1}{n}\right)m^2\operatorname{sech}^2\left(\frac{mx}{n}\right) \quad \text{where} \quad n = 0, 1, 2, \ldots, \tag{3.3.3}$$

where the free theory $V_0(x) = 0$ is given by $n \to 0$. The potentials of this type are symmetric and reflectionless, which implies that the S-matrix is proportional to the identity matrix. The antisymmetric and symmetric phase shifts must therefore be equal and are given by

$$\delta_-(k) = \delta_+(k) = \sum_{j=1}^{n}\arctan\left(\frac{jm}{kn}\right). \tag{3.3.4}$$

Multiples of π must be added to the above equation to make it a smooth function. The bound state energies for these potentials are

$$\omega_j^2 = \left(1 - \frac{j^2}{n^2}\right)m^2 \quad \text{with} \quad j = 0, 1, 2, \ldots, n. \tag{3.3.5}$$

Since the phase shifts are equal in both channels, there must be a half-bound threshold state ($\omega = m$). This is due to Levinson's theorem (2.2.29). This result must hold for all reflectionless potentials.

We now turn back to the kink potential with $n = 2$. The half-bound state is given by $j = 0$, while the zero mode ($\omega_0^2 = 0$), which arises due to translational invariance, is given by $j = 2$. The final bound state is the case $j = 1$ and has $\omega_1^2 = 3m^2/4$. The corresponding wave functions are found to be

$$\eta_0(x) = \sqrt{\frac{3m}{8}}\operatorname{sech}^2\left(\frac{mx}{2}\right) \tag{3.3.6}$$

$$\eta_1(x) = \sqrt{\frac{3m}{4}}\sinh\left(\frac{mx}{2}\right)\operatorname{sech}^2\left(\frac{mx}{2}\right), \tag{3.3.7}$$

for the bound states [45; 46] and

$$\eta_k(x) = \frac{m^2 e^{ikx}}{2\omega\sqrt{4k^2+m^2}}\left[3\tanh^2\left(\frac{mx}{2}\right) - 1 - \frac{4k^2}{m^2} - i\frac{6k}{m}\tanh\left(\frac{mx}{2}\right)\right], \tag{3.3.8}$$

for the continuous scattering states [2; 46]. Since $\eta_k(-x) = \eta_k(x)^*$ we form antisymmetric and symmetric solutions by

$$\eta_-(x) = \frac{1}{2i}[\eta_k(x) - \eta_k(x)^*] \quad \text{and} \quad \eta_+(x) = \frac{1}{2}[\eta_k(x) + \eta_k(x)^*] \tag{3.3.9}$$

with the phase shifts, from Eq. (3.3.4)

$$\delta_-(k) = \delta_+(k) = \arctan\left(\frac{3mk}{2k^2 - m^2}\right). \tag{3.3.10}$$

In Section 2.2.2 we pointed out that we do not need to worry about the energy contribution of the half-bound states when calculating the VPE from Eq. (2.4.2). The first Born approximations to the phase shifts can be calculated as

$$\begin{aligned} \delta_-^{(1)}(k) &= -\frac{1}{k}\int_0^\infty \mathrm{d}x\, \sigma(x)\sin^2(kx) \\ \delta_+^{(1)}(k) &= -\frac{1}{k}\int_0^\infty \mathrm{d}x\, \sigma(x)\cos^2(kx), \end{aligned} \tag{3.3.11}$$

and therefore

$$\delta_-^{(1)}(k) + \delta_+^{(1)}(k) = -\frac{1}{k}\int_0^\infty \mathrm{d}x\, \sigma(x) = \frac{3m}{k}. \tag{3.3.12}$$

We can now compute the VPE using Eq. (2.4.2), which in this case becomes

$$E_{\text{vac}} = \frac{1}{2}\sum_{j=0,1}(\omega_j - m) - \int_0^\infty \frac{\mathrm{d}k}{2\pi}\frac{k}{\sqrt{k^2+m^2}}\left[\delta_-(k) + \delta_+(k) - \frac{3m}{k}\right]. \tag{3.3.13}$$

Performing the integral for the phase shifts (3.3.10) yields

$$E_{\text{vac}} = m\left(\frac{1}{4\sqrt{3}} - \frac{3}{2\pi}\right), \tag{3.3.14}$$

which agrees with the result from literature [22].

3.3.1 Numerical Results

We now complete the demonstration of the spectral method by showcasing that the numerical methods of Sections 2.4 and 2.5 are accurate. Both of these are implementations of the variable phase approach, they only differ in their calculation of the phase shifts. Specifically, the method of Section 2.4 implements a second-order differential equation to calculate the phase shifts, while the method of Section 2.5 utilizes first-order differential equations. For this reason we distinguish between them by referring to the former as the "second-order" method and to the latter as the "first-order" method. For both formulations the relevant potential $\sigma(x)$ is given by equation (3.3.2). We will only be discussing the results obtained by performing these calculations. For an overview on the numerical implementation see Appendices D.1 and D.2.

The results of our numerical computation of the bound states is displayed in Table 3.1. We see that our routine accurately calculates the known analytical bound

		analytic	$\Delta\omega$	error
$m=1$	ω_0	0.00	9.57×10^{-10}	—
	ω_1	0.87	5.32×10^{-11}	6.14×10^{-11}
$m=2$	ω_0	0.00	2.70×10^{-9}	—
	ω_1	1.73	2.37×10^{-11}	1.37×10^{-11}

Table 3.1: Comparison of the analytical and numerical results for the two bound state energies of the kink for two different masses m. $\Delta\omega = |\omega^{(\text{ana})} - \omega^{(\text{num})}|$ where $\omega^{(\text{ana})}$ is the analytical result and $\omega^{(\text{num})}$ is the numerical result. The error is calculated as the relative error $\Delta\omega/|\omega^{(\text{ana})}|$.

	n_-	n_+	second-order		first-order	
			$\delta_-(0)$	$\delta_+(0)$	$\delta_-(0)$	$\delta_+(0)$
$m=1$	1	1	3.1416	3.1403	3.1416	3.1416
$m=2$	1	1	3.1416	3.1416	3.1416	3.1416

Table 3.2: The number of bound states and the value of the phase shift at $k=0$ in each channel for two different masses m.

state energies for the kink. The zero mode, ω_0, is determined to be a bound state from the symmetric channel, while ω_1 arises in the antisymmetric channel. This, of course, agrees with Eqs. (3.3.6) and (3.3.7). Using this result we can test Levinson's theorem by also obtaining the value of the phase shift as $k \to 0$ in each channel. This is illustrated in Table 3.2. We find that Levinson's theorem does hold (as expected) when including the half-bound state in the symmetric channel.

Finally, we use the first-order and second-order formulations to perform the calculation for the VPE. We find that our numerical result in both cases matches the expected analytical result, as is shown in Table 3.3. We therefore conclude that the spectral method, using either implementation, is accurate.

	E_0	second-order		first-order	
		E_1	ε	E_1	ε
$m=1$	$-0.333\,127$	$-0.333\,130$	9.17×10^{-6}	$-0.333\,130$	9.28×10^{-6}
$m=2$	$-0.666\,255$	$-0.666\,350$	1.43×10^{-4}	$-0.666\,264$	1.41×10^{-5}

Table 3.3: Comparison of the analytical and numerical results for the VPE of the kink for two different masses m. The analytical and numerical results are given by E_0 and E_1, respectively. The relative error is given by $\varepsilon = |E_0 - E_1|/|E_0|$.

Chapter 4

The Sine-Gordon Model

We now turn our attention to the sine-Gordon model. Once again, the relevant equation of motion has two soliton solutions of interest. These solutions are also called the kink and antikink solutions, representing a spin-0 particle and antiparticle, as before. The model also has a third soliton solution, called the doublet or breather. We will, however, not discuss it in this thesis. These three solutions are in fact "true" solitons and not just solitary waves [2].

This chapter will be laid out similarly to the previous chapter: in Section 4.1 we define the Lagrangian and basic properties of the sine-Gordon model, while in Section 4.2 we derive the static solutions of the model's field equation. Lastly, Section 3.3 contains the calculation of the quantum correction to the kink solution.

4.1 The Model

We have a single scalar field, $\phi(x,t)$, in (1+1) dimensions with the Lagrangian

$$\mathcal{L}(x,t) = \frac{1}{2}\partial_\mu\phi\,\partial^\mu\phi + \frac{m^4}{\lambda}\left[\cos\left(\frac{\sqrt{\lambda}\phi}{m}\right) - 1\right], \tag{4.1.1}$$

where λ is a positive coupling constant and m is the mass of the field. We can expand this Lagrangian in powers of λ, yielding

$$\mathcal{L}(x,t) = \frac{1}{2}\partial_\mu\phi\,\partial^\mu\phi - \frac{1}{2}m^2\phi^2 + \frac{\lambda}{4!}\phi^4 - \frac{\lambda^2}{6!}\frac{1}{m^2}\phi^6 + \dots \tag{4.1.2}$$

In the limit $\lambda \to 0$, this becomes the free Klein-Gordon model. The $\mathcal{O}(\lambda)$ term is the quartic coupling that we saw in the ϕ^4 model, except that it is attractive in this case. The parameter which characterizes strong or weak coupling is again λ/m^2, due to the dimensionless nature of the field.

4.2 Static Solutions

The field equation which corresponds to the Lagrangian (4.1.1) is

$$\frac{\partial^2\phi}{\partial t^2} - \frac{\partial^2\phi}{\partial x^2} + \frac{m^3}{\sqrt{\lambda}}\sin\left(\frac{\sqrt{\lambda}\phi}{m}\right) = 0. \tag{4.2.1}$$

We simplify this equation by adopting dimensionless variables

$$y = mx, \quad \tau = mt \quad \text{and} \quad \varphi(y,\tau) = \frac{\sqrt{\lambda}}{m}\phi(x,t), \tag{4.2.2}$$

which changes the field equation into

$$\frac{\partial^2\varphi}{\partial\tau^2} - \frac{\partial^2\varphi}{\partial y^2} + \sin\varphi = 0. \tag{4.2.3}$$

The Lagrangian has two discrete symmetries, namely $\varphi \to -\varphi$ and $\varphi \to \varphi + 2\pi q$, where $q \in \mathbb{Z}$. The energy of the field is given by

$$E[\varphi] = \frac{m^3}{\lambda}\int_{-\infty}^{\infty} \mathrm{d}y \left[\frac{1}{2}\left(\frac{\partial\varphi}{\partial\tau}\right)^2 + \frac{1}{2}\left(\frac{\partial\varphi}{\partial y}\right)^2 + (1-\cos\varphi)\right], \tag{4.2.4}$$

which vanishes at the absolute minima of the potential[1]

$$V_\varphi(\varphi) = 1 - \cos\varphi. \tag{4.2.5}$$

These degenerate minima are the constant vacuum solutions $\varphi_{\text{vac}} = 2\pi q$, or

$$\phi_{\text{vac}} = 2\pi q\frac{m}{\sqrt{\lambda}} \quad \text{where} \quad q \in \mathbb{Z}. \tag{4.2.6}$$

4.2.1 Kink and Antikink Solutions

We attempt to construct the static solutions, $\varphi = \varphi(y)$, that must satisfy

$$-\frac{\mathrm{d}^2\varphi}{\mathrm{d}y^2} + \sin\varphi = 0. \tag{4.2.7}$$

Similar as before, we multiply this equation by $\mathrm{d}\varphi/\mathrm{d}y$ and integrate, using the boundary conditions $V_\varphi(\varphi) \to 0$ and $\mathrm{d}\varphi/\mathrm{d}y \to 0$ as $y \to -\infty$, to obtain

$$\frac{\mathrm{d}\varphi}{\mathrm{d}y} = \pm\sqrt{2(1-\cos\varphi)}. \tag{4.2.8}$$

We integrate the above equation

$$y - y_0 = \pm\int_{\varphi(y_0)}^{\varphi(y)} \frac{\mathrm{d}\varphi}{2\sin\left(\frac{\varphi}{2}\right)}, \tag{4.2.9}$$

which leads to

$$\varphi(y) = 4\arctan\left[e^{\mp(y-y_0)}\right], \tag{4.2.10}$$

where the constant y_0 is the point in space where $\varphi(y_0) = 0$. Choosing $y_0 = 0$ and transforming back to the original (physical) variables, we find the kink solution

$$\phi_K(x) = \frac{4m}{\sqrt{\lambda}}\arctan\left(e^{-mx}\right), \tag{4.2.11}$$

[1]The potential of the original field ϕ is given by $V(\phi) = \left(m^4/\lambda\right)V_\varphi(\varphi)$.

and the antikink solution

$$\phi_{\overline{K}}(x) = \frac{4m}{\sqrt{\lambda}} \arctan(e^{mx}), \tag{4.2.12}$$

These two solutions are related by spatial reflection. Neighboring pairs of vacuum solutions are characterized by an integer q:

$$\begin{aligned} \lim_{x\to-\infty} \phi_K(x) &= 2\pi q \frac{m}{\sqrt{\lambda}} \\ \lim_{x\to\infty} \phi_K(x) &= 2\pi(q+1) \frac{m}{\sqrt{\lambda}} \\ \lim_{x\to\pm\infty} \phi_{\overline{K}}(x) &= \phi_K(\mp\infty), \end{aligned} \tag{4.2.13}$$

The solutions (4.2.11) and (4.2.12) are the pairs with $q = 0$. These two solutions are shown in Fig. 4.1(a). The moving solutions can be obtained through the application of a Lorentz boost (3.2.11). The energy of the solutions is calculated by integrating the energy density, illustrated in Fig. 4.1(b), to obtain

$$E[\phi_K] = \int_{-\infty}^{\infty} \mathrm{d}x \, \frac{4m^4}{\lambda} \operatorname{sech}^2(mx) = \frac{8m^3}{\lambda}. \tag{4.2.14}$$

Performing a translation $x \to x + x_0$ on the kink (antikink) solution will not affect its energy. So we again have translational invariance, and hence a zero mode in the bound state spectrum.

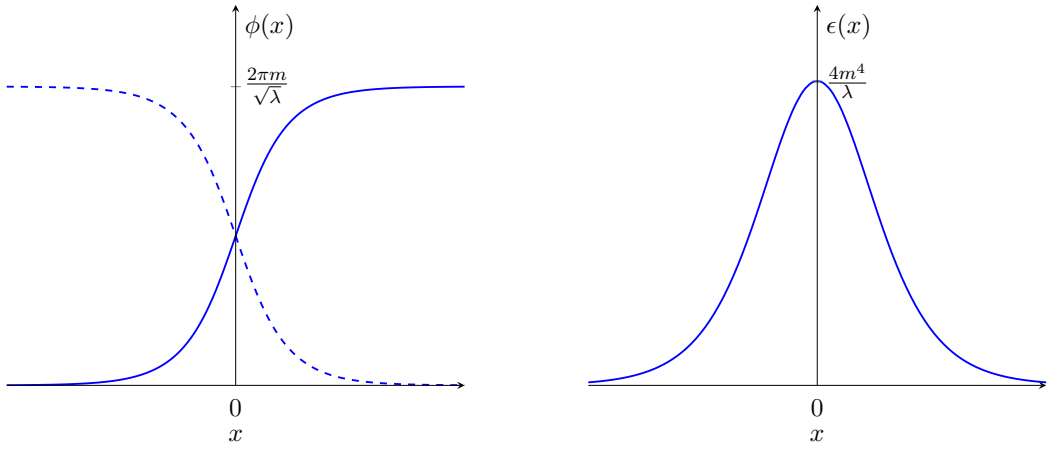

Figure 4.1: (a) The static kink (solid line) and antikink (dashed line) solutions for $q = 0$. (b) The energy density of the sine-Gordon kink.

Finally, the topological sectors of the finite-energy solutions are characterized by the conserved pair of indexes (N_1, N_2), where $N_i = 2\pi q_i m/\sqrt{\lambda}$, which are extracted from the asymptotic values of the field at $x \to -\infty$ and $x \to \infty$, respectively. If only

ϕ modulo 2π is physically meaningful, then only the topological charge[2]

$$Q = \frac{\sqrt{\lambda}}{2\pi m}(N_2 - N_1) = \frac{\sqrt{\lambda}}{2\pi m}\int_{-\infty}^{\infty} \mathrm{d}x\, \frac{\partial \phi}{\partial x}, \tag{4.2.15}$$

will be necessary to specify a sector. The kink solution has $Q = 1$, while the antikink solution has $Q = -1$.

4.3 Quantization of the Kink Solution

Similar to Section 3.3, we calculate the first quantum correction to the kink solution of the sine-Gordon model by considering the fluctuations, η, around the static kink solution $\phi_K(x)$, i.e. $\phi(x,t) = \phi_K(x) + \eta(x,t)$. These fluctuations obey the wave equation (2.3.12)

$$\left[-\frac{\mathrm{d}^2}{\mathrm{d}x^2} + m^2 - 2m^2\,\mathrm{sech}^2(mx)\right]\eta_\omega = \omega^2\eta_\omega, \tag{4.3.1}$$

where we have factorized the time-dependence, $\eta(x,t) = e^{i\omega t}\eta_\omega(x)$, as before. Once again, the fluctuations are quantized as in Section 2.3, and therefore their energy contribution is the leading-order quantum correction to the classical energy. The potential is given by

$$\sigma(x) = -2m^2\,\mathrm{sech}^2(mx), \tag{4.3.2}$$

and corresponds to the $n = 1$ member of the Pöschl-Teller family of potentials (3.3.3). Therefore, from Eq. (3.3.5), this potential must have a half-bound state and a zero mode bound state ($\omega_0^2 = 0$). As mentioned, the latter arises from translational invariance. The half-bound state is located in the antisymmetric channel, since the zero mode is in the symmetric channel. The bound state and scattering wave functions are given by [33]

$$\eta_0(x) = \sqrt{\frac{m}{2}}\,\mathrm{sech}(mx) \tag{4.3.3}$$

$$\eta_k(x) = \frac{e^{ikx}}{\omega}[k + im\tanh(mx)]. \tag{4.3.4}$$

We also form antisymmetric and symmetric wave functions using Eq. (3.3.9). Then the phase shifts are obtained from Eq. (3.3.4) as

$$\delta_-(k) = \delta_+(k) = \arctan\left(\frac{m}{k}\right). \tag{4.3.5}$$

The sum of first Born approximation in the two channels is

$$\delta_-^{(1)}(k) + \delta_+^{(1)}(k) = -\frac{1}{k}\int_0^{\infty} \mathrm{d}x\,\sigma(x) = \frac{2m}{k}. \tag{4.3.6}$$

[2]By modulo 2π, we mean that any single space-time point $\phi(x,t)$ can be chosen modulo 2π, while the other points are then fixed according to continuity requirements.

Finally, we compute the VPE using Eq. (2.4.2), which for this model becomes

$$E_{\text{vac}} = \frac{1}{2}(\omega_0 - m) - \int_0^\infty \frac{\mathrm{d}k}{2\pi} \frac{k}{\sqrt{k^2+m^2}} \left[\delta_-(k) + \delta_+(k) - \frac{2m}{k}\right]. \tag{4.3.7}$$

Performing the integral for the phase shifts (4.3.5) yields

$$E_{\text{vac}} = -\frac{m}{\pi}, \tag{4.3.8}$$

which is the result from literature [23; 24].

4.3.1 Numerical Results

As another test of our numerical methods, we also reproduce the above analytical result using the first-order and second-order formulations. The relevant potential, $\sigma(x)$, for either method is given by Eq. (4.3.2).

		analytic	numeric
$m = 1$	ω_0	0.00	9.54×10^{-6}
$m = 2$	ω_0	0.00	8.57×10^{-6}

Table 4.1: Comparison of the analytical and numerical results for the bound state energies of the kink for two different masses m.

	n_-	n_+	second-order		first-order	
			$\delta_-(0)$	$\delta_+(0)$	$\delta_-(0)$	$\delta_+(0)$
$m = 1$	0	1	1.570	1.571	1.571	1.571
$m = 2$	0	1	1.571	1.571	1.571	1.571

Table 4.2: The number of bound states and the value of the phase shift at $k = 0$ in each channel for two different masses m.

The numerical computation of the bound state energies is displayed in Table 4.1. As expected, the numerical routine correctly obtains only a zero mode bound state for the kink, which lies in the symmetric channel. We once again test Levinson's theorem by calculating the value of the phase shift in each channel as $k \to 0$. This is shown in Table 4.2. We conclude that Levinson's theorem holds, as long as we include the necessary half-bound state in the antisymmetric channel.

Finally, we calculate the VPE using both formulations, with the results shown in Table 4.3. In both cases, the numerical calculation matches the analytical result. Hence, we conclude that both implementations of the spectral method are accurate.

	E_0	second-order		first-order	
		E_1	ε	E_1	ε
$m = 1$	$-0.318\,310$	$-0.318\,313$	9.02×10^{-6}	$-0.318\,308$	5.94×10^{-6}
$m = 2$	$-0.636\,620$	$-0.636\,708$	1.39×10^{-4}	$-0.636\,626$	1.05×10^{-5}

Table 4.3: Comparison of the analytical and numerical results for the VPE of the kink for two different masses m. The analytical and numerical results are given by E_0 and E_1, respectively. The relative error is given by $\varepsilon = |E_0 - E_1|/|E_0|$.

Chapter 5

Kink-Antikink Interaction

In the two previous chapters we showed that both the ϕ^4 model and the sine-Gordon model admit static soliton solutions. For each model these solutions have the interpretation of a particle (kink) and an antiparticle (antikink) pair. In this chapter we consider a background configuration, for both of these models, that consists of a kink and an antikink separated by a distance $2R$. We compute the $\mathcal{O}(\hbar)$ quantum contribution to the classical energy of this kink-antikink pair, at a fixed half-separation R. This calculation is performed for a range of values of R and we thereby construct the VPE as a function of R. The VPE then has the physical interpretation of a quantum correction to the potential for particle-antiparticle interaction. Since we are interested in calculating the VPE at some fixed separation, we require that the quantum fluctuations do not include modes that parameterize changing R.

We begin this chapter by investigating the kink-antikink configuration for the ϕ^4 model in Section 5.1, while in Section 5.2 we discuss the case for the sine-Gordon model.

5.1 The ϕ^4 Model

The kink-antikink configuration for the ϕ^4 model is constructed from Eqs. (3.2.8) and (3.2.9) as

$$\phi_R(x) = \frac{m}{\sqrt{2\lambda}}\Big[\tanh\Big(\frac{m}{2}(x-R)\Big) - \tanh\Big(\frac{m}{2}(x+R)\Big) + 1\Big], \tag{5.1.1}$$

which consists of a kink located at $x = R$ and an antikink at $x = -R$. This configuration is shown in Fig. 5.1. Clearly as $R \to 0$ we obtain the constant vacuum solution $\phi_{\text{vac}} = m/\sqrt{2\lambda}$, while as $R \to \infty$ the configuration becomes a widely separated kink-antikink pair. In both of these limits, the kink-antikink configuration is a solution to the equation of motion of the system. However, for intermediate values of R this is not the case.

To calculate the VPE, we once again begin by defining the fluctuations η around this configuration, such that $\phi(x,t) = \phi_R(x) + \eta(x,t)$. Since the background configuration is not a solution to the relevant equation of motion for all values of R, the Lagrangian will contain terms linear in the fluctuations. These can formally be removed by introducing an additional source term, as mentioned in Section 2.3, which

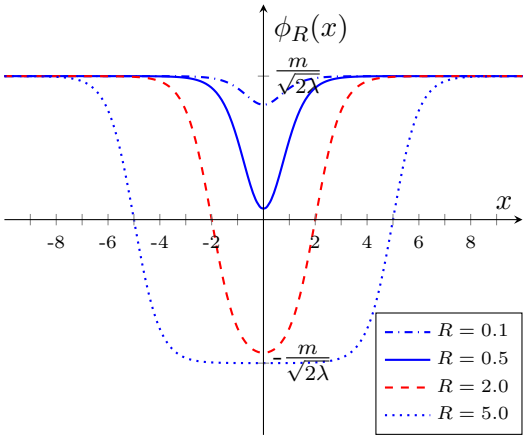

Figure 5.1: The kink-antikink configuration for various values of the half-separation distance R.

vanishes in the limits $R \to 0$ and $R \to \infty$. The above configuration is therefore a stationary point of the classical action and the results of Chapter 2 apply. The fluctuations obey the wave equation (2.3.12),

$$\left[-\frac{\mathrm{d}^2}{\mathrm{d}x^2} + m^2 + \sigma_R(x)\right]\eta_\omega = \omega^2\eta_\omega, \tag{5.1.2}$$

where $\omega^2 = k^2 + m^2$ and we have made the stationary ansatz, $\eta(x,t) = e^{-i\omega t}\eta_\omega(x)$. The fluctuations are quantized as before (see Section 2.3) and are of $\mathcal{O}(\hbar^{1/2})$. Their vacuum energy contribution (which is $\mathcal{O}(\eta^2)$) is therefore the $\mathcal{O}(\hbar)$ quantum correction to the classical energy. The potential for the quantum fluctuations is produced by the background configuration and is given by

$$\sigma_R(x) = \frac{3m^2}{2}\left[\left(\frac{\sqrt{2\lambda}}{m}\phi_R(x)\right)^2 - 1\right], \tag{5.1.3}$$

which is illustrated in Fig. 5.2. We observe that for large R the potential separates into two single (anti)kink potentials located at $x = \pm R$. For $R \to 0$ the potential vanishes, since the background configuration becomes the (positive) constant vacuum solution. We therefore expect the VPE to vanish as $R \to 0$, and to tend to twice the single (anti)kink result for $R \to \infty$.

We calculate the classical energy by using Eqs. (1.3.4) and (1.3.5) with the background (5.1.1) and integrating over the spatial coordinate. By subtracting twice the classical kink mass from this result, we obtain the classical potential

$$V_{\mathrm{cl}}(R) = \frac{2m^3}{\lambda}\left[mR + \frac{3}{\tanh(mR)} - \frac{2+3mR}{\tanh^2(mR)} + \frac{2mR}{\tanh^3(mR)} - 1\right]. \tag{5.1.4}$$

The above result is derived in Appendix C.1. This is interpreted as an (attractive) effective potential between the kink and antikink [47].

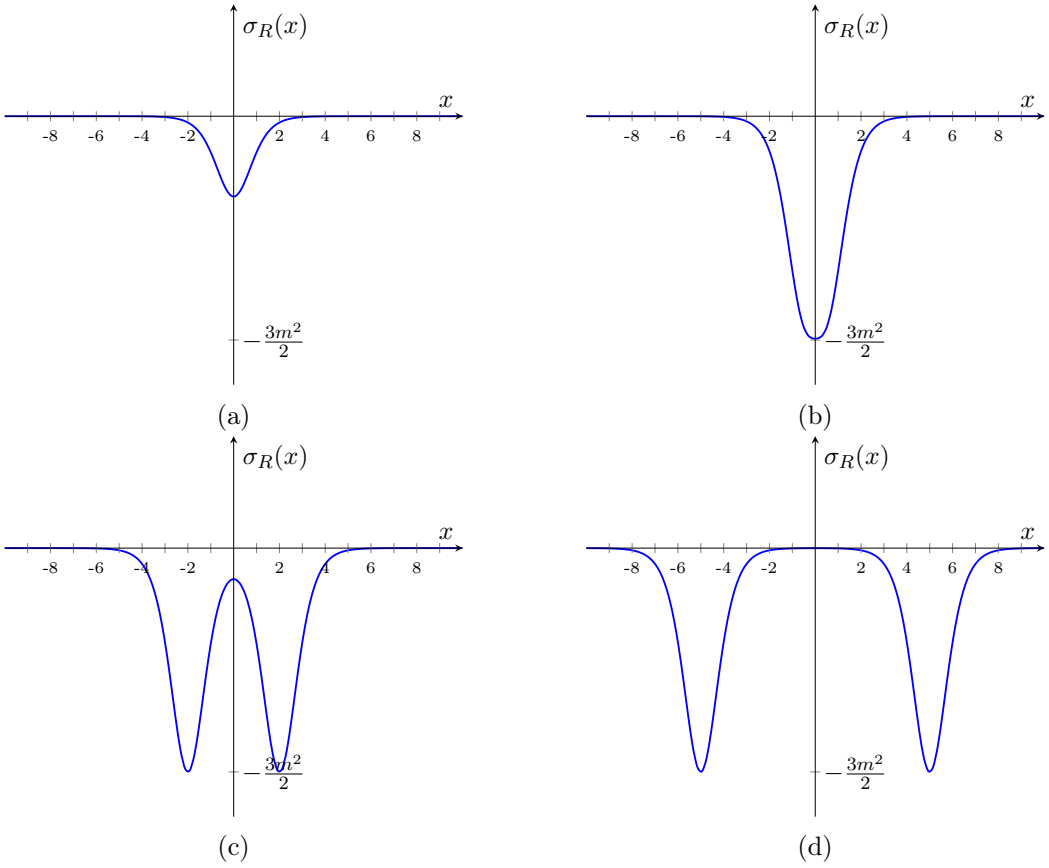

Figure 5.2: Potential for the fluctuations, which is induced by the kink-antikink background, for different values of R, (a) $R = 0.1$ (b) $R = 0.5$ (c) $R = 2.0$ (d) $R = 5.0$.

5.1.1 Introduction of the Constraint

Our goal is to calculate the VPE contribution to the classical potential, which requires solving Eq. (5.1.2). However, this does not lead to a well-defined quantum theory for the fluctuations. To see this, note that for large R (i.e. $R \to \infty$) the background configuration becomes a widely separated kink and antikink, as mentioned before. From Chapter 3 we know that each possesses a translational zero mode, $\omega_0^2 = 0$, and a breather mode, $\omega_1^2 = 3m^2/4$. As we reduce R, the two zero mode solutions split, producing an antisymmetric state with slightly higher energy and a symmetric state with slightly lower energy (i.e. $\omega^2 < 0$). Therefore we have an unstable bound state with an imaginary energy eigenvalue. In this case the field configuration becomes unstable with respect to fluctuations in some direction in field space. Since this unstable mode arises from the symmetric combination of the kink and antikink's individual translational modes, it corresponds to translations which move the kink-antikink pair closer together or further apart. Therefore we note that this mode is equivalent to changing R and should not be included as a small-amplitude fluctuation. This (unstable) mode must be eliminated in order to obtain a well-defined quantum theory for the fluctuations. We do so by recalling that the

half-separation distance R must be fixed and hence no fluctuations in this direction should be allowed. This induces the constraint

$$\int_{-\infty}^{\infty} \mathrm{d}x\, z(x)\eta_\omega(x) = 0, \tag{5.1.5}$$

with

$$z(x) = N\frac{\mathrm{d}}{\mathrm{d}R}\phi_R(x) = N\Big[\tanh^2\Big(\frac{m}{2}(x-R)\Big) + \tanh^2\Big(\frac{m}{2}(x+R)\Big) - 2\Big], \tag{5.1.6}$$

where N is a normalization constant. This constraint only affects the symmetric channel. It is automatically satisfied for large R, where $z(x)$ parameterizes the symmetric combination of two independent translational modes that are, by construction, orthogonal to the remaining fluctuations. This can be observed in Fig. 5.3.

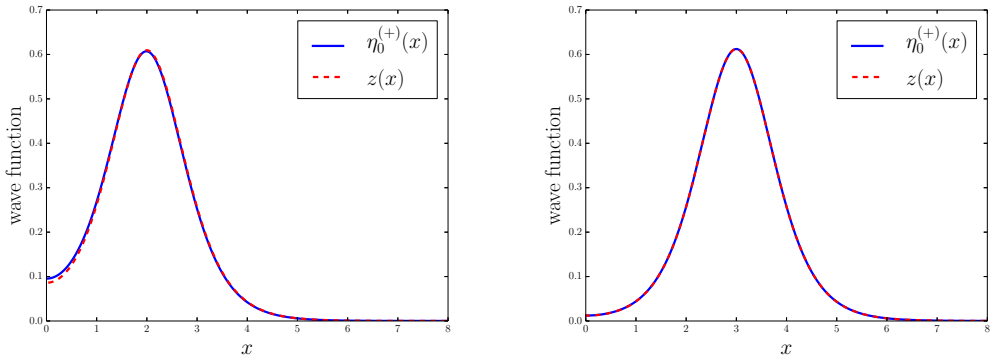

(a) (b)

Figure 5.3: Comparison of the most strongly bound wave function in the symmetric channel of the unconstrained system, $\eta_0^{(+)}(x)$, and the constraint function, $z(x)$, for two values of R, (a) $R = 2$ (b) $R = 3$. Note that the two curves lie on top of each other which is why only one curve is visible.

When applying the constraint, the most strongly bound state in the symmetric channel is turned into a zero mode. So if we apply the constraint in a case where there is no imaginary energy eigenstate, the lowest energy bound state in the symmetric channel will incorrectly appear as a zero mode in the bound state spectrum. The question is then whether the constraint is necessary for all values of R. In the limit $R \to 0$, the background reduces to the constant vacuum solution, $\phi_{\mathrm{vac}} = m/\sqrt{2\lambda}$, and the potential for the fluctuations vanishes. We thus have a free theory which only has a half-bound state in the symmetric channel. For small R, the background is a slight deviation from the constant vacuum solution and the potential is then too weak to bind a state with an imaginary eigenvalue.

From this argument we therefore conclude that there should be a finite, nonzero value R_c where the imaginary eigenvalue first appears. We show numerically that this is the case in Table 5.1; for $m = 2$ we obtain $R_c \simeq 0.367$. This is in agreement with the result $R_c \simeq 0.75/m = 0.375$ which was found by Ref. [48]. We also see that the constraint affects the breather bound state energy (squared) by only about 3%

or less. For large R, the imaginary mode approaches the zero mode, as expected. The bound states in the antisymmetric channel will be discussed later.

		without constraint	with constraint
$R = 0.100$	ω_0^2	2.862	0.000
	ω_1^2	—	—
$R = 0.250$	ω_0^2	1.019	0.000
	ω_1^2	—	—
$R = 0.366$	ω_0^2	0.004	0.000
	ω_1^2	3.933	3.932
$R = 0.367$	ω_0^2	−0.003	0.000
	ω_1^2	3.932	3.931
$R = 0.380$	ω_0^2	−0.092	0.000
	ω_1^2	3.911	3.909
$R = 1.0$	ω_0^2	−0.753	0.000
	ω_1^2	2.616	2.534
$R = 2.0$	ω_0^2	−0.024	0.000
	ω_1^2	2.774	2.773

Table 5.1: Numerical calculation of the bound states in the symmetric channel, without and with the constraint, for $m = 2$.

Lastly, recall that we subtracted the Born approximation from the phase shift in order to render the integral which appears in the VPE finite. The subtracted Born approximation was then added back in as a Feynman diagram that we renormalized in the usual way by adding counterterms to the Lagrangian. If the constraint alters the Born approximation, we do not know with which Feynman diagram to associate it. However, as long as the large k behavior of the exact phase shift remains unaffected by the constraint, we can simply use the unconstrained Born approximation in our renormalization procedure. Thus we need to determine whether the constraint will alter the large k behavior of the phase shift. We therefore investigate the large k behavior of the constraint, where the wave function is well represented by the free case, $\eta_k(x) = \cos(kx)$. In this regime the constraint becomes

$$\int_{-\infty}^{\infty} \mathrm{d}x\, z(x)\eta_k(x) \sim 2\int_0^{\infty} \mathrm{d}x \cos(kx)\big[\tanh^2(x-R) + \tanh^2(x+R) - 2\big], \quad (5.1.7)$$

where we have used $\lambda = m = 2$. This is illustrated in Fig. 5.4. We observe that the constraint approaches zero faster than $1/k$, so it will not modify the large k behavior of the phase shift.

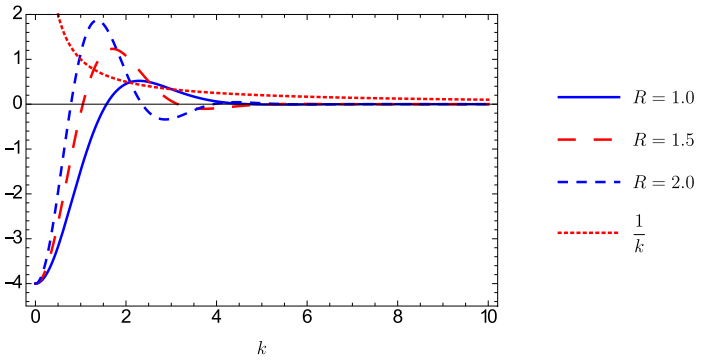

Figure 5.4: Behavior of the constraint (5.1.7) for various values of R.

5.1.2 Numerical Results

Due to the above arguments, we calculate the VPE using the first-order implementation of the VPA from Section 2.5, with the constraint only applied for $R \geq R_c$. In order to produce the numerical results, we redefine the field and the coordinates such that $m = 2$ and $\lambda = 2$. One might be concerned that the introduction of the constraint at R_c could significantly alter the phase shift between $R = R_c - \varepsilon$ and $R = R_c$, where $\varepsilon > 0$ is small. In Fig. 5.5 we compare the phase shifts for two values of R; one ($R = 0.367$) with the constraint active and one ($R = 0.366$) without the constraint. We see no significant alteration.

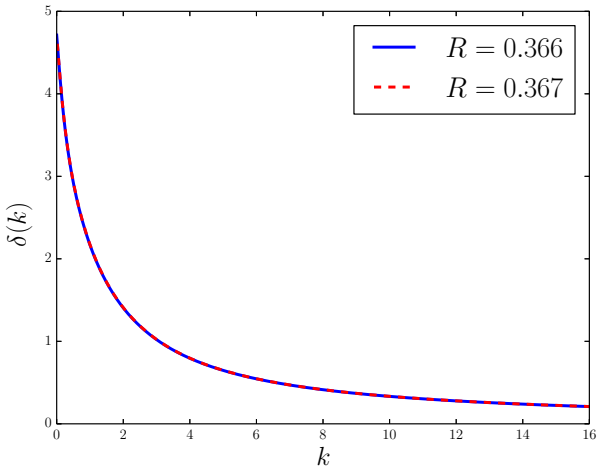

Figure 5.5: Phase shift in the symmetric channel for R near $R_c = 0.367$.

Firstly, we investigate whether Levinson's theorem holds for the kink-antikink system. In Table 5.2 we list the number of bound states along with the value of the phase shift at $k = 0$, in each channel. From this, we see that Levinson's theorem holds even when the constraint is applied. We note that for the last entry, $R = 5$,

$\delta_+(0)$ goes to 2π due to a half-bound state arising in the symmetric channel, similar to the single kink case.

	n_-	n_+	$\delta_-(0)$	$\delta_+(0)$
$R = 0.01$	0	1	0.000	1.571
$R = 0.25$	1	1	3.142	1.571
$R = 0.50$	1	2	3.144	4.695
$R = 1.00$	2	2	6.274	4.710
$R = 5.00$	2	2	6.283	6.270

Table 5.2: The number of bound states and the value of the phase shift at $k = 0$ in each channel.

We list the bound state energies for various values of R in Table 5.3. As $R \to \infty$ the lowest bound state in the antisymmetric channel also turns into a zero mode. In the same limit, the second bound state approaches the breather energy, $\omega = \sqrt{3}$, in both channels. This is expected, since the background turns into a widely separated kink and antikink as $R \to \infty$, as we discussed above.

Finally we compute the VPE as a function of the half-separation distance R. We then subtract twice the single kink result in order to obtain the $\mathcal{O}(\hbar)$ correction to the classical potential as

$$V_{\text{vac}}(R) = E_{\text{vac}}(R) - 2E_{\text{vac}}^{(\text{kink})}. \tag{5.1.8}$$

We compare the classical potential to the quantum correction in Fig. 5.6. Also shown is the total potential, $V_{\text{cl}}(R) + V_{\text{vac}}(R)$. We note that the VPE has the behavior $E_{\text{vac}}(R) \to 0$ as $R \to 0$, and $E_{\text{vac}}(R) \to 2E_{\text{vac}}^{(\text{kink})}$ as $R \to \infty$. This is as we expected from the behavior of the background in these limits. The classical potential is attractive, as we mentioned before. On the contrary, the quantum correction is repulsive, but in magnitude it is not large enough to turn the total potential repulsive. This is consistent with the VPE being a correction. However, the total potential does produce a small barrier at intermediate distances. A secondary barrier also appears at $R \approx R_c$ which is due to the inclusion of the nonzero energy eigenvalue. Since this barrier is caused by disabling the constraint for $R < R_c$, we consider keeping

	$R = 0.25$	$R = 0.5$	$R = 0.75$	$R = 1.0$	$R = 3.0$	$R = 4.0$
$\omega_0^{(+)}$	1.010	0.000	0.000	0.000	0.000	0.000
$\omega_1^{(+)}$	—	1.905	1.719	1.592	1.723	1.731
$\omega_0^{(-)}$	1.815	1.350	0.927	0.606	0.012	0.002
$\omega_1^{(-)}$	—	—	1.999	1.955	1.740	1.733

Table 5.3: Symmetric ($\omega_j^{(+)}$) and antisymmetric ($\omega_j^{(-)}$) bound states for various values of the half-separation distance R. Note that we list the bound states energies, and not the energies squared.

the constraint active in this region. This is illustrated in Fig. 5.7, from which we observe that with the constraint enabled we have $V_{\text{vac}}(0) \neq -2E_{\text{vac}}^{(\text{kink})}$. For $R = 0$ the background is the trivial configuration which has zero VPE and so we must have $V_{\text{vac}}(0) = -2E_{\text{vac}}^{(\text{kink})}$. We also observe that if we choose to enable the constraint from another value of R instead of R_c (eg. $R > 0.9R_c$), we will obtain a large jump in the VPE.

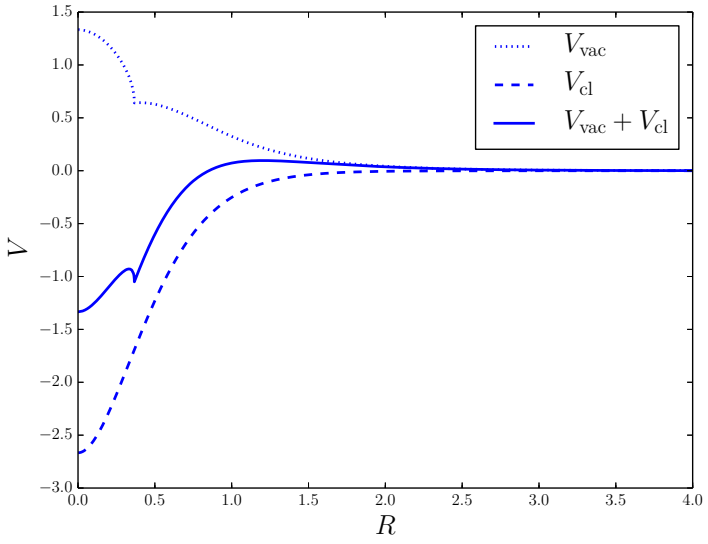

Figure 5.6: Quantum correction to the kink-antikink potential as a function of the half-separation R, defined in Eq. (5.1.8). Also shown is the classical potential from Eq. (5.1.4).

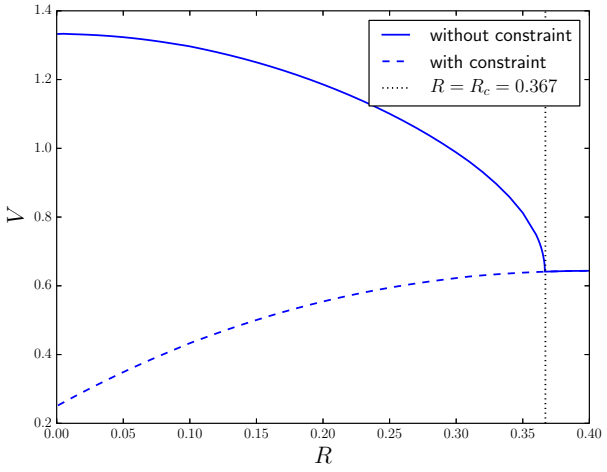

Figure 5.7: $V_{\text{vac}}(R)$ with and without the constraint in the region $R < R_c$. Note that the two graphs agree at $R = R_c$.

The two resulting barriers indicate that the quantum correction does indeed have the potential to stabilize a classically unstable configuration. Our VPE result resembles that of Ref. [48] when we discard the constraint and simply omit the imaginary part from $\omega_0^2 < 0$. The jump in V_{vac} at $R \approx R_c$ is also seen in Ref. [48].

5.2 The Sine-Gordon Model

We now turn our attention to the sine-Gordon model, which was discussed in Chapter 4. Using Eqs. (4.2.11) and (4.2.12), we construct the kink-antikink configuration as a kink located at $x = R$ and an antikink at $x = -R$,

$$\phi_R(x) = \frac{4m}{\sqrt{\lambda}}\left[\arctan\left(e^{-m(x-R)}\right) + \arctan\left(e^{m(x+R)}\right) - \frac{\pi}{2}\right]. \tag{5.2.1}$$

This configuration is illustrated in Fig. 5.8. In the limit $R \to \infty$ the configuration is a widely separated kink and antikink pair, while for $R \to 0$ the trivial vacuum solution is approached. The kink-antikink configuration is only a solution to the system's equation of motion in these two limits.

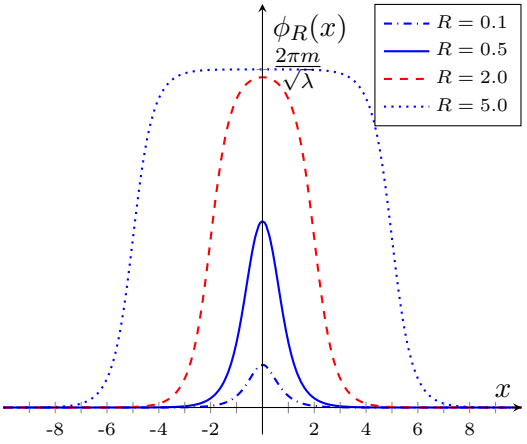

Figure 5.8: The kink-antikink configuration for various values of the half-separation distance R.

As before, we define the fluctuations η around this background configuration, $\phi(x,t) = \phi_R(x) + \eta(x,t)$. The background configuration is not a solution to the field equation for all values of R, so the Lagrangian will contain terms linear in the fluctuations, which (again formally) are removed by introducing an additional source term. The above configuration is then a stationary point of the classical action and so we can use the methods of Chapter 2. The fluctuations obey the stationary wave equation (2.3.12),

$$\left[-\frac{\mathrm{d}^2}{\mathrm{d}x^2} + m^2 + \sigma_R(x)\right]\eta_\omega = \omega^2\eta_\omega, \tag{5.2.2}$$

where $\omega^2 = k^2 + m^2$ and we have made the stationary ansatz, $\eta(x,t) = e^{-i\omega t}\eta_\omega(x)$. Once again, we quantize the fluctuations as in Section 2.3, and so their vacuum

energy contribution is the leading quantum correction to the classical energy. The background configuration produces the potential for the quantum fluctuations as

$$\sigma_R(x) = m^2\left[\cos\left(\frac{\sqrt{\lambda}}{m}\phi_R(x)\right) - 1\right], \tag{5.2.3}$$

which is shown in Fig. 5.9. From this we observe that the potential separates into two single (anti)kink potentials for large R located at $x = \pm R$. In the limit $R \to 0$, the background configuration becomes the trivial vacuum solution and so the potential vanishes. Thus we expect the VPE to approach twice the single (anti)kink VPE as $R \to \infty$, and to tend to zero as $R \to 0$.

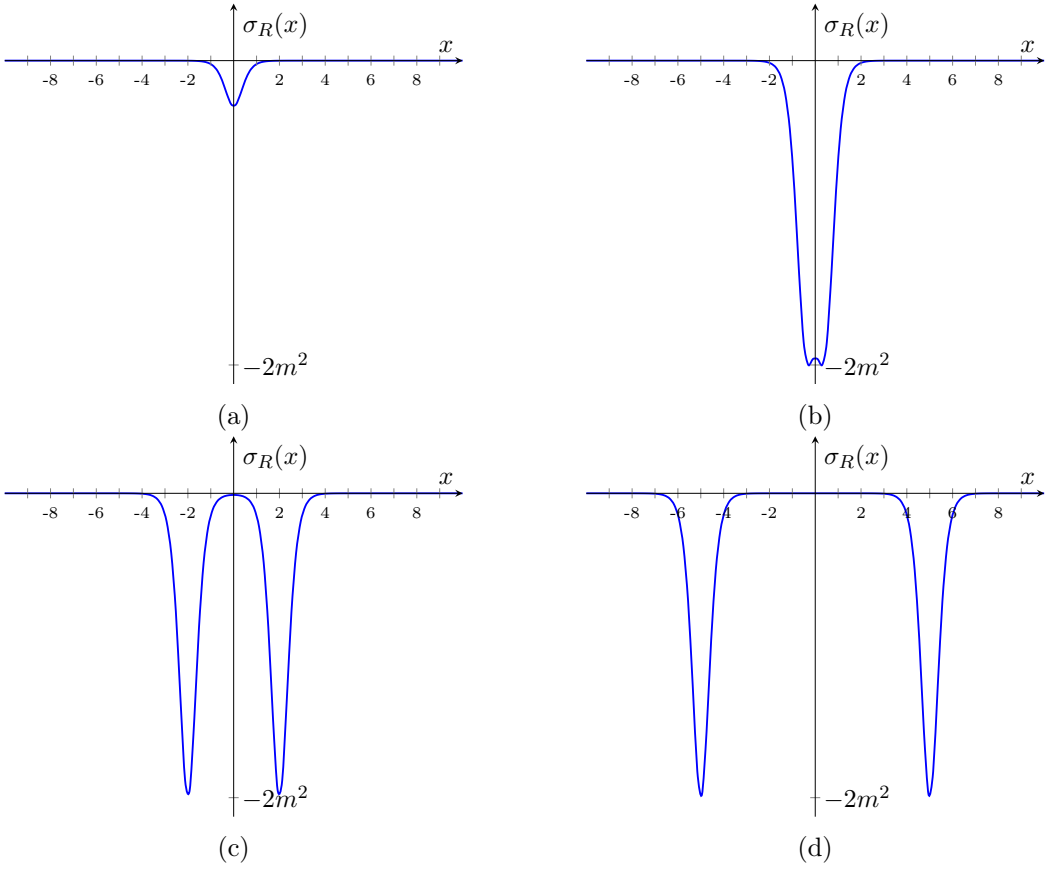

Figure 5.9: Plot of the potential for the fluctuations, which is induced by the kink-antikink configuration, for different values of R, (a) $R = 0.1$ (b) $R = 0.5$ (c) $R = 2.0$ (d) $R = 5.0$.

Using Eqs. (1.3.4) and (1.3.5) with the background configuration (5.2.1), we compute the classical energy. This once again has the interpretation of an effective potential between the kink and antikink. We obtain the classical potential by

subtracting twice the classical kink mass from this result to find

$$V_{\text{cl}}(R) = -\frac{8m^3}{\lambda}\left[\frac{1}{\cosh^2(mR)} + \frac{mR}{\sinh(mR)\cosh^3(mR)}\right]. \tag{5.2.4}$$

The derivation of the above formula is presented in Appendix C.2.

5.2.1 Introduction of the Constraint

As before, we compute the VPE contribution to the classical potential. Recall from Chapter 4, that the (anti)kink has a translational zero mode bound state. As a result, imaginary energy eigenvalues may emerge for fluctuations that are equivalent to changing R. Therefore, using the same arguments as the previous section, we require the constraint

$$\int_{-\infty}^{\infty} \mathrm{d}x\, z(x)\eta_\omega(x) = 0, \tag{5.2.5}$$

with

$$z(x) = N\frac{\mathrm{d}}{\mathrm{d}R}\phi_R(x) = N[\mathrm{sech}(m(x-R)) + \mathrm{sech}(m(x+R))], \tag{5.2.6}$$

where N is a normalization constant. The constraint only affects the symmetric channel and is automatically satisfied in the large R regime for fluctuations η_ω with $\omega \neq 0$. This is indicated in Fig. 5.10: As R increases, $\eta_0(x)$ and $z(x)$ coincide. For $\omega \neq 0$, $\eta_0(x)$ and $\eta_\omega(x)$ are orthogonal.

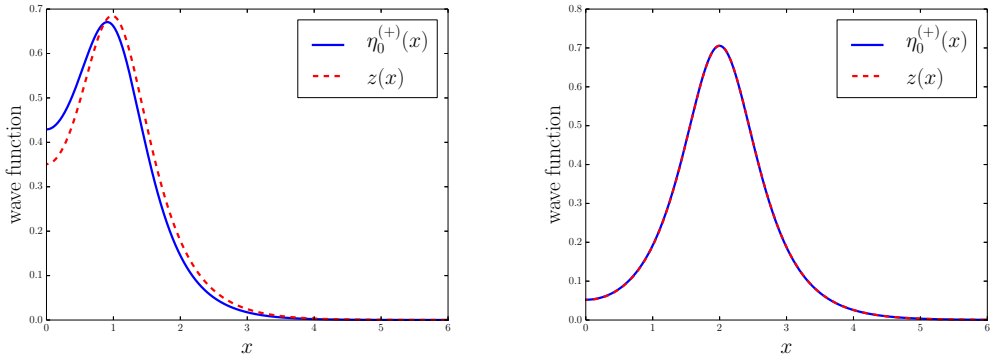

(a) (b)

Figure 5.10: Comparison of the most strongly bound wave function in the symmetric channel of the unconstrained system ($\eta_0^{(+)}(x)$) and the constraint function ($z(x)$), for two values of R, (a) $R = 1$ (b) $R = 2$. Note that the two curves lie on top of each other in (b), which is why only one curve is visible.

The critical value R_c, from which point onwards the constraint is necessary, is found to be $R_c \simeq 0.316$ for $m = 2$. This is shown in Table 5.4; we also see that the constraint affects the second bound state energy (squared), which only appears at intermediate values of R, by less than 1%. The imaginary mode approaches the zero mode in the large R limit.

		without constraint	with constraint
$R = 0.075$	ω_0^2	3.918	0.000
	ω_1^2	—	—
$R = 0.250$	ω_0^2	1.312	0.000
	ω_1^2	—	—
$R = 0.315$	ω_0^2	0.009	0.000
	ω_1^2	—	—
$R = 0.316$	ω_0^2	−0.010	0.000
	ω_1^2	—	—
$R = 0.500$	ω_0^2	−2.004	0.000
	ω_1^2	—	—
$R = 1.0$	ω_0^2	−0.575	0.000
	ω_1^2	3.922	3.889
$R = 2.0$	ω_0^2	−0.009	0.000
	ω_1^2	—	—

Table 5.4: Numerical calculation of the bound states in the symmetric channel, without and with the constraint, for $m = 2$.

Finally, we must determine whether the constraint affects the large k behavior of the phase shift. Consider the large k regime, where the wave function is well approximated by the free wave function, $\eta_k(x) = \cos(kx)$. The constraint then becomes

$$\int_{-\infty}^{\infty} \mathrm{d}x\, z(x)\eta_k(x) \sim 2\int_0^{\infty} \mathrm{d}x \cos(kx)[\mathrm{sech}(2(x-R)) + \mathrm{sech}(2(x+R))], \quad (5.2.7)$$

where we used $\lambda = 4$ and $m = 2$. This is illustrated in Fig. 5.11. We observe that the constraint vanishes faster than $1/k$, and so it will not affect the large k behavior of the phase shift.

5.2.2 Numerical Results

We compute the VPE using the constraint implementation of the VPA from Section 2.5, with the constraint only applied for $R \geq R_c$. We redefine the field and the coordinates such that $m = 2$ and $\lambda = 4$, in order to obtain the numerical results. In Fig. 5.12 we show that the introduction of the constraint at R_c does not significantly alter the phase shift between $R = R_c - \varepsilon$ and $R = R_c$, where $\varepsilon > 0$ is small.

We list the number of bound states along with the value of the phase shift at $k = 0$, for each channel, in Table 5.5. We observe that Levinson's theorem holds when the constraint is applied. Note that for the last entry ($R = 5$), we have $\delta_+(0) \to \pi$ due to a half-bound state arising in the symmetric channel. This differs from the single kink case where the half-bound state appeared in the antisymmetric channel. Recall that the sine-Gordon potential for the single kink is reflectionless, so

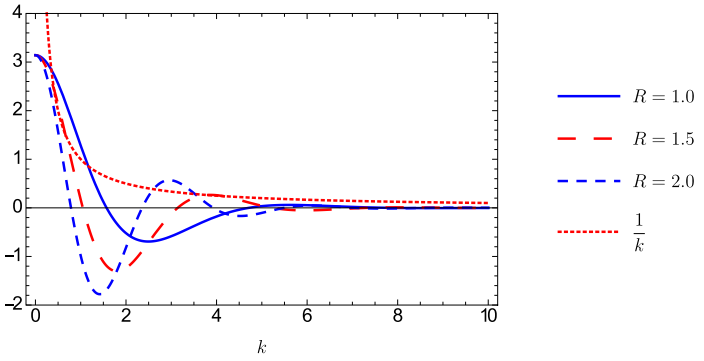

Figure 5.11: Behavior of the constraint (5.2.7) for various values of R.

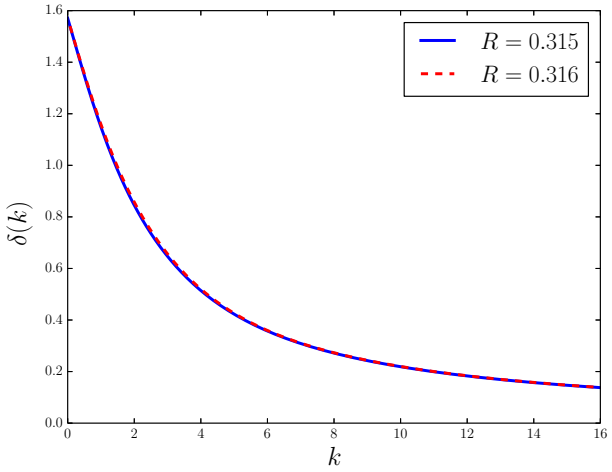

Figure 5.12: Phase shift in the symmetric channel for R near $R_c = 0.316$.

the phase shifts double as $R \to \infty$ in the kink-antikink system. Therefore we should have $\delta_-(0) \to \pi$ and $\delta_+(0) \to \pi$ as $R \to \infty$, and hence the half-bound state comes from the symmetric channel. This is what we obtain numerically.

	n_-	n_+	$\delta_-(0)$	$\delta_+(0)$
$R = 0.25$	0	1	0.000	1.571
$R = 0.50$	1	1	3.138	1.580
$R = 1.00$	1	2	3.141	4.708
$R = 5.00$	1	1	3.142	3.151

Table 5.5: The number of bound states and the value of the phase shift at $k = 0$ in each channel for various values of R.

In Table 5.6 we list the bound state energies for different values of R. For large R, the lowest bound state in the antisymmetric channel also becomes a zero mode.

	$R = 0.25$	$R = 0.5$	$R = 0.75$	$R = 1.0$	$R = 3.0$	$R = 4.0$
$\omega_0^{(+)}$	1.145	0.000	0.000	0.000	0.000	0.000
$\omega_1^{(+)}$	—	—	1.971	1.972	—	—
$\omega_0^{(-)}$	—	1.478	0.796	0.410	0.006	0.001

Table 5.6: Symmetric ($\omega_j^{(+)}$) and antisymmetric ($\omega_j^{(-)}$) bound states for different values of R. Note that we list the bound states energies, and not the energies squared.

This is as we expected, due to the background becoming a widely separated kink and antikink.

The VPE is calculated as a function of the half-separation distance R. This is shown in Fig. 5.13, from which we observe that the VPE is repulsive, except at around $R \approx R_c$, where it briefly turns attractive. Again this originates from the lowest bound state energy being nonzero for $R < R_c$. The VPE has the expected behavior $E_{\text{vac}}(R) \to 0$ as $R \to 0$, and $E_{\text{vac}}(R) \to 2E_{\text{vac}}^{(\text{kink})}$ as $R \to \infty$. We obtain the quantum correction to the classical potential from this result by subtracting twice the single kink VPE,

$$V_{\text{vac}}(R) = E_{\text{vac}}(R) - 2E_{\text{vac}}^{(\text{kink})}. \tag{5.2.8}$$

In Fig. 5.14 we compare the classical potential to the quantum correction. Also shown is the total potential, $V_{\text{cl}}(R) + V_{\text{vac}}(R)$. We observe that the classical potential is attractive and significantly larger (in absolute value) than the VPE. This is consistent with the VPE being a mere correction. Unlike the result for the ϕ^4 model, the VPE is not strong enough to produce any barriers in the total potential and therefore cannot stabilize the classically unstable configuration.

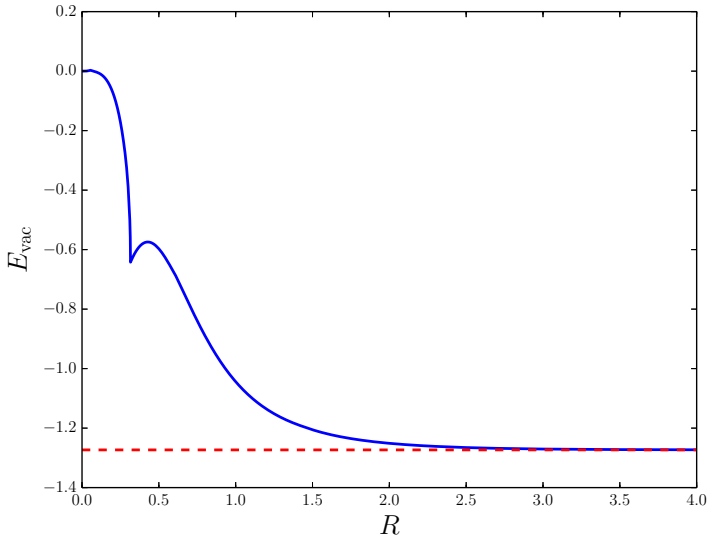

Figure 5.13: VPE as a function of the half-separation R. Also shown is twice the single kink VPE (dashed line).

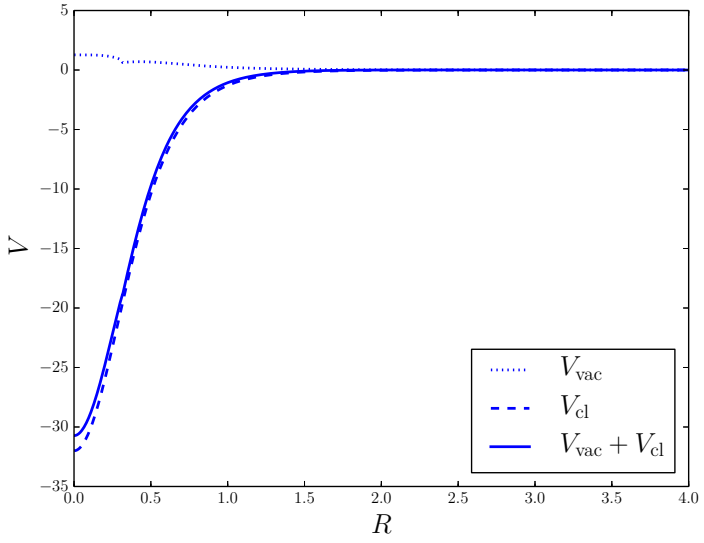

Figure 5.14: Quantum correction to the kink-antikink potential as a function of R, defined in Eq. (5.2.8). Also shown is the classical potential from Eq. (5.2.4).

Chapter 6

Conclusion and Outlook

We briefly summarize what has been achieved over the course of this thesis and comment on possible future work.

We began by utilizing the spectral method to obtain an expression for the vacuum polarization energy (VPE) in terms of scattering data. We discussed the necessary renormalization procedure to be followed in order to obtain sensible, finite results for our calculation. To calculate the necessary phase shifts in an efficient manner we employed generalizations of the variable phase approach (VPA). This lead to two numerical treatments to compute scattering data for potential scattering. We tested both of these treatments by calculating the VPE of the kink solution in the ϕ^4 model. This calculation was also performed for the kink of the sine-Gordon model. In both cases our numerical results reproduced the known results from literature. The main motivation to develop a second treatment was a simpler incorporation of a constraint on the scattering wave function.

We constructed the kink-antikink configuration for the ϕ^4 model from a kink and an antikink separated by some distance $2R$. We found that an unstable mode appeared in the bound state spectrum of the symmetric channel when $R \geq R_c$. This unstable mode arose due to fluctuations that model changing the separation R. These fluctuations should be avoided since the VPE must be calculated for a fixed value of R. We therefore implemented a constraint on the fluctuations for which we developed the second treatment. The constraint turned this unstable mode into a zero mode. We found that Levinson's theorem holds when including this zero mode in the bound state spectrum. We then performed the calculation of the VPE as a function of the half-separation R. This was compared to the classical kink-antikink potential. We observed that the quantum correction, which is repulsive, mitigated the strong attraction of the classical potential. Our findings on the magnitude of the VPE are consistent with the VPE being a correction to the classical energy. Interestingly enough, though, the quantum correction produced two barriers, one at intermediate separation and another at around R_c, in the total potential. This suggests that these corrections stabilize a classically unstable configuration, though the repulsion around R_c may be caused by omitting the constraint for $R < R_c$. We showed that enabling the constraint in this region leads to an incorrect result for the VPE at $R = 0$, while turning the constraint on from another value of R instead of R_c causes a large jump in the VPE.

The kink-antikink configuration of the sine-Gordon model was also investigated. As before, we found an unstable mode in the symmetric channel for $R \geq R_c$ that became a zero mode once the constraint was applied. Including this zero mode in the bound state spectrum showed that Levinson's theorem is valid. The VPE was calculated as a function of the half-separation distance R. We observed that the quantum correction is repulsive, except at around $R \approx R_c$ where it briefly turns attractive. However, comparing this to the classical kink-antikink potential, we found that the quantum correction could not overcome the strong attraction of the classical potential. Therefore the classically unstable configuration is not stabilized by the quantum correction. This result is consistent with the VPE being just a correction to the classical energy.

We have computed the one-loop quantum correction to the kink-antikink potential in both the ϕ^4 and sine-Gordon models. These are prototype calculations of quantum corrections for configurations with different particle numbers. This will eventually illuminate the predictions for classically stable configurations of even large particle numbers such as nuclei [49], for example.

This most obvious avenue for further research would involve considering soliton-antisoliton configurations of other models, such as the kink-antikink or antikink-kink configurations of the ϕ^6 model.

Appendices

Appendix A

Review of Three-Dimensional Scattering Theory

In the main text we discussed potential scattering theory in (1+1) dimensions. Here we link it to the standard formulation in three spatial dimensions.

We will only be considering spherically symmetric potentials, $V(\mathbf{r}) = V(r)$, which satisfy

$$\int_a^\infty \mathrm{d}r\, r|V(r)| < \infty, \quad a \geq 0, \tag{A.1}$$

and are called regular potentials.

Suppose that we have a spinless particle which scatters off a regular potential. We begin by applying the usual separation of variables to the time-independent Schrödinger equation to factorize the wave function as

$$\psi_{E\ell m}(r,\theta,\phi) = R_{E\ell}(r)Y_\ell^m(\theta,\phi), \tag{A.2}$$

where $R_{E\ell}(r)$ is the radial component and $Y_\ell^m(\theta,\phi)$ are the spherical harmonic functions.[1] The partial wave of angular momentum ℓ, $\psi_\ell(k,r) = rR_{E\ell}(r)$, satisfies the reduced radial Schrödinger equation[2]

$$-\frac{\mathrm{d}^2\psi_\ell}{\mathrm{d}r^2} + \left[V(r) + \frac{\ell(\ell+1)}{r^2}\right]\psi_\ell - k^2\psi_\ell = 0. \tag{A.3}$$

In potential scattering theory, the standard method is to find asymptotic solutions to the equation in question. With this in mind, we note that Eq. (A.3) has the free outgoing spherical wave solution

$$w_\ell(kr) = ie^{i\pi\ell}\sqrt{\frac{\pi kr}{2}}H^{(1)}_{\ell+\frac{1}{2}}(kr), \tag{A.4}$$

where $H_\alpha^{(1)}$ is the Hankel function of the first kind [50]. This solution has the behavior

$$w_\ell(kr) \underset{r\to 0}{\simeq} (-1)^\ell(2\ell-1)!!(kr)^{-\ell}, \tag{A.5}$$

[1] In this section we use m to refer to the magnetic quantum number, while μ is reserved for the mass of a particle.

[2] In reduced units we have $\hbar = 2\mu = 1$.

and

$$w_\ell(kr) \underset{r\to\infty}{\simeq} e^{\frac{i\pi\ell}{2}} e^{ikr}. \tag{A.6}$$

There are three important solutions to Eq. (A.3) we need to discuss, each with different boundary conditions. Firstly, we have the regular solution, $\varphi_\ell(k,r)$, which is defined by the boundary condition

$$\lim_{r\to 0} (2\ell+1)!! r^{-(\ell+1)} \varphi_\ell(k,r) = 1. \tag{A.7}$$

Note that this boundary condition is independent of k, and since the Schrödinger equation is even in k, this implies that the regular solution is an even function in k. This solution must exist for regular potentials and it is the only solution which vanishes at the origin [37].

The second solution we are interested in is the physical scattering solution, $\psi_\ell(k,r)$, that is required to have the asymptotic behavior

$$\psi_\ell(k,r) \underset{r\to\infty}{\simeq} e^{i\delta_\ell} \sin\left(kr - \frac{\pi\ell}{2} + \delta_\ell\right), \tag{A.8}$$

where δ_ℓ is the phase shift, which is a real-valued quantity that depends on the energy, and hence depends on k. This solution must also vanish at the origin[3], therefore it must be proportional to the regular solution [37]

$$\psi_\ell(k,r) = A(k)\varphi_\ell(k,r), \tag{A.9}$$

where $A(k)$ is a proportionality factor. This solution differs from the regular solution due to the fact that it has an additional physical boundary condition at $r\to\infty$, while φ_ℓ only has the simple boundary condition (A.7) at $r=0$.

Finally, we have the Jost solution, $f_\ell(k,r)$, with the behavior

$$\lim_{r\to\infty} \left[f_\ell(k,r) - e^{\frac{i\pi\ell}{2}} e^{ikr}\right] = 0, \tag{A.10}$$

and

$$\lim_{r\to\infty} \left[f'_\ell(k,r) - ike^{\frac{i\pi\ell}{2}} e^{ikr}\right] = 0. \tag{A.11}$$

From Eqs. (A.6) and (A.10) we see that the Jost solution reduces to w_ℓ in the free case. There are actually two Jost solutions, $f_\ell(\pm k,r)$, with their Wronskian[4] given by

$$W[f_\ell(k,r), f_\ell(-k,r)] = (-1)^{\ell+1} 2ik, \tag{A.12}$$

which shows that they are linearly independent for $k\neq 0$.[5] This implies that the regular solution can be written in terms of the Jost solutions, because a second-order differential equation only has two linearly independent solutions. We then define the Jost *function* as

$$F_\ell(k) = (-k)^\ell W[f_\ell(k,r), \varphi_\ell(k,r)], \tag{A.13}$$

[3]The solution $\psi_0(k,r)\to 1$ as $r\to 0$ is not allowed, because then we would have $R_{E0}(r)\sim r^{-1}$ as $r\to 0$. This does not satisfy the time-independent Schrödinger equation since $\nabla^2 r^{-1} = -4\pi\delta^3(\boldsymbol{r})$.

[4]The Wronskian of two functions f and g is given by $W(f,g) = fg' - gf'$.

[5]This is the result of a theorem which states that if the Wronskian of two functions f and g is nonzero at some point x_0, then they are linearly independent. The inverse is not necessarily true [51].

and write

$$\varphi_\ell(k,r) = \frac{i}{2}k^{-(\ell+1)}\Big[F_\ell(k)f_\ell(-k,r) - (-1)^\ell F_\ell(-k)f_\ell(k,r)\Big]. \tag{A.14}$$

Recall that the physical scattering solution is proportional to the regular solution, and can thus be written in terms of the Jost solutions as

$$\psi_\ell(k,r) = \frac{k^{\ell+1}}{F_\ell(k)}\varphi_\ell(k,r) = \frac{i}{2}\left[f_\ell(-k,r) - (-1)^\ell\frac{F_\ell(-k)}{F_\ell(k)}f_\ell(k,r)\right], \tag{A.15}$$

where we used the asymptotic behavior of ψ_ℓ and the Jost solutions in order to determine the proportionality factor in Eq. (A.9). This implies that the asymptotic behavior of the two contributions to ψ_ℓ are that of incoming and outgoing spherical waves, respectively. The prefactor of the outgoing waves is the scattering matrix (also called the S-matrix)

$$S_\ell(k) = \frac{F_\ell(-k)}{F_\ell(k)}. \tag{A.16}$$

The Jost function has the property

$$F_\ell(-k) = F_\ell(k)^*, \quad \forall\ k \in \mathbb{R}, \tag{A.17}$$

from which we can deduce that the S-matrix is a pure phase for real k and therefore we may write

$$S_\ell(k) = e^{2i\delta_\ell(k)}. \tag{A.18}$$

This allows us to identify the phase shift $\delta_\ell(k)$ with the negative phase of the Jost function:

$$F_\ell(k) = |F_\ell(k)|e^{-i\delta_\ell(k)}, \quad \forall\ k \in \mathbb{R}. \tag{A.19}$$

The following properties of the Jost function are relevant to the spectral method [37]:

1. The Jost function is holomorphic in the upper complex k-plane ($\operatorname{Im} k \geq 0$).
2. It satisfies the symmetry relation $F_\ell(-k^*) = F_\ell(k)^*$.
3. In the upper complex k-plane ($\operatorname{Im} k \geq 0$) the limit $F_\ell(k) \to 1$ as $|k| \to \infty$ holds.
4. Every zero of the Jost function in the upper complex k-plane ($\operatorname{Im} k \geq 0$) corresponds to a bound state and lies on the imaginary axis, $k_j = i\kappa_j$ with $\kappa_j \in \mathbb{R}$. These zeros are finite in number and simple.

The third property, along with the relation between the phase shift and the Jost function (A.19), implies that

$$\lim_{k\to\infty}\delta_\ell(k) = 0. \tag{A.20}$$

The phase shift also satsifies

$$\delta_\ell(-k) = -\delta_\ell(k) \quad \text{for} \quad k \geq 0,\ k \in \mathbb{R}. \tag{A.21}$$

Appendix B

Proof of Levinson's Theorem for the Antisymmetric Channel

In this appendix we will prove Levinson's theorem for the antisymmetric channel in one spatial dimension. To obtain Levinson's theorem, we must integrate[1]

$$I = \int_0^\infty \frac{\mathrm{d}k}{\pi} \frac{\mathrm{d}\delta(k)}{\mathrm{d}k} = -\frac{1}{2\pi i} \int_0^\infty \mathrm{d}k \, \frac{\mathrm{d}}{\mathrm{d}k} [\ln F(k) - \ln F(-k)], \tag{B.1}$$

where we have used Eq. (2.2.17) to write the phase shift in terms of the Jost function. The above integrand is even in k and thus we may extend the integration range to $-\infty$, which yields

$$I = -\frac{1}{2\pi i} \int_{-\infty}^\infty \mathrm{d}k \, \frac{\dot{F}(k)}{F(k)} = -\frac{1}{2\pi i} \oint_{\mathcal{C}} \mathrm{d}k \, \frac{\dot{F}(k)}{F(k)}, \tag{B.2}$$

where the dot denotes differentiation with respect to k and the contour $\mathcal{C}$ is the real axis plus the semicircle of infinite radius in the upper half plane (see Fig. B.1). The semicircle gives no contribution, because $F(k) \to 1$ as $|k| \to \infty$ (property 3)[2], so $\dot{F}(k)/F(k)$ goes like $|k|^{-2}$ in the upper complex k-plane (property 1). Recall that the zeros of the Jost function lie on the imaginary axis, correspond to the bound states of the system and are finite in number and simple (property 4). In the vicinity of $k \approx i\kappa_j$ we thus have

$$\frac{\dot{F}(k)}{F(k)} \approx \frac{1}{k - i\kappa_j}. \tag{B.3}$$

Since the Jost function has no poles in the upper complex plane (property 1) and no zeros on the contour $\mathcal{C}$ (including at $k = 0$), we can use Cauchy's argument principle to obtain

$$I = -\frac{1}{2\pi i} \oint_{\mathcal{C}} \mathrm{d}k \, \frac{\dot{F}(k)}{F(k)} = -\sum_j^{b.s.} 1 = -n, \tag{B.4}$$

[1] Since we are only working in the antisymmetric channel, we will drop all the channel-specific subscripts to simplify notation.

[2] The properties mentioned in this section refer to the properties of the Jost function found in Section 2.2.

where n is the number of bound states in the antisymmetric channel. Integrating the phase shift in Eq. (B.1) then gives

$$\delta(0) - \delta(\infty) = n\pi, \tag{B.5}$$

which is Levinson's theorem in the antisymmetric channel.

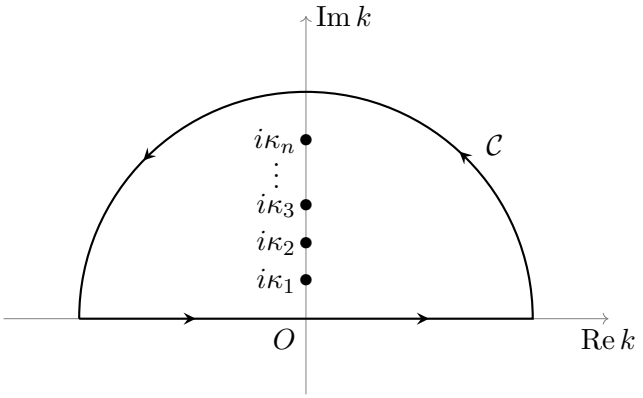

Figure B.1: The integration contour for Levinson's theorem in the antisymmetric channel, where $\kappa_i^2 = m^2 - \omega_i^2$ with ω_i being the bound state energies.

Appendix C

Calculation of the Classical Potentials

Here we outline the calculation of the two classical potentials which appear in Chapter 5. For both the ϕ^4 model and the sine-Gordon model, the classical potential of their respective kink-antikink configurations is given by

$$V_{\mathrm{cl}}(R) = E_{\mathrm{cl}}(R) - 2E_{\mathrm{cl}}^{(\mathrm{kink})}, \tag{C.1}$$

where E_{cl} is the classical energy of the kink-antikink configuration and $E_{\mathrm{cl}}^{(\mathrm{kink})}$ is the classical kink mass. The classical energy is calculated by using Eqs. (1.3.4) and (1.3.5) with the kink-antikink background of the model and integrating over the spatial coordinate,

$$E_{\mathrm{cl}} = \int_{-\infty}^{\infty} \mathrm{d}x \left[\frac{1}{2} \left(\frac{\mathrm{d}}{\mathrm{d}x} \phi_R(x) \right)^2 + V(\phi_R(x)) \right], \tag{C.2}$$

where ϕ_R and V are given by Eqs. (5.1.1) and (3.1.2) for the ϕ^4 model, and Eqs. (5.2.1) and (4.2.5) for the sine-Gordon model, respectively.

We will compute the integrals as limiting cases of Fourier transformations as suggested in Ref. [52]. Our detailed calculation closely follows Ref. [53].

C.1 The ϕ^4 Model

For the kink-antikink configuration of the ϕ^4 model, the classical energy (C.2) is given by

$$E_{\mathrm{cl}}(R) = \frac{m^3}{8\lambda} \int \mathrm{d}x \left\{ \left[\mathrm{sech}^2(x - X) - \mathrm{sech}^2(x + X) \right]^2 + \left[(\tanh(x - X) - \tanh(x + X) - 1)^2 - 1 \right]^2 \right\}, \tag{C.3}$$

where we have rescaled the integration variable and set $X = mR/2$. The terms with a single sign of X are straightforward to calculate. The interesting terms are the

ones which contain both signs of X. As an example we compute

$$I(X) = \int_{-\infty}^{\infty} \mathrm{d}x \left[\tanh^2(x-X)\tanh^2(x+X) - 1\right], \tag{C.4}$$

where the -1 is necessary to render the integral finite. First we define the Fourier integral

$$\begin{aligned} I_k(X) &= \int_{-\infty}^{\infty} \mathrm{d}x\, e^{ikx}\left[\tanh^2(x-X)\tanh^2(x+X) - 1\right] \\ &= \int_{-\infty}^{\infty} \mathrm{d}z\, e^{ikz}\left[\frac{\sinh^2(z-X)\sinh^2(z+X)}{\cosh^2(z-X)\cosh^2(z+X)} - 1\right]. \end{aligned} \tag{C.5}$$

The original integral is obtained by taking the limit $I(X) = \lim_{k\to 0} I_k(X)$. We evaluate the Fourier integral by using analytic integration methods. Note that there are two sets of second order poles at

$$(1)\ z = iy_n + X \quad \text{and} \quad (2)\ z = iy_n - X, \quad \text{where} \quad y_n = (2n+1)\frac{\pi}{2},\ n \in \mathbb{Z}.$$

We close the contour in the upper half plane so that only $n = 0, 1, \ldots$ is relevant. The residues of the first set of poles are found by writing $z = iy_n + X + \epsilon$ and expanding the functions under the integral to linear order in the small parameter ϵ,

$$\begin{aligned} \cosh(z-X) &\sim i(-1)^n\epsilon \\ \cosh(z+X) &\sim i(-1)^n(s_2 + \epsilon c_2) \\ \sinh(z-X) &\sim i(-1)^n \\ \sinh(z+X) &\sim i(-1)^n(c_2 + \epsilon s_2) \\ e^{ikz} &\sim e^{ikX}e^{-ky_n}(1+ik\epsilon), \end{aligned} \tag{C.6}$$

where we have abbreviated $s_2 = \sinh(2X)$ and $c_2 = \cosh(2X)$. The integrand is then expanded as

$$\begin{aligned} &e^{ikz}\left[\frac{\sinh^2(z-X)\sinh^2(z+X)}{\cosh^2(z-X)\cosh^2(z+X)} - 1\right] \\ &\qquad = e^{ikX}e^{-ky_n}(1+ik\epsilon)\frac{1}{\epsilon}\left[\frac{2c_2}{s_2} + \frac{c_2^2}{\epsilon s_2^2} - \frac{2c_2^3}{s_2^3}\right] + \mathcal{O}\big(\epsilon^0\big). \end{aligned} \tag{C.7}$$

The residue is produced by the $\mathcal{O}\big(\epsilon^{-1}\big)$ terms, so therefore

$$R_n^{(1)} = e^{ikX}e^{-ky_n}\left[\frac{2c_2}{s_2} + \frac{ikc_2^2}{s_2^2} - \frac{2c_2^3}{s_2^3}\right]. \tag{C.8}$$

Summing the geometric series

$$\sum_{n=0}^{\infty} e^{-ky_n} = e^{-\frac{\pi k}{2}}\sum_{n=0}^{\infty}\left(e^{-\pi k}\right)^n = \frac{1}{2\sinh\left(\frac{\pi k}{2}\right)}, \tag{C.9}$$

leads to the result

$$\sum_{n=0}^{\infty} R_n^{(1)} = \frac{e^{ikX}}{2\sinh\left(\frac{\pi k}{2}\right)}\left[\frac{2c_2}{s_2} + \frac{ikc_2^2}{s_2^2} - \frac{2c_2^3}{s_2^3}\right]. \tag{C.10}$$

For the residues of the second set of poles we write $z = iy_n - X + \epsilon$ and again expand the functions under the integral to linear order in ϵ,

$$\begin{aligned}
\cosh(z+X) &\sim i(-1)^n\epsilon \\
\cosh(z-X) &\sim -i(-1)^n(s_2 - \epsilon c_2) \\
\sinh(z+X) &\sim i(-1)^n \\
\sinh(z-X) &\sim i(-1)^n(c_2 - \epsilon s_2) \\
e^{ikz} &\sim e^{-ikX}e^{-ky_n}(1+ik\epsilon).
\end{aligned} \tag{C.11}$$

The integrand therefore expands as

$$\begin{aligned}
&e^{ikz}\left[\frac{\sinh^2(z-X)\sinh^2(z+X)}{\cosh^2(z-X)\cosh^2(z+X)} - 1\right] \\
&\qquad = e^{-ikX}e^{-ky_n}(1+ik\epsilon)\frac{1}{\epsilon}\left[-\frac{2c_2}{s_2} + \frac{c_2^2}{\epsilon s_2^2} + \frac{2c_2^3}{s_2^3}\right] + \mathcal{O}\big(\epsilon^0\big),
\end{aligned} \tag{C.12}$$

with the $\mathcal{O}\big(\epsilon^{-1}\big)$ terms producing the residue

$$R_n^{(2)} = e^{-ikX}e^{-ky_n}\left[-\frac{2c_2}{s_2} + \frac{ikc_2^2}{s_2^2} + \frac{2c_2^3}{s_2^3}\right], \tag{C.13}$$

which leads to

$$\sum_{n=0}^{\infty} R_n^{(2)} = \frac{e^{-ikX}}{2\sinh\big(\frac{\pi k}{2}\big)}\left[-\frac{2c_2}{s_2} + \frac{ikc_2^2}{s_2^2} + \frac{2c_2^3}{s_2^3}\right]. \tag{C.14}$$

Summing the two sets of residues, Eqs. (C.10) and (C.14), and multiplying by $2\pi i$ yields

$$I_k(X) = \frac{4\pi}{2\sinh\big(\frac{\pi k}{2}\big)}\left[-\frac{2c_2}{s_2}\sin(kX) - \frac{kc_2^2}{s_2^2}\cos(kX) + \frac{2c_2^3}{s_2^3}\sin(kX)\right]. \tag{C.15}$$

Finally we take the limit $k \to 0$ to obtain

$$I(X) = -8X\coth(2X) - 4\coth^2(2X) + 8X\coth^3(2X). \tag{C.16}$$

The other integrals are calculated using the same techniques. We list them below:

$$\begin{aligned}
\int_{-\infty}^{\infty} \mathrm{d}x\,\mathrm{sech}^4(x \pm X) &= \frac{4}{3} \\
\int_{-\infty}^{\infty} \mathrm{d}x\,\mathrm{sech}^2(x-X)\,\mathrm{sech}^2(x+X) &= [8X\coth(2X) - 4]\big[\coth^2(2X) - 1\big] \\
\int_{-\infty}^{\infty} \mathrm{d}x\,\big[\tanh^2(x \pm X) - 1\big] &= -2 \\
\int_{-\infty}^{\infty} \mathrm{d}x\,\big[\tanh^4(x \pm X) - 1\big] &= -\frac{8}{3} \\
\int_{-\infty}^{\infty} \mathrm{d}x\,[\tanh(x-X)\tanh(x+X) - 1] &= -4X\coth(2X) \\
\int_{-\infty}^{\infty} \mathrm{d}x\,\big[\tanh^3(x \mp X)\tanh(x \pm X) - 1\big] &= -2 + 2\coth^2(2X) - 4X\coth^3(2X),
\end{aligned} \tag{C.17}$$

and

$$\begin{aligned}
\int_{-\infty}^{\infty} \mathrm{d}x \left[\tanh^3(x-X) - \mathrm{sign}(x)\right] &= -2X \\
\int_{-\infty}^{\infty} \mathrm{d}x \left[\tanh^3(x+X) - \mathrm{sign}(x)\right] &= 2X \\
\int_{-\infty}^{\infty} \mathrm{d}x \left[\tanh^2(x-X)\tanh(x+X) - \mathrm{sign}(x)\right] &= -\left[2X + 2\coth(2X) - 4X\coth^2(2X)\right] \\
\int_{-\infty}^{\infty} \mathrm{d}x \left[\tanh(x-X)\tanh^2(x+X) - \mathrm{sign}(x)\right] &= 2X + 2\coth(2X) - 4X\coth^2(2X).
\end{aligned} \tag{C.18}$$

All of the above integrals have been verified by numerical simulation. Using these results and substituting $mR = 2X$, the classical energy (C.3) is found to be [46]

$$E_{\mathrm{cl}}(R) = \frac{2m^3}{\lambda}\left[-\frac{2}{3} + mR + \frac{3}{\tanh(mR)} - \frac{2+3mR}{\tanh^2(mR)} + \frac{2mR}{\tanh^3(mR)}\right]. \tag{C.19}$$

Subtracting twice the classical kink mass (3.2.16) from this result yields the classical potential

$$V_{\mathrm{cl}}(R) = \frac{2m^3}{\lambda}\left[mR + \frac{3}{\tanh(mR)} - \frac{2+3mR}{\tanh^2(mR)} + \frac{2mR}{\tanh^3(mR)} - 1\right]. \tag{C.20}$$

C.2 The Sine-Gordon Model

The classical energy (C.2) of the kink-antikink configuration of the sine-Gordon model is given by

$$\begin{aligned}
E_{\mathrm{cl}}(R) = \frac{2m^3}{\lambda}\int \mathrm{d}x \Bigg\{ &\left[\mathrm{sech}(x+X) - \mathrm{sech}(x-X)\right]^2 \\
&+ \frac{1}{2}\left[1 - \cos\left[4\arctan\left(e^{-(x-X)}\right) + 4\arctan\left(e^{(x+X)}\right)\right]\right]\Bigg\},
\end{aligned} \tag{C.21}$$

where we have rescaled the integration variable and set $X = mR$. Using the identities

$$\begin{aligned}
\cos(4A+4B) &= \cos(4A)\cos(4B) - \sin(4A)\sin(4B) \\
\cos\left[4\arctan(e^x)\right] &= 2\tanh^2(x) - 1 \\
\sin\left[4\arctan(e^x)\right] &= -2\tanh(x)\,\mathrm{sech}(x),
\end{aligned} \tag{C.22}$$

the above equation becomes

$$\begin{aligned}
E_{\mathrm{cl}}(R) = -\frac{4m^3}{\lambda}\int \mathrm{d}x \Big\{ &\left[\tanh^2(x-X)\tanh^2(x+X) - 1\right] \\
&+ \mathrm{sech}(x-X)\,\mathrm{sech}(x+X)[1 + \tanh(x-X)\tanh(x+X)]\Big\}.
\end{aligned} \tag{C.23}$$

We calculate

$$I(X) = \int_{-\infty}^{\infty} \mathrm{d}x\,\mathrm{sech}(x-X)\tanh(x-X)\,\mathrm{sech}(x+X)\tanh(x+X), \tag{C.24}$$

in detail, as an example. We begin by defining the Fourier integral

$$\begin{aligned} I_k(X) &= \int_{-\infty}^{\infty} \mathrm{d}x\, e^{ikx} \operatorname{sech}(x-X)\tanh(x-X)\operatorname{sech}(x+X)\tanh(x+X) \\ &= \int_{-\infty}^{\infty} \mathrm{d}z\, e^{ikz} \frac{\sinh(z-X)\sinh(z+X)}{\cosh^2(z-X)\cosh^2(z+X)}. \end{aligned} \tag{C.25}$$

Taking the limit $I(X) = \lim_{k\to 0} I_k(X)$ yields the original integral. The Fourier integral is evaluated using analytic integration methods. There are two sets of second order poles at

$$(1)\ z = iy_n + X \quad \text{and} \quad (2)\ z = iy_n - X, \quad \text{where} \quad y_n = (2n+1)\frac{\pi}{2},\ n \in \mathbb{Z}.$$

The contour is closed in the upper half plane such that $n = 0, 1, \ldots$ is relevant. To extract the residues of the first set of poles we write $z = iy_n + X + \epsilon$ and expand the functions under the integral to linear order in the small parameter ϵ,

$$\begin{aligned} \cosh(z-X) &\sim i(-1)^n\epsilon \\ \cosh(z+X) &\sim i(-1)^n(s_2 + \epsilon c_2) \\ \sinh(z-X) &\sim i(-1)^n \\ \sinh(z+X) &\sim i(-1)^n(c_2 + \epsilon s_2) \\ e^{ikz} &\sim e^{ikX}e^{-ky_n}(1+ik\epsilon), \end{aligned} \tag{C.26}$$

where we have abbreviated $s_2 = \sinh(2X)$ and $c_2 = \cosh(2X)$. The integrand then expands as

$$\begin{aligned} &e^{ikz}\frac{\sinh(z-X)\sinh(z+X)}{\cosh^2(z-X)\cosh^2(z+X)} \\ &\qquad = e^{ikX}e^{-ky_n}(1+ik\epsilon)\frac{1}{\epsilon}\left[-\frac{1}{s_2} - \frac{c_2}{\epsilon s_2^2} + \frac{2c_2^2}{s_2^3}\right] + \mathcal{O}\big(\epsilon^0\big). \end{aligned} \tag{C.27}$$

The $\mathcal{O}\big(\epsilon^{-1}\big)$ terms produce the residue

$$R_n^{(1)} = e^{ikX}e^{-ky_n}\left[-\frac{1}{s_2} - \frac{ikc_2}{s_2^2} + \frac{2c_2^2}{s_2^3}\right]. \tag{C.28}$$

Summing the geometric series

$$\sum_{n=0}^{\infty} e^{-ky_n} = e^{-\frac{\pi k}{2}}\sum_{n=0}^{\infty}\left(e^{-\pi k}\right)^n = \frac{1}{2\sinh\left(\frac{\pi k}{2}\right)}, \tag{C.29}$$

yields the result

$$\sum_{n=0}^{\infty} R_n^{(1)} = \frac{e^{ikX}}{2\sinh\left(\frac{\pi k}{2}\right)}\left[-\frac{1}{s_2} - \frac{ikc_2}{s_2^2} + \frac{2c_2^2}{s_2^3}\right]. \tag{C.30}$$

For the residues of the second set of poles we write $z = iy_n - X + \epsilon$ and again expand the functions under the integral to linear order in ϵ,

$$\begin{aligned}
\cosh(z+X) &\sim i(-1)^n\epsilon \\
\cosh(z-X) &\sim -i(-1)^n(s_2 - \epsilon c_2) \\
\sinh(z+X) &\sim i(-1)^n \\
\sinh(z-X) &\sim i(-1)^n(c_2 - \epsilon s_2) \\
e^{ikz} &\sim e^{-ikX}e^{-ky_n}(1+ik\epsilon).
\end{aligned} \tag{C.31}$$

The integrand is then expanded as

$$\begin{aligned}
&e^{ikz}\frac{\sinh(z-X)\sinh(z+X)}{\cosh^2(z-X)\cosh^2(z+X)} \\
&\qquad = e^{-ikX}e^{-ky_n}(1+ik\epsilon)\frac{1}{\epsilon}\left[\frac{1}{s_2} - \frac{c_2}{\epsilon s_2^2} - \frac{2c_2^2}{s_2^3}\right] + \mathcal{O}\big(\epsilon^0\big).
\end{aligned} \tag{C.32}$$

The residue is obtained from the $\mathcal{O}\big(\epsilon^{-1}\big)$ terms,

$$R_n^{(2)} = e^{-ikX}e^{-ky_n}\left[\frac{1}{s_2} - \frac{ikc_2}{s_2^2} - \frac{2c_2^2}{s_2^3}\right], \tag{C.33}$$

which leads to

$$\sum_{n=0}^{\infty} R_n^{(2)} = \frac{e^{-ikX}}{2\sinh\left(\frac{\pi k}{2}\right)}\left[\frac{1}{s_2} - \frac{ikc_2}{s_2^2} - \frac{2c_2^2}{s_2^3}\right]. \tag{C.34}$$

We multiply the two sets of residues, Eqs. (C.30) and (C.34), by $2\pi i$ and sum them to obtain

$$I_k(X) = \frac{4\pi}{2\sinh\left(\frac{\pi k}{2}\right)}\left[\frac{1}{s_2}\sin(kX) + \frac{kc_2}{s_2^2}\cos(kX) - \frac{2c_2^2}{s_2^3}\sin(kX)\right] \tag{C.35}$$

Taking the limit $k \to 0$ yields

$$I(X) = 4\,\mathrm{csch}(2X)\big[X + \coth(2X) - 2X\coth^2(2X)\big]. \tag{C.36}$$

We use the same techniques to evaluate the other two integrals. We list them below:

$$\begin{aligned}
&\int_{-\infty}^{\infty} \mathrm{d}x\,\mathrm{sech}(x-X)\,\mathrm{sech}(x+X) = 4X\,\mathrm{csch}(2X) \\
&\int_{-\infty}^{\infty} \mathrm{d}x\,\big[\tanh^2(x-X)\tanh^2(x+X) - 1\big] = -2\coth(2X)\,\mathrm{csch}^2(2X)[\sinh(4X) - 4X].
\end{aligned} \tag{C.37}$$

We have verified all of the above integrals by numerical simulation. The classical energy (C.23) is then calculated using these results and substituting $mR = X$ [47],

$$E_{\mathrm{cl}}(R) = -\frac{8m^3}{\lambda}\left[\frac{1}{\cosh^2(mR)} + \frac{mR}{\sinh(mR)\cosh^3(mR)} - 2\right]. \tag{C.38}$$

Subtracting twice the classical kink mass (3.2.16) from this result yields the classical potential

$$V_{\mathrm{cl}}(R) = -\frac{8m^3}{\lambda}\left[\frac{1}{\cosh^2(mR)} + \frac{mR}{\sinh(mR)\cosh^3(mR)}\right]. \tag{C.39}$$

Appendix D

Numerical Methods

In this appendix we provide a succinct overview of the numerical methods used during the course of this thesis. All of the mentioned algorithms were implemented in Fortran 90.

D.1 Numerical Calculation of Bound State Energies

In order to calculate the VPE of a system we must be able to accurately and efficiently calculate the bound state energies of the system. Consider the two-channel problem

$$\left[-\frac{\mathrm{d}^2}{\mathrm{d}x^2}+\sigma(x)\right]\phi_{\pm}(x)=k^2\phi_{\pm}(x). \tag{D.1}$$

The antisymmetric channel is specified by the boundary condition $\phi_-(0)=0$, while the symmetric channel corresponds to $\phi'_+(0)=0$. The system is discretized by placing it inside a 'box' of length L and imposing the boundary condition $\phi_{\pm}(kL)=0$. In the free case ($\sigma(x)=0$) this leads to

$$\phi_-^{(0)}(x)=\sqrt{\frac{2}{L}}\sin(k_n x), \quad \text{where} \quad k_n=\frac{n\pi}{L},\ n=1,2,\ldots,N, \tag{D.2}$$

and

$$\phi_+^{(0)}(x)=\sqrt{\frac{2}{L}}\cos\left(\tilde{k}_n x\right), \quad \text{where} \quad \tilde{k}_n=\left(n-\frac{1}{2}\right)\frac{\pi}{L},\ n=1,2,\ldots,N. \tag{D.3}$$

The prefactor $\sqrt{2/L}$ is necessary for normalization. We construct the interacting Hamiltonian as

$$H_{nm}^{(I)}=\int_0^L \mathrm{d}x\,\phi_{\pm,n}^{\dagger(0)}(x)\sigma(x)\phi_{\pm,m}^{(0)}. \tag{D.4}$$

The above integration is performed using the 5-point closed Newton-Cotes formula, otherwise known as Boole's rule.[1] A numerical implementation of this formula can be found in Ref [55, pg. 126]. The full Hamiltonian is then calculated from

$$H_{nm}=E_n^2\,\delta_{nm}+H_{nm}^{(I)}, \tag{D.5}$$

[1] As a result of a typographical error that propagated from Ref. [50, pg. 886], this is widely known as Bode's rule, but it is actually due to Boole [54].

where $E_n^2 = k_n^2 + m^2$ is obtained using the relativistic dispersion relation. We diagonalize this Hamiltonian using the Jacobi method, which consists of performing a sequence of orthogonal similarity transformations equivalent to plane rotations, known as Jacobi rotations. This algorithm appears in Ref. [55, pg. 456]. After diagonalization, the eigenvalues correspond to the squares of the energies. These will depend on the both of the numerical parameters N (the upper limit of the momentum of the system) and L (the length of the 'box'). Nevertheless, if these two parameters are chosen 'large enough' then the eigenvalues below the threshold (given by the square of the mass of the system) are stable because their wave functions are localized. These eigenvalues correspond to the bound state energies squared. The eigenvalues above this threshold are the scattering states which depend on the discretization parameters. This is not a problem, since we evaluate their contribution to the VPE in another manner.

In the case where we apply a constraint to system, as we discussed in Section 2.5, we need to modify our calculation in the symmetric channel. We compute the full Hamiltonian as defined in Eq. (D.5). We then calculate the matrix elements of the projector

$$\hat{P} = \mathbb{1} - |z\rangle\langle z|\,, \tag{D.6}$$

in the symmetric channel basis (D.3). The matrix is diagonalized in order to obtain its eigenvectors, and the full Hamiltonian is transformed into this new basis with the zero mode of $\hat{P}$ decoupled. The bound state energies squared are obtained from the eigenvalues below the threshold of the resulting Hamiltonian, which is diagonalized using Jacobi rotations. Note that this always causes a zero mode to appear for the solution that is annihilated by the projector.

D.2 Numerical Implementation of the VPA

The calculation of the VPE requires computing the integral

$$E_{\text{int}} = -\sum_{p=\pm}\int_0^\infty \frac{\mathrm{d}k}{2\pi}\frac{k}{\sqrt{k^2+m^2}}\Big[\delta_p(k) - \delta_p^{(1)}(k)\Big], \tag{D.7}$$

where the phase shift and its first Born approximation are obtained by solving the relevant differential equations. This requires the implementation of a numerical integration technique, as well as an efficient method for solving differential equations.

D.2.1 Numerical Integration of the VPE

The VPE integral (D.7) must be evaluated numerically over an unbounded interval. This requires the calculation of an infinite number of points on a computer, which is not possible. To avoid this limitation, consider the integral

$$I = \int_0^\infty \mathrm{d}k\, f(k), \tag{D.8}$$

where for some value $\varkappa$ we have

$$f(k) \approx \frac{C}{k^n}, \quad \forall\, k \geq \varkappa, \tag{D.9}$$

where C is a constant and n is an integer. The above integral then becomes

$$\begin{aligned} I &= \int_0^{\varkappa} \mathrm{d}k\, f(k) + \int_{\varkappa}^{\infty} \mathrm{d}k\, \frac{C}{k^n} \\ &= \int_0^{\varkappa} \mathrm{d}k\, f(k) + \frac{C}{(n-1)\varkappa^{n-1}} \\ &= \int_0^{\varkappa} \mathrm{d}k\, f(k) + \frac{\varkappa}{n-1} f(\varkappa). \end{aligned} \tag{D.10}$$

The VPE integrand in Eq. (D.7) is known to be $\mathcal{O}\big(1/k^3\big)$ when $k \to \infty$ [37]. Therefore we may make use of this method, as long as we choose $\varkappa$ sufficiently large.

All that remains is to calculate the bounded integral

$$E_{\mathrm{int}} = -\int_0^{\varkappa} \frac{\mathrm{d}k}{2\pi} \frac{k}{\sqrt{k^2+m^2}} \sum_{p=\pm} \Big[\delta_p(k) - \delta_p^{(1)}(k)\Big]. \tag{D.11}$$

To do so, we convert it into the differential equation

$$\frac{\mathrm{d}}{\mathrm{d}k} E_{\mathrm{int}}(k) = -\frac{1}{2\pi} \frac{k}{\sqrt{k^2+m^2}} \sum_{p=\pm} \Big[\delta_p(k) - \delta_p^{(1)}(k)\Big], \tag{D.12}$$

with the boundary condition $E_{\mathrm{int}}(0) = 0$. This differential equation is solved numerically to evaluate $E_{\mathrm{int}}(\varkappa)$ which gives precisely the bounded integral result (D.11). This is done by using a 4^{th}-order Runge-Kutta (RK) algorithm with adaptive step-size control [55, pg. 706].

The process for calculating the integral contribution to the VPE using the standard implementation of the VPA (from Section 2.4) is as follows:

1. We use a RK algorithm to solve the energy differential equation (D.12), from $k = \varepsilon$ to $k = \varkappa$, where $\varepsilon > 0$ is sufficiently small.

2. At every step, we solve the differential equations (2.4.5) and (2.4.10) with the boundary conditions (2.4.6) and (2.4.12), from $x = x_{\max}$ to $x = x_{\min}$, to obtain $\beta(k, x_{\min})$, $\beta'(k, x_{\min})$, $\beta^{(1)}(k, x_{\min})$ and $\beta'^{(1)}(k, x_{\min})$. This is done by another RK algorithm. The parameter $x_{\max}$ represents spatial infinity and must be chosen adequately large (where "large" depends on the length scale of the potential) while $x_{\min} \to 0$ is positive.

3. These values are then used to calculate the phase shift and its Born approximation in each channel via the relations (2.4.9), (2.4.13), (2.4.15) and (2.4.16).

4. The phase shift and its Born approximation is then used by the RK algorithm from step 1 to advance k.

In the case where a constraint is implemented, the above procedure must be modified, since we instead use the constraint implementation of the VPA, from Section 2.5. The integral contribution to the VPE is then calculated as:

1. We use a RK algorithm to solve the energy differential equation (D.12), from $k = \varepsilon$ to $k = \varkappa$, where ε is an adequately small and positive.

2. At every step, we take a guess for the Lagrange multiplier α and use another RK algorithm to solve the differential equations (2.5.23) (with initial conditions (2.5.26)), (2.5.29), (2.5.39) (with initial conditions $\delta_a(x_{\min}) = 0$) and (2.5.41), from $x = x_{\min}$ to $x = x_{\max}$. The parameter $x_{\max}$ represents spatial infinity and must be chosen sufficiently large (where "large" is dependent on the length scale of the potential) while $x_{\min} > 0$ is small.

3. We determine whether the constraint is satisfied by calculating Eq. (2.5.27). This is done by applying the trapezoidal rule at each point evaluated during the RK algorithm from step 2.

4. If the constraint is satisfied, i.e. the absolute value of the integral is less than a prescribed tiny value, the resulting value of α is tested using Eq. (2.5.28) to ensure consistency. The physical phase shifts are then calculated from the limits (2.5.19), (2.5.30), (2.5.40) and (2.5.42). If the constraint is not satisfied, we use a root-finding algorithm to refine α and step 2 is repeated. In our case we used Ridders' method (see Ref. [55, pg. 351])

5. Once the phase shift and its Born approximation is found, they are used by the RK algorithm from step 1 to advance k.

Bibliography

[1] Aoyama, T., Hayakawa, M., Kinoshita, T. and Nio, M.: Tenth-order QED contribution to the electron $g-2$ and an improved value of the fine structure constant. *Phys. Rev. Lett.*, vol. 109, p. 111807, Sep 2012.
Available at: `http://link.aps.org/doi/10.1103/PhysRevLett.109.111807`

[2] Rajaraman, R.: *Solitons and Instantons: An introduction to solitons and instantons in Quantum Field Theory.* North Holland, Amsterdam, 1987. ISBN 0-444-87047-4.

[3] Russell, J.S.: Report on waves. *Fourteenth meeting of the British Association for the Advancement of Science*, 1844.

[4] Korteweg, D.J. and Vries, G.D.: On the change of form of long waves advancing in a rectangular canal, and on a new type of long stationary waves. *Philos. Mag. Ser*, vol. 39, no. 240, pp. 422–443, 1895.
Available at: `http://dx.doi.org/10.1080/14786449508620739`

[5] Perring, J.K. and Skyrme, T.H.R.: A model unified field equation. *Nucl. Phys.*, vol. 31, pp. 550–555, 1962. ISSN 0029-5582.
Available at: `http://www.sciencedirect.com/science/article/pii/0029558262907745`

[6] Zabusky, N.J. and Kruskal, M.D.: Interaction of "solitons" in a collisionless plasma and the recurrence of initial states. *Phys. Rev. Lett.*, vol. 15, pp. 240–243, Aug 1965.
Available at: `http://link.aps.org/doi/10.1103/PhysRevLett.15.240`

[7] Segev, M., Crosignani, B., Yariv, A. and Fischer, B.: Spatial solitons in photorefractive media. *Phys. Rev. Lett.*, vol. 68, pp. 923–926, Feb 1992.
Available at: `http://link.aps.org/doi/10.1103/PhysRevLett.68.923`

[8] Trapani, P.D., Caironi, D., Valiulis, G., Dubietis, A., Danielius, R. and Piskarskas, A.: Observation of temporal solitons in second-harmonic generation with tilted pulses. *Phys. Rev. Lett.*, vol. 81, pp. 570–573, Jul 1998.
Available at: `http://link.aps.org/doi/10.1103/PhysRevLett.81.570`

[9] Stegeman, G.I. and Segev, M.: Optical spatial solitons and their interactions: Universality and diversity. *Science*, vol. 286, no. 5444, pp. 1518–1523, 1999. ISSN 0036-8075.
Available at: `http://science.sciencemag.org/content/286/5444/1518`

[10] Kevrekidis, P.G., Frantzeskakis, D.J. and Carretero-González, R.: *Emergent Nonlinear Phenomena in Bose-Einstein Condensates: Theory and Experiment*. 1st edn. Springer-Verlag, Berlin, Heidelberg, 2008. ISBN 978-3-540-73590-8.

[11] Carretero-González, R., Frantzeskakis, D.J. and Kevrekidis, P.G.: Nonlinear waves in Bose-Einstein condensates: physical relevance and mathematical techniques. *Nonlinearity*, vol. 21, no. 7, p. R139, 2008.
Available at: `http://stacks.iop.org/0951-7715/21/i=7/a=R01`

[12] Ivanov, B.A., Kichizhiev, A.N. and Mitsai, Y.N.: Nonlinear dynamics and relaxation of strongly anisotropic ferromagnets. *J. Exp. Theor. Phys.*, vol. 75, no. 2, p. 329, 1992.
Available at: `http://www.jetp.ac.ru/cgi-bin/e/index/e/75/2/p329?a=list`

[13] Bishop, A.R., Krumhansl, J.A. and Trullinger, S.E.: Solitons in condensed matter: A paradigm. *Physica D*, vol. 1, no. 1, pp. 1–44, 1980. ISSN 0167-2789.
Available at: `http://www.sciencedirect.com/science/article/pii/0167278980900032`

[14] Vachaspati, T.: *Kinks and Domain Walls: An Introduction to Classical and Quantum Solitons*. 1st edn. Cambridge University Press, UK, 2010. ISBN 978-0521141918.

[15] Davydov, A.S.: Solitons in molecular systems. *Phys. Scr.*, vol. 20, no. 3–4, p. 387, 1979.
Available at: `http://iopscience.iop.org/1402-4896/20/3-4/013`

[16] Yakushevich, L.V.: *Nonlinear Physics of DNA*. 2nd edn. Wiley, New York, 2004. ISBN 978-3-527-40417-9.

[17] Heimburg, T. and Jackson, A.D.: On soliton propagation in biomembranes and nerves. *Proc. Natl. Acad. Sci. U.S.A.*, vol. 102, no. 28, pp. 9790–9795, 2005.
Available at: `http://www.pnas.org/content/102/28/9790.abstract`

[18] Skyrme, T.H.R.: A unified field theory of mesons and baryons. *Nucl. Phys.*, vol. 31, pp. 556–569, 1962. ISSN 0029-5582.
Available at: `http://www.sciencedirect.com/science/article/pii/0029558262907757`

[19] Weigel, H.: *Chiral Soliton Models for Baryons*. Lect. Notes Phys. 743. Springer-Verlag, Berlin, Heidelberg, 2008. ISBN 978-3-540-75435-0.

[20] Skyrme, T.H.R.: The origins of skyrmions. *Int. J. Mod. Phys.*, vol. 3, no. 12, pp. 2745–2751, 1988. Article reconstructed by I. Aitchison.
Available at: `http://dx.doi.org/10.1142/S0217751X88001156`

[21] Adkins, G.S., Nappi, C.R. and Witten, E.: Static properties of nucleons in the Skyrme model. *Nucl. Phys. B*, vol. 228, no. 3, pp. 552–566, 1983. ISSN 0550-3213.

Available at: http://www.sciencedirect.com/science/article/pii/055032138390559X

[22] Dashen, R.F., Hasslacher, B. and Neveu, A.: Nonperturbative methods and extended-hadron models in field theory. II. two-dimensional models and extended hadrons. *Phys. Rev. D*, vol. 10, pp. 4130–4138, Dec 1974.
Available at: https://dx.doi.org/10.1103/PhysRevD.10.4130

[23] Dashen, R.F., Hasslacher, B. and Neveu, A.: Particle spectrum in model field theories from semiclassical functional integral techniques. *Phys. Rev. D*, vol. 11, pp. 3424–3450, Jun 1975.
Available at: http://link.aps.org/doi/10.1103/PhysRevD.11.3424

[24] Faddeev, L.D. and Korepin, V.E.: Quantum theory of solitons. *Phys. Rep.*, vol. 42, no. 1, pp. 1–87, 1978. ISSN 0370-1573.
Available at: http://www.sciencedirect.com/science/article/pii/0370157378900583

[25] Moussallam, B. and Kalafatis, D.: On the Casimir energy of a skyrmion. *Phys. Lett. B*, vol. 272, no. 3, pp. 196–201, 1991. ISSN 0370-2693.
Available at: http://www.sciencedirect.com/science/article/pii/037026939191819H

[26] Holzwarth, G. and Walliser, H.: Quantum corrections to the skyrmion mass. *Nucl. Phys. A*, vol. 587, no. 4, pp. 721–746, 1995. ISSN 0375-9474.
Available at: http://www.sciencedirect.com/science/article/pii/037594749500012P

[27] Meier, F. and Walliser, H.: Quantum corrections to baryon properties in chiral soliton models. *Phys. Rep.*, vol. 289, no. 6, pp. 383–448, 1997. ISSN 0370-1573.
Available at: http://www.sciencedirect.com/science/article/pii/S0370157397000124

[28] Achúcarro, A. and Vachaspati, T.: Semilocal and electroweak strings. *Phys. Rep.*, vol. 327, no. 6, pp. 347–426, 2000. ISSN 0370-1573.
Available at: http://www.sciencedirect.com/science/article/pii/S0370157399001039

[29] Graham, N., Quandt, M., Schröder, O. and Weigel, H.: Quantum energies of strings in a (2+1)-dimensional gauge theory. *Nucl. Phys. B*, vol. 758, no. 1–2, pp. 112–143, 2006. ISSN 0550-3213.
Available at: http://www.sciencedirect.com/science/article/pii/S0550321306007565

[30] Balachandran, A.P., Barducci, A., Lizzi, F., Rodgers, V.G.J. and Stern, A.: Doubly strange dibaryon in the chiral model. *Phys. Rev. Lett.*, vol. 52, pp. 887–890, Mar 1984.
Available at: http://link.aps.org/doi/10.1103/PhysRevLett.52.887

[31] Scholtz, F.G., Schwesinger, B. and Geyer, H.B.: The Casimir energy of strongly bound $B = 2$ configurations in the Skyrme model. *Nucl. Phys. A*, vol. 561, no. 4, pp. 542–556, 1993. ISSN 0375-9474.
Available at: `http://www.sciencedirect.com/science/article/pii/0375947493900645`

[32] Noether, E.: Invariante Variationsprobleme. *Nachrichten von der Gesellschaft der Wissenschaften zu Göttingen, Mathematisch-Physikalische Klasse*, vol. 1918, pp. 235–257, 1918.
Available at: `http://eudml.org/doc/59024`

[33] Graham, N., Quandt, M. and Weigel, H.: *Spectral Methods in Quantum Field Theory*. Springer, Berlin, Heidelberg, 2009. ISBN 3-642-00138-6.

[34] Graham, N., Jaffe, R.L. and Weigel, H.: Casimir effects in renormalizable quantum field theories. *Int. J. Mod. Phys. A*, vol. 17, no. 06n07, pp. 846–869, 2002.
Available at: `https://dx.doi.org/10.1142/S0217751X02010224`

[35] Graham, N., Jaffe, R.L., Khemani, V., Quandt, M., Scandurra, M. and Weigel, H.: Calculating vacuum energies in renormalizable quantum field theories: A new approach to the Casimir problem. *Nucl. Phys. B*, vol. 645, no. 1–2, pp. 49–84, 2002. ISSN 0550-3213.
Available at: `https://dx.doi.org/10.1016/S0550-3213(02)00823-`

[36] Newton, R.G.: *Scattering Theory of Waves and Particles*. 2nd edn. Springer-Verlag, New York, 1982. ISBN 978-3-642-88130-5.

[37] Chadan, K. and Sabatier, P.C.: *Inverse Problems in Quantum Scattering Theory*. 2nd edn. Springer-Verlag, New York, 1989. ISBN 978-3-642-83319-9.

[38] Levinson, N.: On the uniqueness of the potential in a Schrödinger equation for a given asymptotic phase. *Danske. Vid. Selsk. Math. Fys. Medd.*, vol. 25, pp. 1–29, 1949.

[39] Barton, G.: Levinson's theorem in one dimension: heuristics. *J. Phys. A*, vol. 18, no. 3, p. 479, 1985.
Available at: `http://stacks.iop.org/0305-4470/18/i=3/a=023`

[40] Collins, J.C.: *Renormalization. An Introduction to Renormalization, the Renormalization Group, and the Operator Product Expansion*. Cambridge University Press, UK, 1986. ISBN 978-0521311779.

[41] Calogero, F.: *Variable Phase Approach to Potential Scattering*. Academic Press, New York and London, 1967.

[42] Vidal, F. and LeTourneux, J.: Multichannel scattering with nonlocal and confining potentials. I. general theory. *Phys. Rev. C*, vol. 45, pp. 418–429, Jan 1992.
Available at: `https://dx.doi.org/10.1103/PhysRevC.45.418`

[43] Ma, Z.Q. and Dai, A.Y.: Levinson's theorem for non-local interactions. *J. Phys. A*, vol. 21, no. 9, p. 2085, 1988.
Available at: `https://dx.doi.org/10.1088/0305-4470/21/9/022`

[44] Weinberg, E.J.: *Classical Solutions in Quantum Field Theory: Solitons and Instantons in High Energy Physics*. Cambridge University Press, UK, 2012. ISBN 978-0-521-11463-9.

[45] Pöschl, G. and Teller, E.: Bemerkungen zur Quantenmechanik des anharmonischen Oszillators. *Zeitschrift für Physik*, vol. 83, no. 3, pp. 143–151, 1933. Available at: `https://dx.doi.org/10.1007/BF01331132`

[46] Sugiyama, T.: Kink-antikink collisions in the two-dimensional ϕ^4 model. *Progr. Theoret. Phys.*, vol. 61, no. 5, pp. 1550–1563, 1979. Available at: `https://dx.doi.org/10.1143/PTP.61.1550`

[47] Rajaraman, R.: Intersoliton forces in weak-coupling quantum field theories. *Phys. Rev. D*, vol. 15, pp. 2866–2874, May 1977. Available at: `http://link.aps.org/doi/10.1103/PhysRevD.15.2866`

[48] Graham, N. and Jaffe, R.L.: Unambiguous one-loop quantum energies of 1+1 dimensional bosonic field configurations. *Phys. Lett. B*, vol. 435, no. 1–2, pp. 145–151, 1998. ISSN 0370-2693. Available at: `http://www.sciencedirect.com/science/article/pii/S0370269398007953`

[49] Feist, D.T.J., Lau, P.H.C. and Manton, N.S.: Skyrmions up to baryon number 108. *Phys. Rev. D*, vol. 87, p. 085034, Apr 2013. Available at: `http://link.aps.org/doi/10.1103/PhysRevD.87.085034`

[50] Abramowitz, M. and Stegun, I.A.: *Handbook of Mathematical Functions with Formulas, Graphs, and Mathematical Tables*. Tenth edn. U.S. Department of Commerce, National Bureau of Standards, 1972. ISBN 0-486-61272-4.

[51] Bôcher, M.: On linear dependence of functions of one variable. *Bull. Amer. Math. Soc.*, vol. 7, pp. 120–121, 1900. Available at: `https://dx.doi.org/10.1090/S0002-9904-1900-00771-3`

[52] Campbell, D.K., Schonfeld, J.F. and Wingate, C.A.: Resonance structure in kink-antikink interactions in ϕ^4 theory. *Physica D*, vol. 9, no. 1, pp. 1–32, 1983. ISSN 0167-2789. Available at: `http://www.sciencedirect.com/science/article/pii/0167278983902890`

[53] Takyi, I. and Weigel, H.: Collective coordinates in one-dimensional soliton models revisited. *Phys. Rev. D*, vol. 94, p. 085008, Oct 2016. Available at: `http://link.aps.org/doi/10.1103/PhysRevD.94.085008`

[54] Boole, G. and Moulton, J.F.: *A Treatise on the Calculus of Finite Differences*. 2nd edn. Dover, New York, 1960. ISBN 0-828-41121-2.

[55] Press, W.H., Flannery, B.P., Teukolsky, S.A. and Vetterling, W.T.: *Numerical Recipes in Fortran 77: The Art of Scientific Computing*. 2nd edn. Cambridge University Press, UK, 1992. ISBN 0-521-43064-X.